ARCHIVES OF ACOUSTICS
11, 3, 203-229 (1986)

ESTIMATION OF GUITAR SOUND QUALITY

TOMIRA BOEHM, KACPER MIKLASZEWSKI

Frederik Chopin Academy of Music
(Warsaw, ul. Okólnik 2)

FRIEDRICH BLUTNER, EBERHARD MEINEL

Institut für Musikinstrumentenbau, Zwota (GDR)

The described investigation was aimed at the determination of the subjective and objective quality of sound of four classic guitars. The investigation of the subjective sound quality — carried out in the Laboratory of Music Acoustics, Academy of Music in Warsaw — consisted of two parts: general and parametric. The following parameters was used: brightness, timbre dispersion over the instrument scale, fullness, carrying power, clearness, dynamics. The listeners were students and co-workers in this laboratory. Investigations of the objective quality carried out in Zwota (GDR) resulted in sound pressure level histograms — presented in 20 diagrams for 20 frequency bands covering the full range of sound frequencies produced by the investigated instruments. The analysis of these histograms shows a significant correlation with the results of the subjective quality estimation.

1. Introduction

Among investigations of music instruments, which constitute a large part of acoustics — the examinations of string instruments, particularily violins, have an important place. These investigations concern also other string instruments, including guitars. Most measurements were carried out in order to determine improvements of the instrument design, essential to make the instrument better in view of its physical parameters and sound quality. It is obvious that physical properties, or even mechanical properties, are closely related to the sound quality of a given instrument.

However, many investigations concerned only the measureable guitar parameters. The resonance box and its properties, as a secondary source, were the main objects of interest. It appeared that the frequency characteristic of the sound radiated by the box contained, in its lower range, several resonances (formants) which significantly influenced the quality of sound. In the frequency range up to 800 Hz, these formants are clearly perceptible and can be simply investigated. The important problem, which presently is given a great deal of attention, is the location of these resonances (f_r) and their width (Q), peak level and level exceeding the rest of the signal. Resonances of the top plate were investigated widely. For example, [8] constructed systems of harmonic oscillators moving a piston, acting as individual sources, with a unipolar sound radiation. Every oscillator corresponds to one formant in the frequency response. Investigations conducted on 5 guitars have proved a significant correlation of the experimental results with the frequency response obtained theoretically from the analysis of a system of several oscillators. The author stated, that in the frequency range up to 800 Hz the parameters of 4–6 harmonic oscillators are sufficient. This procedure is much simpler that the investigation of the frequency response of the guitar box. One of CHRISTENSEN'S earlier works [6] was concerned with the first two guitar resonances only. These resonances were defined as the result of overlapping of the fundamental vibration of the top plate and the Helmholtz resonance of air inside the guitar box. Also in this case a theoretical model of the frequency characteristics in the low frequency range was proposed. It was found that the Helmholtz resonance was not equivalent with the air resonance. The Helmholtz resonance appeared as an antiformant between the first and second formant of the plate. The proposed model (oscillator design obtained on the basis of the Newton equation) precisely described the variation of the sound pressure level and the motion of the top plate of the guitar in terms of frequency. In another paper, [7] investigated the middle frequency range. The signal was recorded and than analysed with the application of the Fourier transform, in order to obtain the acoustical power density spectrum (*APDS*). Through averaging the levels in 1/3 octave bands and calculating the energy distribution, a curve with many informations about the sound, was achieved. This curve usually has the same characteristic jump-growing shape (the jumps are the regions of succeeding resonances) for every instrument. The greatest amount of energy comes from the 224–445 Hz range (this leads to a conclusion that it is a very important range for guitar sound quality). The following distinct jump occurs about 400 and 550 Hz — for the III and IV resonance. In this last range about 50 per cent (or more) of the energy is radiated. This accounts for the main interest in the low and medium frequency ranges (to about 800 Hz) in further investigations.

Among others, also CALDERSMITH [5] investigated the problem of vibrations of the plate and the air mass contained in the resonance box. This research also resulted in a theoretical model of the reflective casing, which was physically

applicable and convincingly determined the most important parameters of the investigated box — the location and width of the fundamental set of two resonances (of plate air). The casing dimensions and the material it was made of, have been taken into account. The model also pointed out the significance of the location of the rose in the plate, in relation to the formant location in the frequency scale (this relationship results from the influence of air vibrations on the complete characteristic of sound radiation).

Similar research was also conducted by FIRTH [10], [9] and JANSSON [12], [13].

In the first mentioned work, Jansson discussed acoustical tests of vibrations of the guitar top plate. Vibrations modes, corresponding to succeeding formants of the frequency characteristic, were studied with the application of holograph interferometric method. This method leads to the determination of the resonance frequency, f, and the quality factor, Q. The characteristic obtained from acoustical measurements was compared with interferograms. Acoustic investigations were conducted with the application of 6 various box excitation points and 6 (different) measuring points of the characteristic. It was stated that the frequency of individual formants obtained from these two methods are constant with an error not exceeding 1 per cent, while Q — with an error not exceeding 13 per cent. Therefore, both values can be achieved from acoustical measurements, on condition that the measuring points of the characteristic are carefully chosen.

In order to explain acoustical properties of resonance holes another series of investigations were carried out. Boxes of various shapes have been investigated. The frequency response of the vibrations of air contained in these casings, was measured. It appeared that guitars and violins had the same vibration modes and generally they corresponded with rectangular and cylindrical casings. The resonance density did not depend on the shape of the box, if the volume, wall surface and lengths of the edges were identical. On the other hand, the density calculated from geometrical data for guitars, differed from the real density by 60 per cent. Whereas, vibration modes changed even at the slightest change of the box shape.

In his paper of 1977, FRITH [10] described a physical model representing the functioning of a guitar. For the reason to construct this model, the following measurements were carried out: the resonance frequency (defined as the formant at 0 Hz — the Helmholtz resonance), the shape of vibration modes (with the application of Chladni figures), input admittance in the central point of the bridge (in the first and second resonance range), and the input sound pressure level and its phase.

All mentioned above papers were concerned exclusively with the physical aspect of the vibrations of the guitar resonance box. Methods of acoustic measurements and various models allowing mathematical calculation of various parameters, have been hitherto described.

The works of KRÜGER [15], MEYER [17] and JAROSZEWSKI, RAKOWSKI, ZERA [14] dealed with a different aspect of the problem. However, KRÜGER still taked up the problem of frequency response of the top plate vibrations, but he conducted research on 20 guitars, which were subjectively rated as good, middle and bad. He tried to relate certain characteristic estimations of physical parameters of instruments to their individual ranks (e.g. a master guitar displays a distinctly higher sound pressure level from any other instrument in the 200–800 Hz range and somewhat less in the range of the so-called "bass"). In the course of his experiments KRÜGER introduced variants of the design structure of the top plate and studied their influence on the sound character. He reached a conclusion that at a constant energy the lesser the losses during the process of bending a plate (during vibrations) and the lesser its rigidity, the greater the vibration amplitude (and thus the sound radiation level for a given frequency).

Energy losses caused by these two factors decrease with the decrease of the plate thickness.

The other two papers described research concerned with the subjective evaluation of the guitar sound quality. JAROSZEWSKI et al. [14] limited their studies to one parameter, i.e. onset time. Subjective evaluations were carried out by experts during individual 0.5–1.5 hour sessions. The sound arise time was measured from a perceptible moment of the beginning of the signal to the moment it reached 90 or 100 per cent of the maximal amplitude (in dependence on shape of arise). A comparison between the obtained results and the experts' evaluation showed distinct correlation between them. Instruments with longer attack were rated as a better. These better instruments had also a lower relative dispersion of the onset time values (30 sounds for 13 guitars have been investigated). MEYER'S paper [17] includes more criteria. It was aimed at finding such resonance properties of the instrument, which would significantly influence its quality. 15 guitars have been studied and 40 persons have subjectively evaluated instruments on the basis of an auditory test. Correlation of obtained rank arrangements of instruments with data obtained from various modifications of the frequency response was calculated (level averaging in 1/3 octave and wider bands of various ranges; determining formant levels and widths, as well as determining how much this range exceeds the rest of the frequency region; establishing the distances between the box resonances and the nearest sound, etc.). A distinct correlation was observed here between certain criteria of the physical and subjective quality evaluation. E.g. the high level in the 80–1000 Hz region occurred only in highly rated guitars — the better the instrument, the higher level of the third resonance (but a smaller width), the additional formant between the main formants was also a positive feature of the instrument.

In the final stage of these studies the correlation coefficient between the results of subjective and objective evaluation was calculated for all 20 parameters. The correlation was very high, namely $r = 0.88$, and excluding the guitar with an unstable pitch, it equaled $r = 0.97$. However, even only seven criteria

gave a very high correlation coefficient of 0.85. It was found that for a high correlation between subjective and objective evaluation, the most important factors are: the level of third resonrence, level values in the 80–125 Hz 250–400 Hz and 315–500 Hz, and the occurrence of a formant between the first and second resonance. Unfortunately, during the investigations it appeared that there is a rather significant dependence on the kind of music played on the instrument. This to a certain extent shakes the universality of the achieved results.

It should be mentioned here that musicians always select instruments to the kind of music they are to play (solo, accompaniament, melody or rather harmonic structures).

The experiment presented in this paper, performed by KAM in Warsaw and the IfM in Zwota (GDR), was aimed at similar goals as the last discussed paper. 4 guitars have been subjectively rated (auditory test). The comparison and correlation of the achieved results were the final goal. Investigations of the subjective sound quality were carried out in the Laboratory of Music Acoustics at the Academy of Music in Warsaw, while the objective parameters were measured in IfM in Zwota (GDR).

2. Experimental materials

Guitars for investigations were chosen only from among concert instruments of medium quality, corresponding to a class of higher quality instruments produced in large-scale. However, due to various designs, certain differences in sound timbre were expected. Instrument no. 1 (test guitar, produced by a violin maker) was a hand-made experimental model, which had a modified resonance plate in the bridge region, in order to improve radiation of low frequencies. Other guitars were standard instruments produced by industry and widely sold. Instrument no. 2 was one of the "Resonata" models, till now produced by VEB Musima in Markneukirchen. Instrument no. 3 was a new achievement, named "Musima Classic", model 136. The new range of products from the "Classic" series was developed in cooperation between VEB Musima and Institute of Music Instruments Construction (IfM) in Zwota and it replaced the "Resonata" assortment. It had an optimised radiation power in comparison with previous models. Furthermore, this new assortment had a vaulted plate.

Instrument no. 4 (Marlin MC 315) has been included in tests as an instrument for comparison, due to its high acoustic value distinguishing it from other instruments produced by industry.

3. Subjective evaluation — arrangement of tests

The test was constructed under the method of comparing in pairs. Excerpts of recordings of individual instruments were grouped in pairs, so every instrument was compared with every other instrument. This way six pairs were formed (from four elements).

However, since an arrangement of two instruments was presented two times — in a different sequence every time (*AB*, *BA*) — there were twelve test items. Their sequence in a test was randomly chosen. Such a twelve — task test constituted one out of three parts of the whole test material. These parts differed from each other in the sequence of test items and, first of all in the music material, i.e. in every part a different music composition was used: in part I — Preludium no. 1 by Villa-Lobos, in part II — the second variation from the Variation on Mozart by Ferynand Sor, in part III — Rondetto by Napoleon Coste.

4. Conduction of tests

The subjective auditory estimation was divided into two parts:

1. So-called general evaluation (general impression) of the instrument quality;

2. Estimation of six subjective parameters: brightness, timbre dispersion over the instrument scale, fullness, carrying power, clearness (clarity, absence of disturbances and deformations) and dynamics (dynamic range).

In the second part the listeners were to estimate which instrument posseses a given feature in a greater extend. That is, which one, within the pair, is brighter, has better dispersion, has better sound fullness etc. If the instruments differed greatly the listener was to give two points, when they differed less-one point. The instrument with a given feature estimated lower, obtained zero points. In the case of the general evaluation (part I) listeners gave one or two points to this guitar out of a pair, which they liked more. This evaluation was performed on the whole test material — on all three parts — while every parameter was rated with the application of only one part of the test. The brightness and timbre dispersion were evaluated only for guitars in the first part of the test; fullness and carrying power — in the second part; sound clearness and dynamics — in the third part. Therefore every listener listened to the whole test two times: first time — applying the uniform criterion of the general evaluation and second time — applying the criterion of the parametric estimation, different for every one of the three parts of the test.

The group of listeners consisted of 24 persons. These were students and workers of the Academy of Music in Warsaw. Two persons were students of a guitar class of the instrumental faculty, the rest of group consisted of students and graduates of the Faculty of Sound Recording.

The test was reproduced on a Revox B 77 tape recorder and listeners were equipped with SN 60 earphones.

5. Results

In the results analysis first of all it had to be checked whether the kind of music significantly influenced the results. If the general evaluation gave by listeners would depend on the character of the stimulus, then it would not be possible to sum up the results — points obtained for every guitar in individual parts of the test, and the parametric estimation should have to be conducted for all three parts separately. Moreover, due to the interdependence of results and the test itself, it would be impossible finally to rank the instruments in a certain order. In order to state, whether there is such a dependence, a two-factor analysis an variance was performed [4]. ANOVA table is presented in

Table 1. Complete results of two-factor variance analysis — general estimation

Type of variability	ϑ	Sum square	σ^2	F	$F(\alpha, \vartheta_I, \vartheta_{II})$	
					1%	5%
A (test)	2	0.337	0.1685	0.0543	4.68	3.03
B (guitars)	3	357.674	125.225	40.363	3.85	2.63
AB	6	427.857	71.3095	22.984	2.86	2.13
E	276	856.292	3.1025			
total	287	1660.16				

Tab. 1. The application of such two-factor analysis was possible under an assumption of a uniform group of listeners. Without such an assumption a multifactor analysis would be necessary, where the listeners would be the third variable. This would seriously complicate the calculations. But since all listeners were workers or students of the Academy of Music mainly from the Faculty of Sound Recording, the group could have been considered as uniform and the differences between individual persons could have been neglected.

An additional information about the group of listeners was obtained by calculating the reliability coefficient for every listener. As the test was done in such manner, that it could be easily divided into two halves (all pairs of instruments occurred in both halves, but in a reversed sequence), then we could apply the RULON'S equation [11]:

$$r = \frac{\sigma_d^2}{\sigma_x^2}$$

σ_d^2 — variance of differences between the two halves, σ_x^2 — variance of all test results, which is a useful measure of reliability.

All data from every listener are presented in tables, confronting results of corresponding pairs (e.g. 3–4 and 4–3, 1–2 and 2–1, ...). Then, both variances

and reliability (r) were calculated by choosing randomly external or internal columns.

Finally, the guitars were ordered on the rank scale according to the estimation of the subjective quality. To this aim points given to every instrument by all listeners were added up/an instrument could have obtained a maximum amount 864 points: 6 presentations of the instrument $\times 24$ listeners $\times 2$ points $\times 3$ parts of the test (Table 2). Also the mean values of estimations were calculated — their arithmetic mean, $M = \Sigma X/N$, and the standard deviations, $\sigma = \sqrt{\frac{\Sigma x^2}{N}}$ (Table 3, Fig. 1).

ΣX — the sum of points of all listeners,
Σx^2 — the sum of squares of deviations of every result from the mean,
N — number of results,
M — arithmetic mean.

Table 2. Classification of the instruments on the rank scale — general estimation

Guitars	Points	Rank
1	232	III
2	136	IV
3	350	I
4	313	II

1 — master instrument (Markneukirchen)
2 — industrial guitar (Musima)
3 — investigated guitar
4 — Japanese industrial guitar (Marlin MC 315)

Table 3. Means and standard deviations for points obtained by all instruments — general estimation

Guitars	M	σ
1	3.222	1.863
2	1.888	1.939
3	4.861	2.519
4	4.347	2.124

On the basis of this data we can set instruments in an order from the "best" to the "worst", but we still do not know anything about the absolute differentiation of these instruments, or what the "best" and "worst" means. For in the case of a subjective rating we can not fix an absolute zero or any unit, which would determine how many times one instrument is better (worse) than another, we can only place instruments on a rank scale. Therefore, the only information that could been obtained here, was the significance of differences between mean values for individual instruments. To this aim a Student's t test was applied for differences between non-correlated means in samples of equal quantity,

$$t = \frac{M_1 - M_2}{\sqrt{\frac{\Sigma X_1^2 - \Sigma X_2^2}{N(N-1)}}},$$

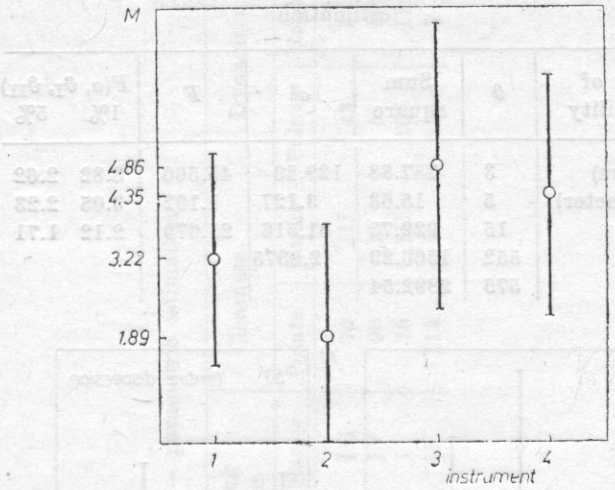

Fig. 1. Means and standard deviations — general estimation

M_1, M_2 — means in two samples (in this case — mean results for two instruments), ΣX_1^2, ΣX_2^2 — sums of squares in both samples.

Obtained quantities show which guitars significantly differ from each other, and for which these differences may be neglected (Table 4).

Results of parametric estimations were processed in the same way.

Table 4. Significancy of differences between means for individual instruments — general estimation

Guitars	t	Significance level
3–1	2.09	0.05
2–3	2.91	0.01
4–2	2.8	0.01
1–2	2.45	0.05

1 — master instrument (Markneukirchen)
2 — industrial guitar (Musima)
3 — investigated guitar
4 — Japanese industrial guitar (Marlin MC 315)

First, it was checked with the application of a two-factor analysis of variance whether the obtained differentiation of results is caused by differences between instruments or criteria (parameters) according to which listeners conducted the estimation. Results of the analysis are presented in Table 5.

Table 5. Results of the two-factor variance analysis — parametric estimation

Type of variability	ϑ	Sum square	σ^2	F	$F(\alpha, \vartheta_I, \vartheta_{II})$ 1%	5%
A (guitars)	3	387.88	129.29	45.566	3.82	2.62
B (parameter)	5	15.63	3.127	1.102	3.05	2.23
AB	15	922.73	61.516	21.679	2.12	1.71
E	552	1566.29	2.8375			
total	575	2892.54				

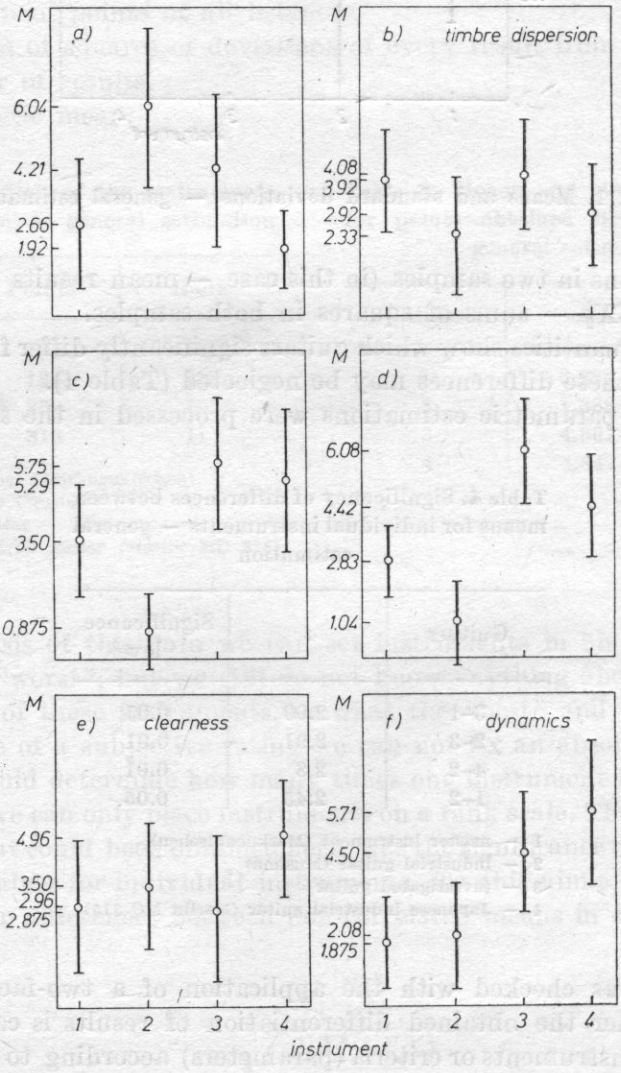

Fig. 2. Means and standard deviations — parametric estimation: a. brightness, b. timbre dispersion over the instrument scale, c. fullness, d. carrying power, e. clearness, f. dynamics

Table 6. Classification of the instruments on the rank scale — parametric estimation

Parameter	Brightness		Timbre dispersion		Fullness		Carrying power		Clearness		Dynamics	
Guitars	Points	Ranks	Points	Ranks	Points	Ranks	Points	Ranks	Points	Ranks	Points	Ranks
1	64	III	98	II	84	III	70	III	70	III	43	IV
2	146	I	54	IV	21	IV	24	IV	90	II	51	III
3	100	II	99	I	138	I	145	I	70	III	109	II
4	46	IV	68	III	130	II	116	II	119	I	138	I

1 — Master instrument (Markneukirchen)
2 — Industrial guitar (Musima)
3 — Investigated guitar
4 — Japanese industrial guitar (Marlin MC 315)

Table 7. Means and standard deviations of individual data for all of instruments — parametric estimation

Parameter	Brightness		Timbre dispersion		Fullness		Carrying power		Clearness		Dynamics	
Guitars	M	σ	M	σ	M	σ	M	σ	M	σ	M	σ
1	2.66	1.88	3.916	1.5	3.5	1.615	2.833	1.007	2.958	1.88	1.875	1.329
2	6.04	2.349	2.333	1.76	0.875	1.115	1.041	1.232	3.5	1.841	2.083	1.585
3	4.21	2.206	4.083	1.639	5.75	1.916	6.083	1.471	2.875	2.132	4.5	1.719
4	1.92	1.176	2.516	1.442	5.291	2.095	4.416	1.501	4.958	1.731	5.708	2.095

1 — Master instrument (Markneukirchen)
2 — Industrial guitar (Musima)
3 — Investigated guitar
4 — Japanese industrial guitar (Marlin MC 315)

Table 8. Significancy of differences between means for individual instruments — parametric estimation

Parameter	Guitars	t	Significance level
Brightness	1–2	2.24	0.05
	3–4	2.1	0.05
	2–4	2.89	0.01
Timbre dispersion	all differences insignificant		
Fullness	2–3	3.77	0.01
	2–4	3.62	0.01
	1–2	3.08	0.01
Carrying power	1–3	2.25	0.05
	2–3	3.75	0.01
	1–2	2.53	0.05
	2–4	3.29	0.01
Clearness	all differences insignificant		
Dynamics	2–4	2.63	0.05
	1–4	2.84	0.01
	2–3	2.12	0.05
	1–3	2.37	0.05

1 — Master instrument (Markneukirchen)
2 — Industrial guitar (Musima)
3 — Investigated guitar
4 — Japanese industrial guitar (Marlin MC 315)

Also for the parametric estimation instruments were classified on rank scales according to the possession of a given feature from the brightest to the least bright, from most to least dispersed, etc. (Table 6, 7, Fig. 2). The significance of differences between the mean value of points obtained by individual instruments was checked with application of the Student's t test. These results are presented in Table 8.

6. Conclusions concerning the subjective estimation

The evaluation reliability of listeners was found to be in the greater part high. Only for six persons the r coefficient dropped below 0.8, while for seven persons it exceeded 0.95. The high reliability consistently chose the better (according to them) instrument; that they had a certain constant quality criterion according to which they rated instruments. On the basis of these coefficients also a conclusion can be drawn that the sequence of instruments in a pair test item is not significant in such tests. The reliability coefficient, calculated from the RULON'S formula brings information about the conformity between both halves of the test. Since in this case, in the second half the sequence of stimuli was reversed in comparison to the first half (AB and BA) and in spite of that listeners chose the same instrument, then it means that it was not significant which one occurred as the first and which as the second within the pair.

Another important matter was to check whether the results were influenced by the kind of music played on tested instruments. Results of the analysis of variance, presented in Table 1, bring an answer to this question. It was found that individual guitars were the only significant factor — the value F is higher from the critical value of the 1 per cent level. Whereas, the kind of music material, on which the evaluation was conducted, was statistically insignificant.

Therefore, it was possible to carry out the parametric estimation on only one out of three parts of the test — not on the whole test. Obtained results can be considered representative.

The analysis of variance, where guitars are one factor and the subjective parameters — the second, give an interesting information. It was stated that results was significantly influenced by the evaluation criterion on 1 per cent, level while the variability caused by instruments was insignificant. This can mean that the differences between guitars in respect to a certain feature are small and that every feature classifies instruments differently. E.g. the guitar which achieved the most points in respect to the criterion of brightness, will not have the best timbre dispersion or carrying power. These suppositions have been confirmed by the number of points achieved by each guitar. Rank of instruments in respect to particular parameters are shown in Table 6. And indeed various features classified instruments differently. The classification in respect to the criterion of brightness proved itself to be the least similar to other parameters, while the fullness and carrying power gave the same results. A similar classification was obtained in respect to the timbre dispersion over the instrument scale; slightly different in respect to dynamics and clearness. However, further conclusions could not be drawn from these results before it was stated whether the differences between instruments with succeeding ranks are signifi-

cant. It was stated that only some of them are significant. The dispersion over the instrument scale and clearness were found insignificant as a parameter- even the difference between the first and fourth rank was insignificant. The difference between the first and second rank is insignificant for all criteria. In respect to fullness, one instrument (no. 2) proved itself distinctly worse from other instruments. The differences between this and any other instrument are significant on the 1 per cent level. All other differences (between guitars with ranks: I, II and III) were insignificant. Therefore, in respect to fullness two groups can be formed: first — including guitars no. 1, 3 and 4, second — guitar no. 2. In respect to the criterion of dynamics, differences between the guitar with rank I (no. 4) and guitars with ranks III (no. 2) and IV (no. 1), and between guitar with rank II (no. 3) and guitars with ranks III and IV, were proved to be significant. This way two classes were obtained: the first one includes instruments no. 3 and 4, the second — no. 1 and 2. Differences between no. 1 and 4 are significant on the 1 per cent level the other — on the 5 per cent level.

It was difficult to determine similar classes in respect to the criteria of carrying power and brightness. In respect to carrying power, the instrument with rank IV (no. 2) distinctly differed from others, while first three ranks formed one class. The difference between the first and third rank (no. 3 and 1) is significant on the 5 per cent level. The classes in respect to brightness were slightly different. The first rank (no. 2) constitutes one class the second (no. 3) and third (no. 1) — the second class, the fourth rank — the third class. The differences between instruments no. 2 and 3, and no. 1 and 4 are insignificant. The difference between the I and IV rank is significant on the 1 per cent level while the others — on the 5 per cent level. The final classification of instruments according to subjective parameters is presented in Fig. 3.

The criterion of the general evaluation gives another, different classification. In this case guitar no. 2 proved itself to be the worst. It significantly differs on the 1 per cent level from guitars with the I (no. 3) and II (no. 4) ranks. In relations to the guitar with the III rank (no. 1), the difference is significant on the 5 per cent level. Thus, in this case three classes of instruments have been formed: first — including guitars no. 3 and 4, second — no. 1, third — no. 2. But it has to be remembered that guitars no. 1 and no. 4 do not differ significantly (Fig. 4).

As it can be seen from the above discussion, the general evaluation criterion classifies guitars in the same way as the criterion of carrying power, fullness and timbre dispersion (because the reverse classification of guitars no. 1 and 4 is not significant). The criterion of dynamics classifies them in a very similar way — only the change of ranks of guitars no. 1 and 2 is important, because the difference between these instruments is significant according to the general estimation. The classification in respect to the criterion of sound clearness is different, but it does not distinguish or disqualify any instrument, therefore it can be left out of account. Instead the different sequence of instruments obtained

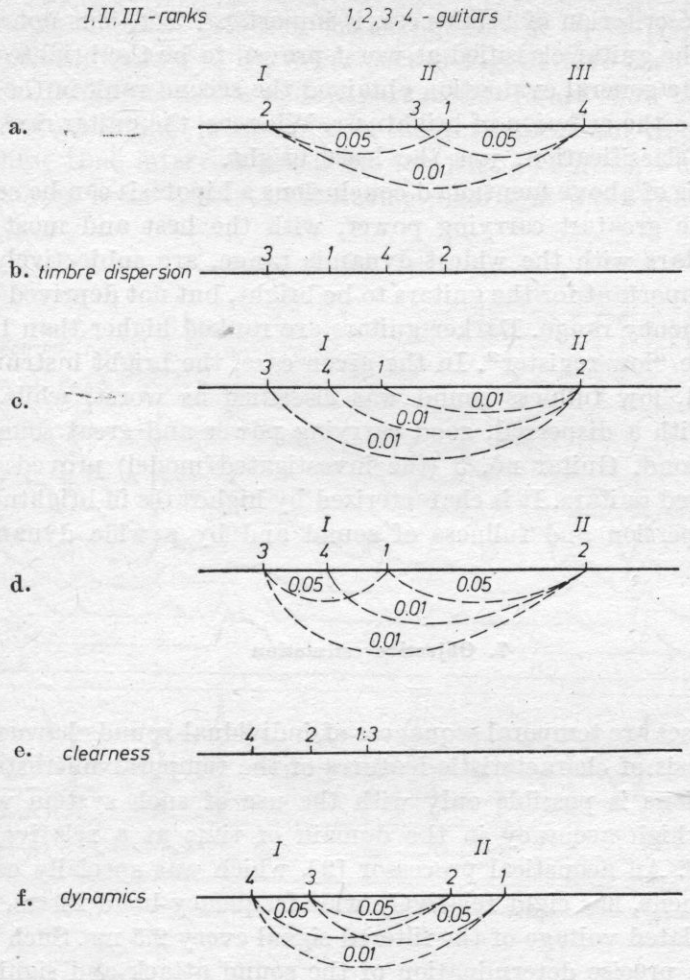

Fig. 3. Levels of significancy of differences between means for individual instruments — parametric estimation: a. brightness, b. timbre dispersion, and so on as in Fig. 2

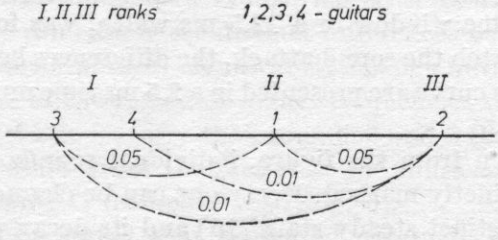

Fig. 4. Levels of significancy of differences between means for individual instruments — general estimation

according to the criterion of brightness, is important. Yet, it is not a reversed classification. The guitar classified as worst proved to be the brightest, but the best guitar in the general evaluation obtained the second rank in the classification in respect to the criterion of brightness. Whereas, the guitar ranked second in the general classification, was the least bright.

On the basis of above mentioned conclusions a hipotesis can be set up, that guitars with the greatest carrying power, with the best and most dispersed sound, and guitars with the widest dynamic range, are subjectively rated as the best. It is important for the guitars to be bright, but not deprived of fullness in the low frequency range. Darker guitars are ranked higher than bright guitars without the "low register". In the given case, the bright instrument with a non-dispersed, low fullness sound was classified as worst, while the least bright guitar with a dispersed, good carrying power and great sound fullness was ranked second. Guitar no. 3 (the investigated model) proved itself best among four tested guitars. It is characterized by high rates in brightness, carrying power, dispersion and fullness of sound and by a wide dynamic range.

7. Objective estimation

Music phrases are temporal sequences of individual sounds harmonic structures. An analysis of characteristic features of the temporal microstructure of observed functions is possible only with the use of such system which give a particularily high accuracy in the domain of time at a relatively narrow frequency band. An acoustical processor [2], which was specially constructed for this experiment, has eight relatively wide frequency band filters. It processes the demodulated voltage of the filtered signal every 2.5 ms. Such a high accuracy allows a precise determination of the sound attack and significant dynamic features of the arise and decay part of sound.

Fig. 5 presents exemplary results of an analysis of the first bars of a melody played in the high register (III part of the test) of the Marlin MC 315 instrument (no. 4). The short time spectrum (upper part of the figure) was obtained by putting together five, in this case, values of neighbouring points of the envelope curve. This way a time window of a 12.5 ms width, was formed. However, in order to accurately catch the sound attack, the differences between neighbouring values of the envelope curve are presented in a 2.5 ms time units (in the lower part of the figure).

As it can be seen from the figure, individual sounds of the phrase have been clearly and distinctly marked. Every one can be characterized by its onset time, more or less distinct steady state [16] and its decay phase. According to Fig. 5 these three "fragments" of a music sound should be clearly presented in the form of two-dimensional diagrams. The left part of Fig. 6 presents arise

phase diagrams. Maximal values of the changes of the envelope curve (i.e. level "peaks" appearing clearly in the lower part of Fig. 5) have been marked on the ordinate axis. Diagrams in the middle part of this figure show the steady state for the individual sounds in the form of maximal spectrum values. Thus, they represent these time intervals (from the top part of Fig. 4), which correspond to the maximum level value. A measuring algorithm was applied here, which

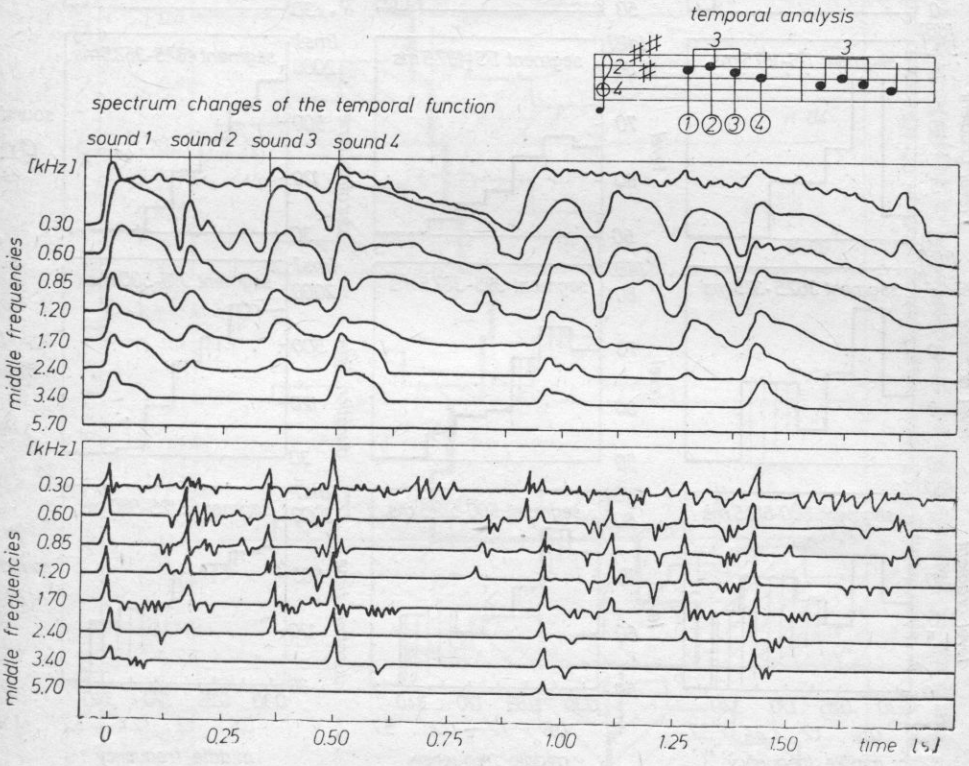

Fig. 5. Temporal analysis of melody from the high register of the Marlin MC 315 instrument

was developed during a psychoacoustic test concerning the subjective duration time of piano and guitar sounds [1]. Comparing with each other columns from diagrams in Fig. 6, we can clearly see distinct differences between them. Individual sounds of the music phrases significantly change in their timbre features. And thus, in this case in the region of higher frequencies sounds 1 and 4 show more distinct characteristic features than sounds 2 and 3 (lined areas in Fig. 6). Most probably this results from the fact that the musician wanted to accent these two sounds (1 and 4) (compare with Fig. 5).

Generally it can be stated that presented parameters of a chosen sound give an important ectosemantic information about music, i.e. such an information which can not be obtained directly from the score. In particular this

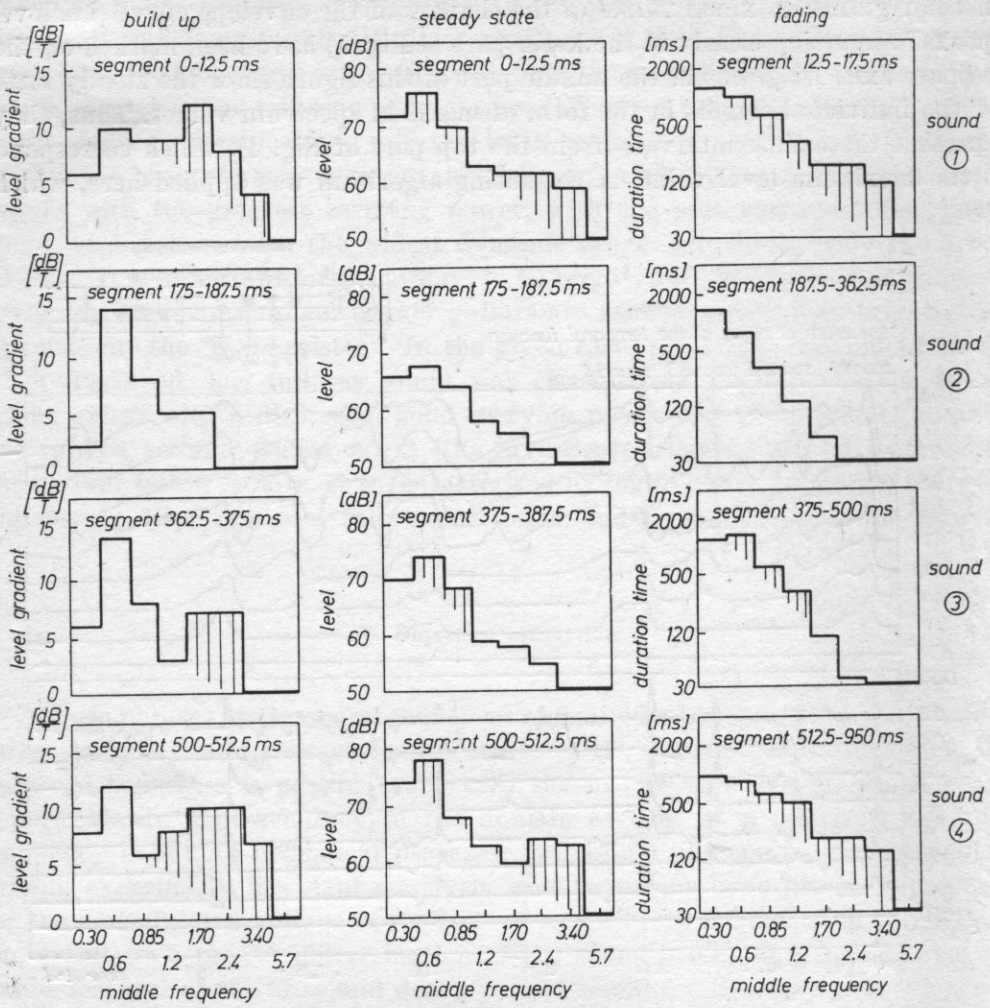

Fig. 6. Diagrams of characteristic parameters in different frequency regions for some time intervals in the melody from the high register of the Marlin MC 315 instrument (left: values of maximum differences of the frequency characteristic; middle: spectrum envelope over maximal values; right: characteristic parameters of signal decay obtained from perceptional estimation)

concernes the presentation of the emotional state of the performer and the problem of emphasis in music. The "inner states" of the musicians are converted through analogue coding into acoustical parameters of the sound. The emotion causes an increase of the size and power of adequate features. When the emotion passes these parameters weaken until they fade in the noise. The possibility of determining such slight changes of these parameters can be recognized as a significant criterion of the sound quality of music instruments. Beside the estimation of these sound features, based on computer calculations, also typical identifi-

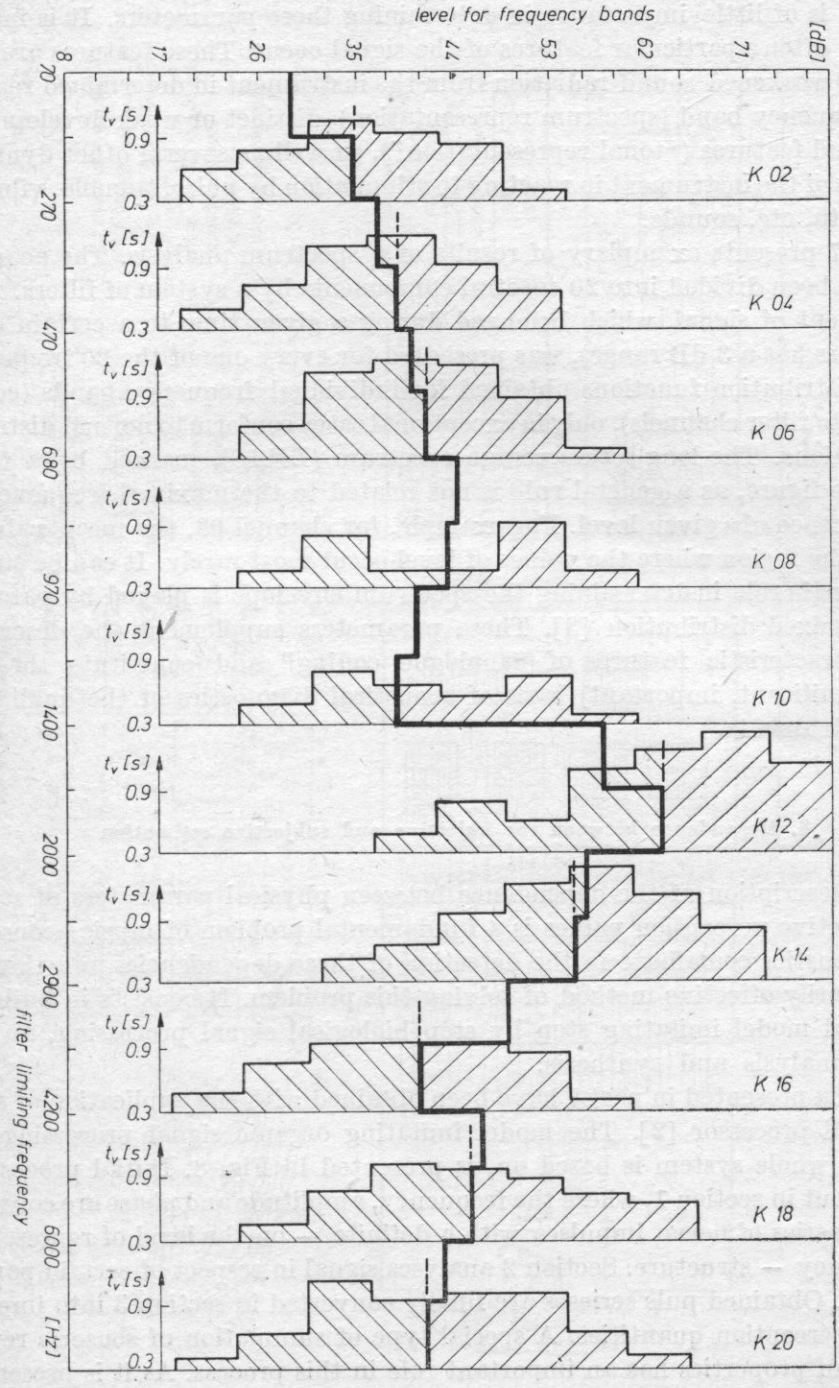

Fig. 7. Example of statistical representation of the spectrum. Thick line: long-time spectrum of the averaged data; individual histograms: frequency of occurrance of particular sound pressure levels in separate filter bands

cation — diagnostic parameters of instruments are significant. The sequence of sounds is of little importance in determining these parameters. It is important, how often a particular features of the signal occur. These features are amplified or weakened sound radiation from the instrument in determined regions of the frequency band (spectrum representation), distinct or weak development of the tonal features ("tonal representation"), as well as several other dynamic properties of the instrument in reacting to stimulation by pulse, tremolo, vibrato, portamento, etc. sounds.

Fig. 7 presents exemplary of results of a spectrum analysis. The acoustic signal has been divided into 20 spectral components by a system of filters. A 10 sec fragment of signal, which belonged during a given time to a certain class (every class has a 3 dB range), was presented for every one of the 20 frequency bands. Distribution functions obtained for individual frequency bands (corresponding to filter channels), only in exceptional cases conform to normal distribution functions. The long-term average spectrum (*LTAS*), marked by a thick line in the figure, as a general rule is not related to the maximal frequency of the occurrence of a given level. For example, for channel 08, the mean value is found in the region where the values of level occur most rarely. It can be stated that the main role in determining the spectrum envelope is played by parameters of a mixed distribution [3]. These parameters supplement the described above characteristic features of "analogue coding" and constitute the real (main, significant, important) basis of acoustical diagnostics of the quality of music instruments.

8. Dependence between the objective and subjective estimation

The description of the dependence between physical parameters of sound and subjective perception values is a fundamental problem of music acoustics. Psychoacoustics contribute in the detection of these dependencies and there is a particularily effective method of solving this problem. It consists in building a technical model imitating step by step biological signal processing, on the basis of analysis and synthesis.

Results presented in part 7 have been obtained with the application of such a technical processor [2]. The model imitating organic signal processing, on which the whole system is based on, is presented in Fig. 8. Initial processing is carried out in section 1, where the frequency, amplitude and phase are converted into a series of nerve impulses with a definite — on the level of representation accuracy — structure. Section 2 analyses signal in respect of certain partial properties. Obtained puls serieses are finally converted in section 3 into impression and perception quantities. A special type of summation of sensoric representation of properties has an important role in this process. As it is presented in the top part of Fig. 8, specific weight functions, which should determine the

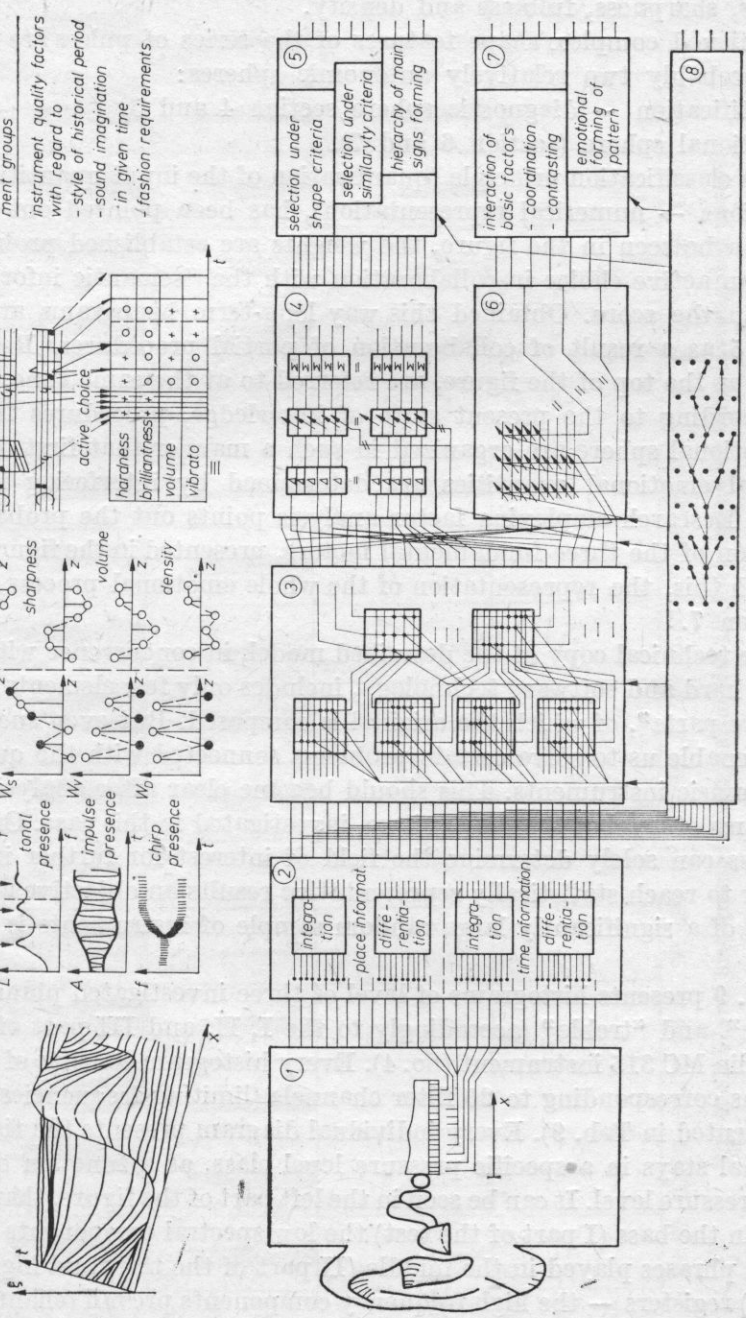

Fig. 8. Model of "organic" transformation of music with particular emphasis on emotional and identification — diagnosis spheres

various degree of dependence on the fundamental frequency of sound, can be determined for the most important spectral features of the macrostructure: loudness, sharpness, fullness and density.

Achieved complex shape features of the series of pulses are then processed in probably two relatively autonomic spheres:
— identification — diagnostic sphere section 4 and 5,
— emotional sphere (section 6 and 7).

The classification principle (quantization of the input quantities → sensoric impressions → numerical representation), has been pointed out in section 5. As it can be seen in the figure, the weights are established probably as a result of an active choice in collaboration with the "semantic information" contained in the score. Obtained this way long-term histograms are reduced in section 5 as a result of collaboration of partial procedures. Reference data, marked at the top of the figure, are referred to at the same time.

According to the present state of knowledge, procedures functioning in the emotional sphere are organized in such a manner that first of all the fundamental emotional quantities are determined by interfering in the limbic system. Research employing factor analysis points out the probability of collaboration of the three fundamental factors, presented in the figure. In connection with this, the representation of the whole emotional process is carried out in section 7.

The technical copy of the described model, in concurrence with the present state of hard and software technology, includes only few elements of the "lower structure parts", of which the original is composed. But even such elementary models enable us to solve certain problems connected with the quality evaluation of music instruments. This should become clear after analysing long-term histograms of level of the four guitars, investigated in this case. Of course these examples can solely determine the field of interest for further investigations. In order to reach statistically representative results an objective and subjective analysis of a significantly large random sample of instruments is to be carried out.

Fig. 9 presents histograms of level of three investigated phrases in "bass", "middle", and "treble" (accordingly to the I, II, and III part of the test) for the Marlin MC 315 instrument (no. 4). Every histogram consists of 20 individual diagrams corresponding to 20 filter channels (limiting frequencies of the filters are presented in Tab. 9). Every individual diagram presents the time (t_v), which the signal stays in a specific pressure level class, as a function of the general sound pressure level. It can be seen in the left part of the figure, that for a melody played in the bass (I part of the test) the low spectral components predominate, while in phrases played in the middle (II part of the test) and high (III part of the test) registers — the high frequency components prevail (channels 11–18 are "taken up" in a greater part).

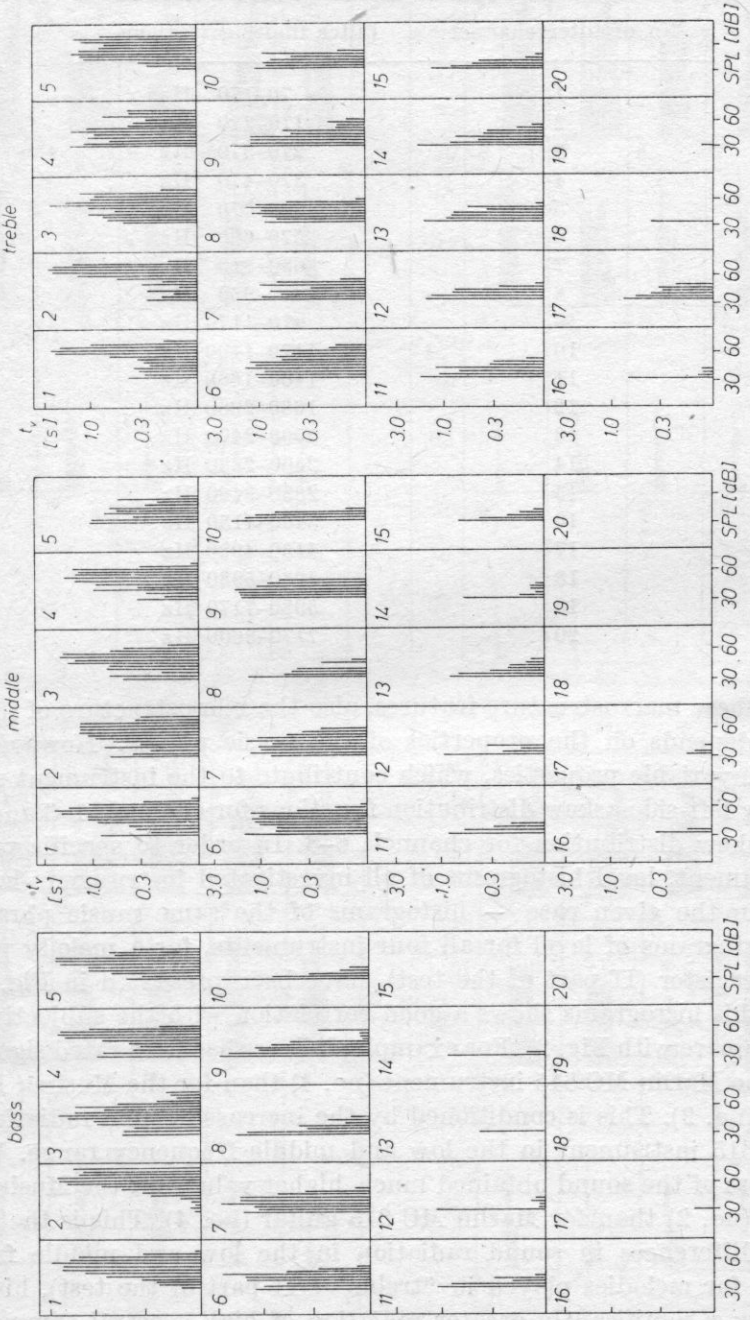

Fig. 9. *SPL* level histograms for the Marlin MC 315 instrument for three investigated phrases

Table 9. Limiting frequencies used in the computer

No of filter channel	Filter limiting frequency
1	70–170 Hz
2	170–270 Hz
3	270–370 Hz
4	370–470 Hz
5	470–570 Hz
6	570–680 Hz
7	680–810 Hz
8	810–970 Hz
9	970–1170 Hz
10	1170–1400 Hz
11	1400–1680 Hz
12	1680–2000 Hz
13	2000–2400 Hz
14	2400–2880 Hz
15	2880–3460 Hz
16	3460–4150 Hz
17	4150–4980 Hz
18	4980–5980 Hz
19	5980–7170 Hz
20	7170–8600 Hz

Beside these macrostructure features, also the microstructure of individual histograms depends on the properties of the music phrase. However, there are several invariable properties, which contribute to the instrument specifity, e.g. typically left-side askew distribution functions for channels 1–3 and a more right-side askew distribution for channels 6–8. In order to specific properties of the instrument, level histograms of all investigated instruments have been compared; in the given case — histograms of the same music phrases. For example, histograms of level for all four instruments, for a melody played in the middle register (II part of the test), have been presented in Fig. 10. The analysis of this histograms shows a good correlation with the subjective sound features (compare with Fig. 2). For example, fullness has been rated significantly higher for the Marlin MC 315 instrument (no. 4) than for the Musima Resonata instrument (no. 2). This is conditioned by the increased sound radiation of the Marlin MC 315 instrument in the low and middle frequency range. Whereas, the brightness of the sound obtained much higher values for the Musima Resonata guitar (no. 2) than for Marlin MC 315 guitar (no. 4). This is the result of mentioned differences in sound radiation in the low and middle frequency range. Also, for melodies played in "treble" (III part of the test), histograms of level show a significantly greater radiation of high spectral components in the 1.7 — 4 kHz range (not shown in the figure) in the case of the Musima Resonata instrument.

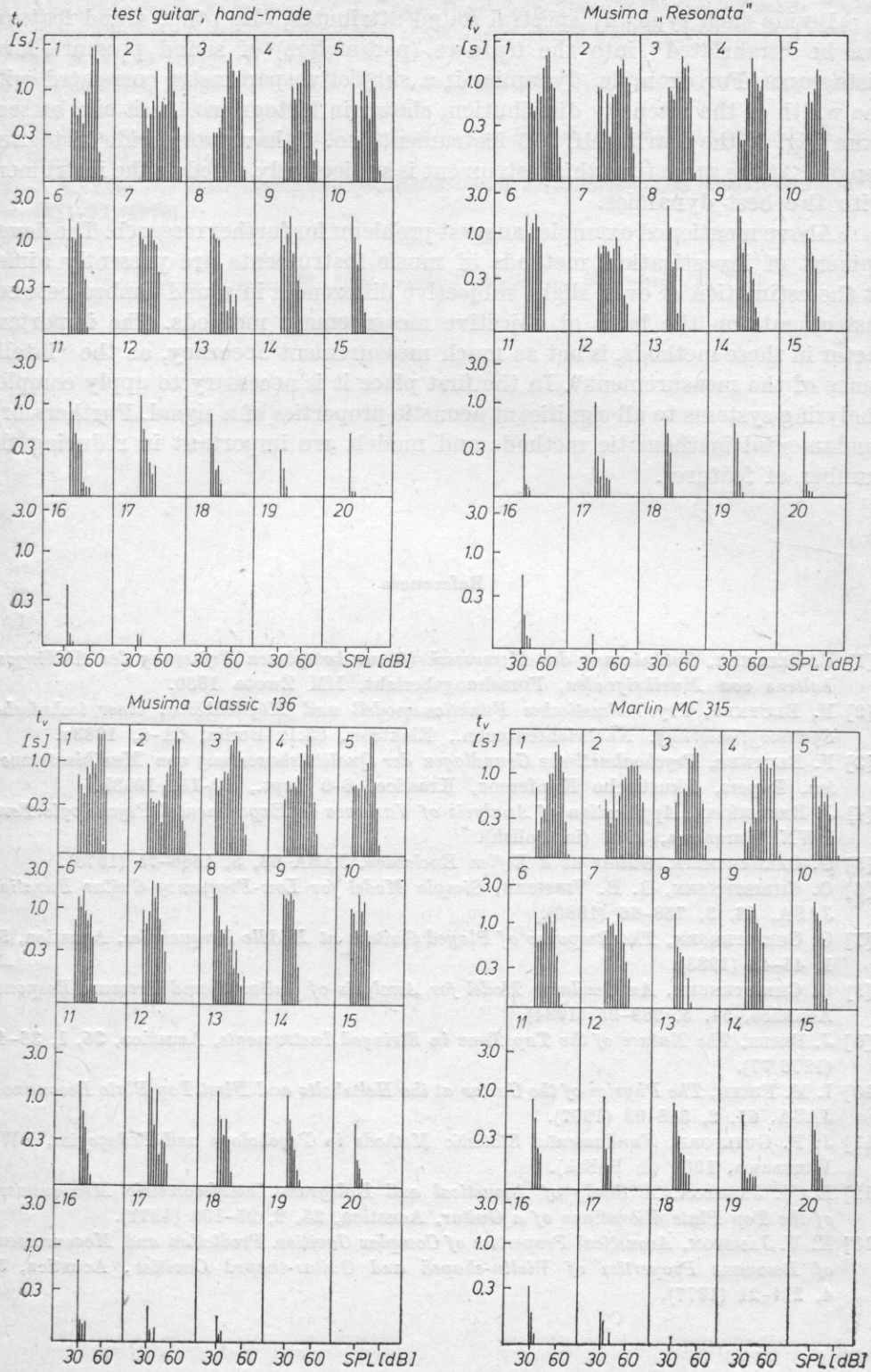

Fig. 10. ***SPL*** **level histograms for four investigated instruments for the melody performed in the middle register**

Beside such typically spectral sound attributes, also other sound features can be "translated" into the features (parameters) of sound pressure level histograms. For example, dynamics is a subjective parameter correlated with the width of the intensity distribution, shown in histograms. As it can be seen from Fig. 6, the Marlin MC 315 instrument (no. 4) have very wide histogram ranges. At the same time this instrument is subjectively rated as the instrument with the best dynamics.

Above mentioned examples suggest problems for further research. The development of investigation methods of music instruments are presently aimed at the estimation of even slight subjective differences in sound timbre between instruments on the basis of objective measurement methods. The important factor in these methods, is not as much measurement accuracy, as the "intelligence of the measurement". In the first place it is necessary to apply complex analysing systems to all significant acoustic properties of a signal. Furthermore, fundamental mathematic methods and models are important in reducing the number of features.

References

[1] F. Blutner, *Optimierung der Messvorschrift zur komplexen Erfassung des Abklingverhaltens von Musiksignalen*, Forschungsbericht, IfM Zwota 1980.

[2] F. Blutner, *Psychoakustisches Funktionsmodell und Möglichkeiten einer technischen Systemoptimierung*, Nachrichtentechn., Elektron. 33.1, Berlin, 21–6, 1983a.

[3] F. Blutner, *Psychoakustische Grundlagen der Qualitätsbewertung von Musikinstrumenten*, Papers, Akustische Konferenz, Kraslice, 6–9 Sept., 10–15, 1983b.

[4] J. Brzeziński, *Application of Analysis of Variance in Experimental Psychologic Tests*, PWN Warszawa, 1981 (in Polish).

[5] G. Caldersmith, *Guitar as a Reflex Enclosure*, JASA **63**, 5, 1566–75 (1978).

[6] O. Christensen, B. B. Vistisen, *Simple Model for Low-Frequency Guitar Function*, JASA, **68**, 3, 758–66 (1980).

[7] O. Christensen, *The Response of Played Guitars at Middle Frequencies*, Acustica, **53**, 1, 45–48 (1983).

[8] O. Christensen, *An Oscilator Model for Analysis of Guitar Sound Pressure Response*, Acustica, **54**, 5, 289–95 (1984).

[9] J. Firth, *The Nature of the Tap Tone in Stringed Instruments*, Acustica, **36**, 1, 36–41, (1976/77).

[10] I. M. Firth, *The Physics of the Guitar at the Helmholtz and First Top Plate Resonances*, JASA, **61**, 2, 588–93 (1977).

[11] J. P. Guilford, *Fundamental Statistic Methods in Psychology and Pedagogics*, PWN Warszawa, 1960 (in Polish).

[12] E. V. Jansson, *A Study of Acoustical and Hologram Interferometric Measurements of the Top Plate Vibrations of a Guitar*, Acustica, **25**, 2, 95–100 (1971).

[13] E. V. Jansson, *Acoustical Properties of Complex Cavities. Prediction and Measurements of Resonans Properties of Violin-shaped and Guitar-shaped Cavities*, Acustica, **37**, 4, 211–21 (1977).

[14] A. Jaroszewski, A. Rakowski, J. Żera, *Dependence Between the Onset Time in Classic Guitars and the Subjective Estimation of the Guitar Sound Quality*, Archiwum Akustyki, **13**, 2, 81–86 (1972) (in Polish).

[15] W. Krüger, *Erfahrungen bei der Bearbeitung von Gitarrendecken*, Das Musikinstrument, **10**, 1220–22 (1981).

[16] E. Lieber, *Systematische akustische Testung von Pianos. Paper IV*, Akustische Konferenz, Budapest 1967.

[17] J. Meyer, *Die Bestimmung von Qualitätskriterien bei Gitarren*, Das Musikinstrument **9**, 1211–22 (1976).

Received on October 26, 1984; revised version on February 17, 1986.

ARCHIVES OF ACOUSTICS
11, 3, 231 237 (1986)

PROPAGATION OF NOISE GENERATED BY A TRAM MOVING WITH UNIFORM MOTION

KRYSTYNA BEREZOWSKA-APOLINARSKA

Centre of the Investigation and Control of Environment
(61-812 Poznań, ul. Kantaka 4)

The registration of level changes of sound generated by a single source (e.g. a rail-vehicle – tram) allows the determination of the resultant level of noise emitted by sets of mobile sources (e.g. rail-vehicle lines). Research was aimed at the determination of the relationship between parameters a and L_{AX}, which characterize the noise of a single source, and the distance from the observation point, d. Investigations were conducted in a not built-over, flat and covered by grass area, for various types of trams and several speeds.

1. Introduction

A tram is one of the main sources of traffic noise. The noise it generates determines the acoustic climate of the human environment. Among others, the acoustic climate depends on the acoustic field generated by single sources, e.g. a rail-vehicle. If certain parameters of such a field are known, then the values of the evaluation indicators of noise emitted by sets of these sources (e.g. rail-vehicle lines) can be predicted. The equivalent sound level for averaging time T, L_{eqT}, was accepted as the best noise evaluation criterion for the external environment. It is used in international regulations concerning the acoustic climate. The high suitability of the equivalent level, L_{eqT}, in acoustic comfort classification is due to a high degree of correlation between its value and the subjective evaluation of noise oppressiveness (correlation coefficient 0.96–0.98 [4]).

In order to predict the numerical value of the equivalent level, L_{eqT}, the value of parameter a_i and the traffic volume N_i/T has to be known; where N_i is the number of vehicles of the i-type, which pass the observation point in time T (e.g. at night measurements were conducted from 10 P.M. to 6 A. M. — 8 hours). Parameter a_i is the measure of noise reaching the observation point

from a single vehicle of the i-type, e.g. tram 102 N. (In road traffic two types of vehicles are distinguished light: motorcars and delivery vans, $i = 1$, and heavy: trucks and buses, $i = 2$.)

The relation between a_i and the noise exposure level, L_{AXi}, is as follows [1]:

$$L_{AXi} = 10 \log(a_i/t_0) \tag{1}$$

where $t_0 = 1$ s.

Let us accept that there is a track-way at a distance d from the observation point O and that during the time T it is passed by N_1 trams of the 1-st type, N_2 trams of the 2-nd type, etc. Then, the equivalent level for time T is:

$$L_{eqT} = 10 \log \left\{ \sum_i (N_i/T) a_i + 10^{0.1\bar{L}_{eq}} \right\} \tag{2}$$

where $\bar{L}_{eq}$ is the equivalent sound level at the observation point when the tram traffic is held up; it is the so called acoustic background.

Values of parameter a_i can be determined from expression

$$a_i = \int_{-\infty}^{+\infty} 10^{0.1L_i(t)} dt \tag{3}$$

when the changes of frequency weighted sound level, according to the correlation curve A, $L_i(t)$, are known [2].

2. The method of determining parameter a

The value of a can be determined from the direct measurement of L_{AX} (Eq. (1)). If we do not have an adequate measuring device, then in order to determine the value of parameter a_i and the equivalent level, L_{eqT}, according to equation (2), the actual values of the sound level for the noise generated by a single source $L_i(t)$ (equation (3)) has to be known. $L_i(t)$ can not be measured at daytime, because of strong signals from other sources, which reach the observation point. These signals are weaker at night. Nevertheless the acoustic background $L^{(0)}(t)$ occurs in every case. Therefore, changes of the sound level registered for a single source are described by the following function:

$$L^{(i)}(t) = 10 \log \{10^{0.1L_i(t)} + 10^{0.1L^{(0)}(t)}\}. \tag{4}$$

If we accept that the acoustic background $L^{(0)}(t)$ is constant in time, $L^{(0)}(t) \cong L^{(0)}$, then for a measurement done during η seconds, we have (equations (3)

and (4)):

$$a_i = \Delta t \sum_{k=0}^{N} 10^{0.1L^{(i)}(t_k)} - \eta \; 10^{0.1L^{(0)}} \tag{5}$$

where $L^{(i)}(t_k)$ are actual values of the sound level at the observation point O, while $t_0 = 0$, $t_N = \eta$ (Fig. 1). 1 second is the unit of parameter a.

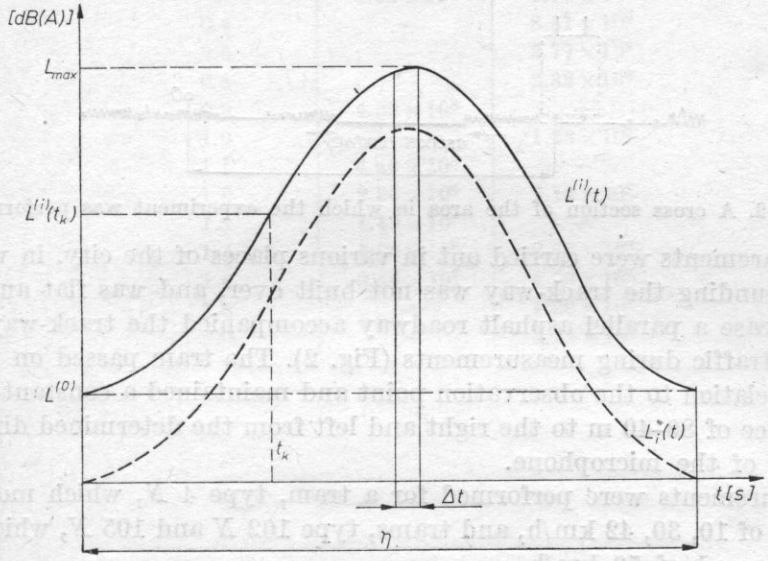

Fig. 1. Sound level $L^{(i)}(t)$ — superposition of noise generated by a single source $L_i(t)$ and the acoustic background $L^{(0)}$

3. Research method

Measurements were performed in order to determine the value of parameter a. They consisted in the registration at different distances from the track-way of changes of the sound level of trams passing with various speeds.

Measurements were carried out at night (12 P.M. — 3 A.M.), when the acoustic background was at the level of 30–45 dB(A). The value of the acoustic background was registered and included in calculations of parameter a. The weather was rainless and windless. The air temperature fluctuated from 10 to 15°C.

The apparatus produced by Bruel-Kjaer was used in the course of investigations. It consisted of: a 1′ microphone (type 4145), sound level meter (type 2209) and sound level recorder (type 2306). The apparatus was calibrated with a pistonphone (type 4220) before every measurement.

The microphone was placed 1.2 m above the ground level at various distances from the track-way, beginging at 1 m. The distance was measured from the outer rail head.

The following three types of trams have been investigated [3]:
— type 4 N — consists of 2 wagons, maximal speed — 42 km/h,
— type 102 N — jointed, developing higher speeds; has wheel shields (especially for middle wheels), resulting from the construction of the body,
— type 105 Na — has the greatest maximal speed, reaching 70 km/h (only one wagon was used in the course of measurements).

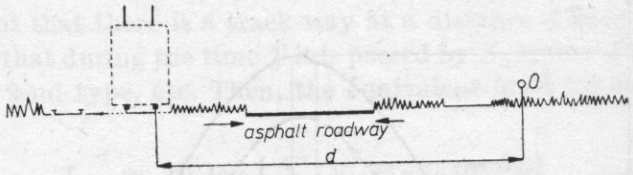

Fig. 2. A cross section of the area in which the experiment was performed

Measurements were carried out in various places of the city, in which the area surrounding the track-way was not built over, and was flat and grassy. In every case a parallel asphalt roadway accompanied the track-way. It was closed to traffic during measurements (Fig. 2). The tram passed on the track closer in relation to the observation point and maintained a constant speed on the distance of 80–40 m to the right and left from the determined direction of relocation of the microphone.

Measurements were performed for a tram, type 4 N, which moved with the speed of 10, 30, 42 km/h, and trams, type 102 N and 105 N, which moved with the speed of 50 km/h.

4. Research results

Measurements of the changes of the sound level $L^{(i)}(t)$ and calculations, done according to Eq. (5), have resulted in the determination of parameters, α and L_{AX}, at various distances from the source of noise and at various speeds.

Table 1. Mean values of parameter α [s] at various distances of the observation point from the tram (type 4 N moving with constant speed V)

d[m]	V[m/s]		
	2.(7)	8.(3)	11.(6)
1.0	1.68×10^8	2.34×10^9	5.56×10^9
8.0	1.25×10^7	4.38×10^8	9.04×10^8
10.0	—	2.44×10^8	2.87×10^8
12.6	3.91×10^6	—	—
15.8	1.66×10^7	7.77×10^7	1.33×10^8
20.0	1.36×10^6	3.64×10^7	8.92×10^7
25.0	5.22×10^6	3.29×10^7	6.94×10^7
40.0	2.66×10^6	1.24×10^7	1.30×10^7
63.0	8.33×10^5	5.70×10^6	7.65×10^6

Table 2. Mean values of parameter a [s] at various distances of the observation point from the trams (type 102 N and 105 Na) moving with a constant speed of 50 km/h (13.(8) m/s)

log$d$	Type of tram	
	102 N	105 Na
0	1.03×10^9	1.14×10^{10}
0.4	—	8.51×10^9
0.6	—	3.77×10^9
0.8	—	2.32×10^9
0.9	4.59×10^8	—
1.0	—	1.28×10^9
1.1	4.46×10^8	—
1.2	2.94×10^8	7.12×10^8
1.3	1.49×10^8	—
1.4	1.36×10^8	2.56×10^8
1.6	3.44×10^7	4.56×10^7
1.8	—	1.28×10^7
2.0	—	3.22×10^6

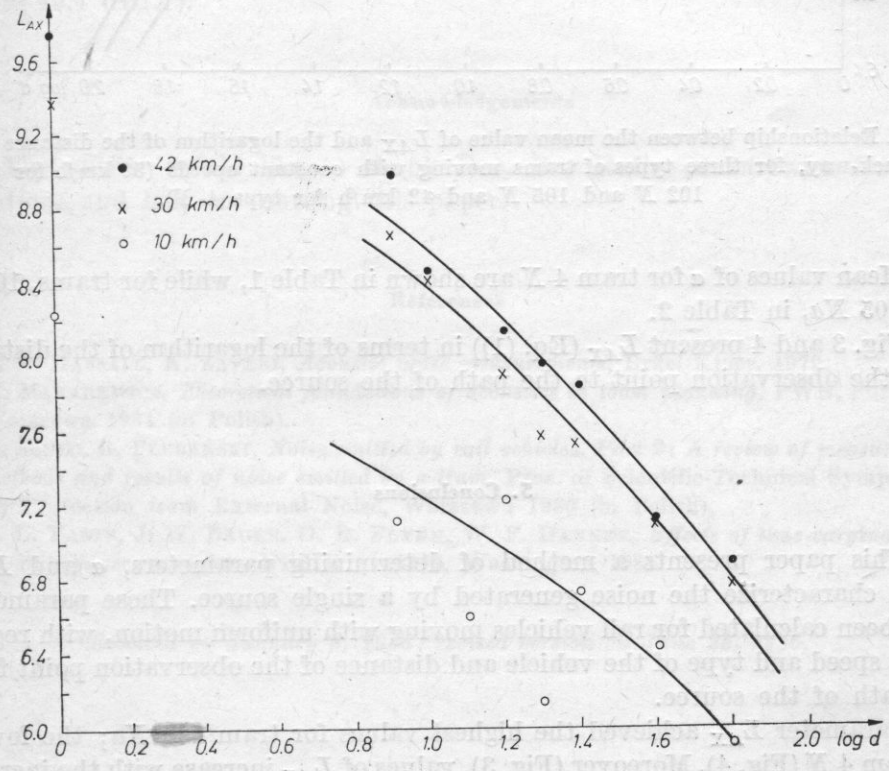

Fig. 3. Relationship between the mean value of L_{AX} and the logarithm of the distance from the track-way, for tram 4 N moving with uniform motion with the speed of 10, 30, 42 km/h

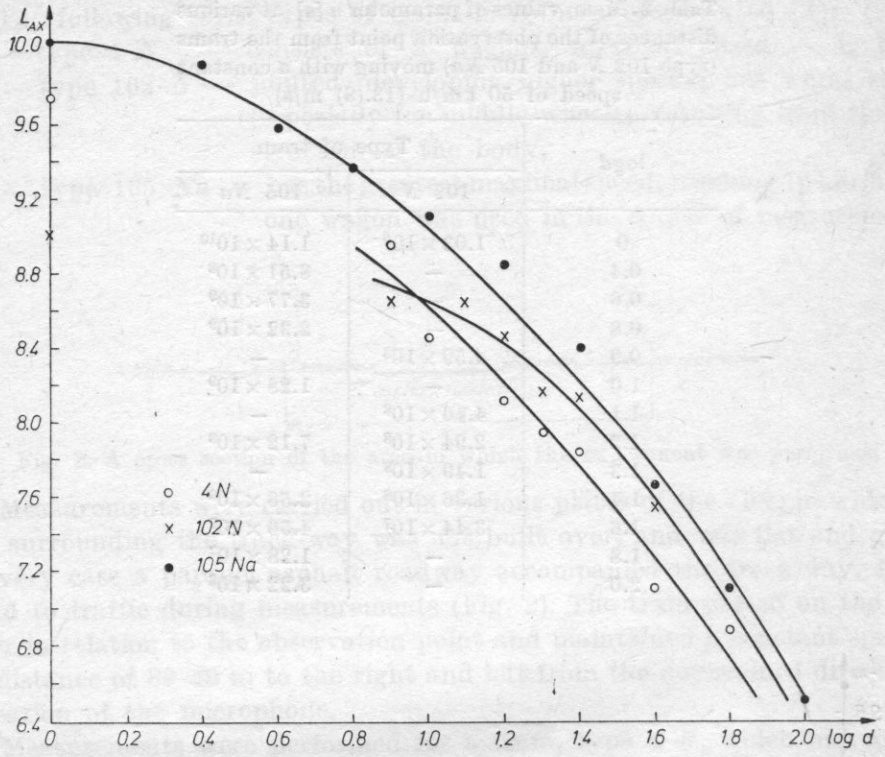

Fig. 4. Relationship between the mean value of L_{AX} and the logarithm of the distance from the track-way, for three types of trams moving with constant speeds (50 km/h for types 102 N and 105 N and 42 km/h for type 4 N).

Mean values of a for tram 4 N are shown in Table 1, while for trams, 102 N and 105 Na, in Table 2.

Fig. 3 and 4 present L_{AX} (Eq. (1)) in terms of the logarithm of the distance from the observation point to the path of the source.

5. Conclusions

This paper presents a method of determining parameters, a and L_{AX}, which characterize the noise generated by a single source. These parameters have been calculated for rail vehicles moving with uniform motion, with regard to the speed and type of the vehicle and distance of the observation point from the path of the source.

Parameter L_{AX} achieved the highest values for tram 105 Na; the lowest for tram 4 N (Fig. 4). Moreover (Fig. 3), values of L_{AX} increase with the increase of speed (type 4 N).

Hence, it results that trams 105 Na are the loudest. Trams 102 N are slightly less loud and trams 4 N are the least disturbing to the environment. Similar results have been obtained in paper [3].

The relationship between parameter L_{AX} and the logarithm of the distance (Fig. 4) for tram 102 N differs from such relationships for other types of trams. This is due to the construction of the body of the tram-shields placed especially on the middle wheels, cause that part of the energy does not reach the observation point, i.e. the microphone placed at a distance of about 10 m and 1.2 m above ground level.

Derived values of parameter a can be applied in calculations of the equivalent level L_{eqT} in town planning, but only at distances not exceeding 90 m. For example, at a distance of $d = 25$ m ($\log 25 = 1.4$) we have from Table 2 for tram 105 Na that $a = 2.49\ 10^8$. If during $T = 8$ hours $= 28800$ s (at night) $N = 10$ trams pass, then from Eq. (2) we have:

$$L_{eqT} = 10 \log\left\{\frac{N}{28800}\, a + 10^{0.1\bar{L}_{eq}}\right\}.$$

If we accept the background sound level at $\bar{L}_{eq} = 30$ dB(A), then the equivalent sound level during 8 hours of the night, from 10 P.M. to 6 A.M., will be $L_{eqT} = 49.4$ dB(A).

Acknowledgements

The author would like to thank Doc. Dr. Rufin Makarewicz for consultations and help in drafting this paper.

References

[1] J. R. Hassall, K. Zaveri, *Acoustic noise measurements*, Brüel-Kjaer, 1979.

[2] R. Makarewicz, *Theoretical foundations of acoustics in town planning*, PWN, Poznań – Warszawa 1984 (in Polish).

[3] B. Szulc, B. Plebański, *Noise emitted by rail vehicles. Part 2: A review of measurement methods and results of noise emitted by a tram*, Proc. of Scientific-Technical Symposium on Protection from External Noise, Warszawa 1980 (in Polish).

[4] S. L. Yaniv, J. W. Bauer, D. R. Flynn, W. F. Danner, *Effects of time-varying noise on annoyance: a review*, NBSIR 81–2377, Washington 1981.

Received on January 8, 1986; revised version on June 25, 1986.

ARCHIVES OF ACOUSTICS
11, 3, 239-251 (1986)

MUTUAL IMPEDANCE OF AXIALLY-SYMMETRIC MODES OF A CIRCULAR PLATE

WITOLD RDZANEK

Department of Physics, Higher Pedagogical School
(35–310 Rzeszów, ul. Rejtana 16)

This paper presents an exact calculation of the mutual radiation impedance of axially-symmetric modes of a fixed at the edge circular plate. Linear and harmonic processes in respect to time have been considered and it has been accepted that the plate radiates acoustic waves into a lossless gas medium. Included here expressions for the mutual impedance in the form of single integrals have been adopted on the basis of several simplifying assumptions to numerical calculations for low and high frequencies of radiated waves. Achieved results are used in the analysis of the impedance and sound power radiated by a circular plate excited to vibrate by a known (from the assumption) superficial distribution of the exciting force.

Notations

a — plate radius
B — flexural rigidity
b_n — constant quantity for n-mode (10)
c — propagation velocity of a wave in a gas medium
f_n — frequency of free vibrations for mode $(0, n)$ (4)
h — plate thickness
$H_m^{(1)}(x)$ — first type, m-order Hankel function
$H_m^{(2)}(x)$ — second type, m-order Hankel function
$I_m(x)$ — first type, m-order modified Bessel function
$J_m(x)$ — m-order Bessel function
k_0 — wave number
$K_m(x)$ — m-order cylindrical MacDonald function
$N_m(x)$ — m-order Neumann function
N_{ns} — mutual power of modes, $(0, n)$ and $(0, s)$, of the circular plate (6)
p_{ns} — acoustic pressure produced by the vibrating plate through mode $(0, n)$ and exerted on the same plate through mode $(0, s)$
r — radial variable of point on the surface of the plate, in polar coordinates
$S_m(x)$ — m-order Struve function

t — time
v_n — vibration velocity of points on the surface of the plate for mode $(0, n)$ (2)
Z_{ns} — mechanical impedance of modes, $(0, n)$ and $(0, s)$ of the circular plate (3)
γ_n — n-root of the characteristic equation (3)
δ_{nm} — Kronecker delta
ζ_{ns} — normalized mutual impedance (12)
θ_{ns} — normalized mutual resistance (13)
λ — length of an acoustic wave in a gas medium
ξ — transverse dislocation of points on the surface of the plate
ϱ — density of the material of the plate
ϱ_0 — rest density of the gas medium
σ — area of the plate
χ_{ns} — normalized mutual reactance (14)
ω_n — angular frequency of free vibrations, corresponding to mode $(0, n)$

1. Introduction

Only few published papers in the field of the generation of acoustic waves by superficial sources are concerned with the problem of acoustic mutual interactions of plates or circular membranes. The carried out analysis was done for a system of two plates or circular membranes for a case of axially-symmetric free vibrations.

Besides theoretical work on acoustic mutual interactions between two sources, research is also performed on acoustic interactions of two different vibration modes of only one source. Results of the analysis of a circular membrane are presented in papers [6] and [7].

Hitherto the problem for a circular plate has not been solved.

This paper undertakes the problem of acoustic interactions by calculating the mutual impedance of two different axially-symmetric, $(0, n)$ and $(0, s)$, vibration modes of a circular plate fixed at the edge, which radiates acoustic waves into a lossless gas medium. Linear and harmonic in time processes have been examined.

Obtained expressions for mutual impedance can be a basis for further investigations of the radiation impedance of a circular plate with a determined superficial distribution of the force exciting vibrations.

2. Superficial distribution of the vibration velocity

The motion equation for free axially-symmetric vibrations of a circular plate, made from a homogeneous material of density ϱ, and of small in respect to the diameter $2a$ thickness h, is as follows [2]:

$$B\left[\frac{1}{r}\frac{\partial}{\partial r}\left(r\frac{\partial}{\partial r}\right)\right]^2 \xi(r,t)+\varrho h\frac{\partial^2\xi(r,t)}{\partial t^2}=0 \tag{1}$$

where ξ is the transverse dislocation of points on the surface of the plate, B — flexural rigidity of the plate.

Solving this equation for effects which are sinusoidal in time, in the case of a plate fixed at the edge leads to a formula for the vibration velocity [2]

$$v_n(r) = v_{0n}\left\{J_0\left(\frac{r}{a}\gamma_n\right) - \frac{J_0(\gamma_n)}{I_0(\gamma_n)} I_0\left(\frac{r}{a}\gamma_n\right)\right\}. \tag{2}$$

In paper [2], v_{0n} denotes the maximal value of the vibration velocity of the central point of the plate for mode $(0, n)$. Occurring here special function $I_0(x)$ is a zero order modified Bessel function of the first type, which can be expressed by a Bessel function $J_0(ix)$ of an imaginary argument, i.e. $I_m(x) = i^{-m}J_m(ix)$ for $m = 0, 1, 2, \ldots$

From the frequency equation (2)

$$I_0(\gamma_n)J_1(\gamma_n) + I_1(\gamma_n)J_0(\gamma_n) = 0 \tag{3}$$

we obtain an infinite number of values $k = k_n (ka = \gamma_n)$, which determine frequencies of free vibrations

$$f_n = \frac{1}{2\pi a^2}\gamma_n^2 \sqrt{\frac{B}{\varrho n}} \tag{4}$$

while for $n = 1, 2, 3$ we have (e.g. [3]): $\gamma_1 = 3.195 \ldots$; $\gamma_2 = 6.306 \ldots$; $\gamma_3 = 9.439 \ldots$ If n is sufficiently large, then according to relationship [3] $\gamma_n \simeq n\pi$, instead of $ka = \frac{2\pi}{\lambda}a = \gamma_n$ we have $n\lambda = 2a$.

3. Integral expression for mutual impedance

The mechanical mutual impedance between axially-symmetric free vibration modes, $(0, n)$ and $(0, s)$, of a circular plate placed in a rigid and flat acoustic baffle is calculated on the basis of the definition (compare [7])

$$Z_{ns} = \frac{1}{2\sqrt{\langle|v_n|^2\rangle\langle|v_s|^2\rangle}} \int_\sigma p_{ns}v_s d\sigma \tag{5}$$

where p_{ns} is the acoustic pressure produced by the vibrating plate through mode $(0, n)$ and exerted on the same plate through vibration mode $(0, s)$,

$$N_{ns} = \frac{1}{2}\int_\sigma p_{ns}v_s d\sigma \tag{6}$$

is the mutual power of modes, $(0, n)$ and $(0, s)$, of the circular plate, while

$$\langle |v_n|^2 \rangle = \frac{1}{2\sigma} \int_{\sigma} v_n^2(r)\, d\sigma \tag{6a}$$

is the mean of the square of velocity of the vibration mode $(0, n)$.

On the basis of paper [4] the mutual impedance (5) can be expressed by the following formula

$$Z_{ns} = \frac{\pi \varrho_0 c k_0^2}{\sqrt{\langle |v_n|^2 \rangle \langle |v_s|^2 \rangle}} \int_0^{\pi/2+i\infty} M_n(\vartheta) M_s(\vartheta) \sin\vartheta\, d\vartheta \tag{7}$$

where

$$M_n(\vartheta) = v_{0n} \int_0^a \left\{ J_0\left(\frac{r}{a}\gamma_n\right) - \frac{J_0(\vartheta_n)}{I_0(\gamma_n)} I_0\left(\frac{r}{a}\gamma_n\right) \right\} J_0(k_0 r \sin\vartheta) r\, dr \tag{8}$$

c_0 — propagation velocity of a wave in a gas medium of a rest density of ϱ_0, $k_0 = 2\pi/\lambda$ — wave number, λ — acoustic wave length in a gas medium. Applying the integral formula (A3) and the frequency equation (3), we achieve

$$M_n(\vartheta) = 2\, v_{0n} \frac{a^2}{\gamma_n} \frac{J_0(\gamma_n)}{1 - \left(\frac{k_0 a}{\gamma_n}\right)^4 \sin^4\vartheta} \left\{ b_n J_0(k_0 a \sin\vartheta) - \right.$$

$$\left. - \frac{k_0 a}{\gamma_n} \sin\vartheta J_1(k_0 a \sin\vartheta) \right\}, \tag{9}$$

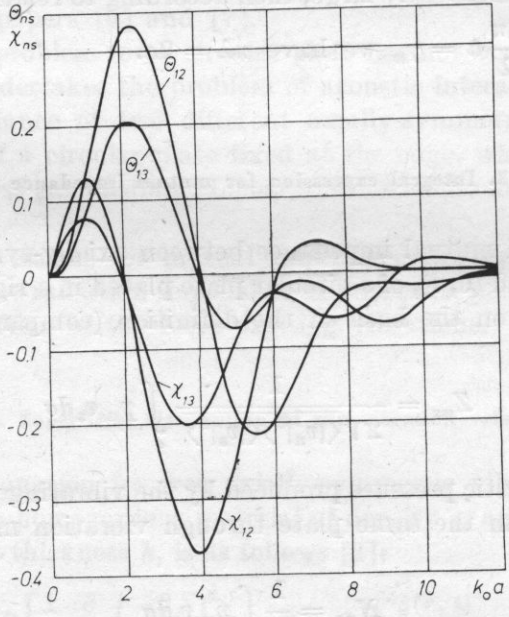

Fig. 1. Normalized mutual impedance of two, $(0, n)$ and $(0, s)$, axially-symmetric vibrations modes of a circular plate in terms of parameter $k_0 a$

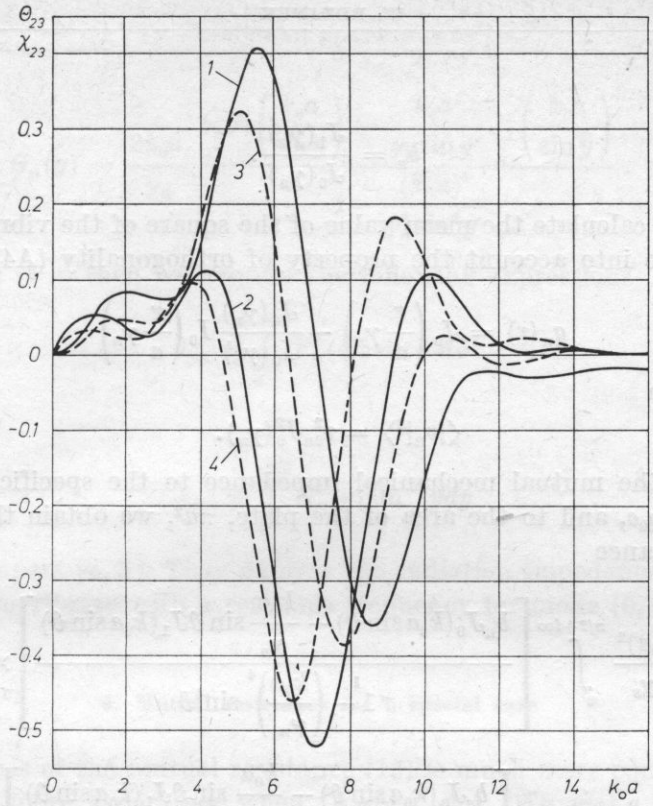

Fig. 2. Normalized mutual impedance of two, (0, 2) and (0, 3), axially-symmetric vibration modes of a circular plate in terms of parameter k_0a: *1* — plate resistance, *2* — plate reactance, *3* — membrane resistance [6], *4* — membrane reactance [6]

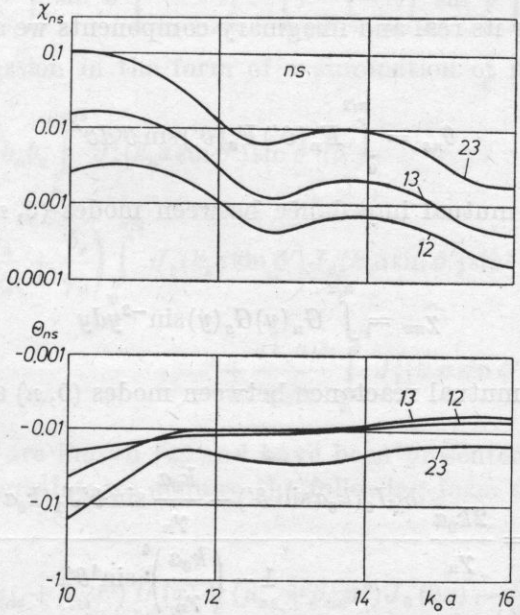

Fig. 3. Normalized mutual impedance of two, (0, *n*) and (0, *s*), axially-symmetric vibration modes of a circular plate in terms of parameter k_0a

where

$$b_n = \frac{J_1(\gamma_n)}{J_0(\gamma_n)}. \tag{10}$$

In order to calculate the mean value of the square of the vibration velocity $\langle |v_n|^2 \rangle$ we take into account the property of orthogonality (A4) for function

$$q_n(r) = J_0\left(\frac{r}{a}\gamma_n\right) - \frac{J_0(\gamma_n)}{I_0(\gamma_n)} I_0\left(\frac{r}{a}\gamma_n\right)$$

and we obtain

$$\langle |v_n|^2 \rangle = v_{0n}^2 J_0^2(\gamma_n). \tag{11}$$

Relating the mutual mechanical impedance to the specific resistance of the medium, $\varrho_0 c$, and to the area of the plate, πa^2, we obtain the normalized mutual impedance

$$\zeta_{ns} = \frac{(2k_0a)^2}{\gamma_n\gamma_s} \int_0^{\pi/2+i\infty} \left[\frac{b_n J_0(k_0a\sin\vartheta) - \frac{k_0a}{\gamma_n}\sin\vartheta J_1(k_0a\sin\vartheta)}{1-\left(\frac{k_0a}{\gamma_n}\right)^4\sin^4\vartheta} \right] \times$$

$$\times \left[\frac{b_s J_0(k_0a\sin\vartheta) - \frac{k_0a}{\gamma_s}\sin\vartheta J_1(k_0a\sin\vartheta)}{1-\left(\frac{k_0a}{\gamma_s}\right)^4\sin^4\vartheta} \right] \sin\vartheta d\vartheta \tag{12}$$

and after separating its real and imaginary components we attain the following expressions

$$\theta_{ns} = \int_0^{\pi/2} F_n(\vartheta') F_s(\vartheta') \sin\vartheta' d\vartheta' \tag{13}$$

for the normalized mutual impedance between modes $(0, n)$ and $(0, s)$ of the circular plate, and

$$\chi_{ns} = \int_0^{\pi/2} G_n(y) G_s(y) \sin^{-2} y dy \tag{14}$$

for the normalized mutual reactance between modes $(0, n)$ and $(0, s)$ of the circular plate, where

$$F_n(\vartheta') = \frac{2k_0a}{\gamma_n} \frac{b_n J_0(k_0a\sin\vartheta') - \frac{k_0a}{\gamma_n}\sin\vartheta' J_1(k_0a\sin\vartheta')}{1-\left(\frac{k_0a}{\gamma_n}\right)^4\sin^4\vartheta'}, \tag{15}$$

$$G_n(y) = \frac{2k_0a}{\gamma_n} \frac{b_n J_0\left(\frac{k_0a}{\sin y}\right) - \frac{k_0a}{\gamma_n \sin y} J_1\left(\frac{k_0a}{\sin y}\right)}{1 - \frac{(k_0a)^4}{\gamma_n^4 \sin^4 y}}. \tag{16}$$

If we accept $s = n$, then we acquire the following expressions

$$\theta_{nn} = \int_0^{\pi/2} F_n^2(\vartheta') \sin \vartheta' d\vartheta' \tag{17}$$

and

$$\chi_{nn} = \int_0^{\pi/2} G_n^2(y) \sin^{-2} y dy \tag{18}$$

known from papers [4, 5]. They express the radiation impedance of a circular plate excited to vibrate with a resonans frequency for mode $(0, n)$.

4. Mutual resistance for a special case

The analysis of the mutual resistance (13) is much more convenient when $k_0a/\gamma_n < 1$, or more accurately when $(k_0a/\gamma_n)^4 \ll 1$. We make the following simplifications in formula (13)

$$\left[1 - \left(\frac{k_0a}{\gamma_n}\right)^4 \sin^4 \vartheta'\right]^{-1} \simeq 1, \quad \left[1 - \left(\frac{k_0a}{\gamma_s}\right)^4 \sin^4 \vartheta'\right]^{-1} \simeq 1 \tag{19}$$

and reach an expression in the form of a summation of integrals

$$\Theta_{ns} \simeq \frac{(2k_0a)^2}{\gamma_n\gamma_s} \left\{ b_n b_s \int_0^{\pi/2} J_0^2(k_0a \sin \vartheta') \sin \vartheta' d\vartheta' - \right.$$

$$- k_0a \left(\frac{b_n}{\gamma_s} + \frac{b_s}{\gamma_n}\right) \int_0^{\pi/2} J_1(k_0a \sin \vartheta') J_0(k_0a \sin \vartheta') \sin^2 \vartheta' d\vartheta' +$$

$$\left. + \frac{(k_0a)^2}{\gamma_n\gamma_s} \int_0^{\pi/2} J_1^2(k_0a \sin \vartheta') \sin^3 \vartheta' d\vartheta' \right\}. \tag{20}$$

These integrals are known [4] and have been presented in formulae (A5), (A6) and (A7). Integrating we acquire the following form of the mutual resistance (20)

$$\theta_{ns} \simeq (2x)^2 \left[(a_{ns} + \beta_{ns}x^2) U(x) + (\mu_{ns} + \beta_{ns}x^2) J_0(2x) - \frac{3}{2} \beta_{ns} x J_1(2x) \right] \tag{21}$$

where: $x = k_0 a$, $U(x) = \frac{\pi}{2}[J_1(2x)S_0(2x) - J_0(2x)S_1(2x)]$, $S_m(x)$ is the m-order Struve function,

$$a_{ns} = \frac{1}{\gamma_n \gamma_s}\left[b_n b_s + \frac{1}{2\gamma_n \gamma_s}\left(\frac{3}{4} - b_n\gamma_n - b_s\gamma_s\right)\right], \tag{22}$$

$$\beta_{ns} = \frac{1}{2\gamma_n^2 \gamma_s^2}, \tag{23}$$

$$\mu_{ns} = \frac{b_n b_s}{\gamma_n \gamma_s}. \tag{24}$$

If moreover $x = k_0 a \ll 1$, then we can apply approximate formulae, (A9) and (A11), and thus

$$\theta_{ns} \simeq (2x)^2 \frac{b_n b_s}{\gamma_n \gamma_s}\left[1 - \frac{1}{3}\left(1 + \frac{1}{\gamma_s b_s} + \frac{1}{\gamma_n b_n}\right)x^2\right] \tag{25}$$

whereas for $n = s$

$$\theta_{nn} = (2x)^2 \left(\frac{b_n}{\gamma_n}\right)^2 \left[1 - \frac{1}{3}\left(1 + \frac{2}{\gamma_n b_n}\right)x^2\right]. \tag{26}$$

We will also analyse the mutual reistance when $k_0 a > \gamma_n, \gamma_s$, or more accurately when $(k_0 a)^4 \gg \gamma_n^4, \gamma_s^4$.

We perform a change of variables in formulae (13) and (15)

$$\theta_{ns} = 4(\gamma_n \gamma_s)^3 \int_0^{k_0 a} \frac{\left[b_n J_0(t) - \frac{t}{\gamma_n} J_1(t)\right]\left[b_s J_0(t) - \frac{t}{\gamma_s} J_1(t)\right]}{(\gamma_n^4 - t^4)(\gamma_s^4 - t^4)} \frac{t\,dt}{\sqrt{1 - \left(\frac{t}{k_0 a}\right)^2}}. \tag{27}$$

We use the approximate formula

$$\left[1 - \left(\frac{t}{k_0 a}\right)^2\right]^{-1/2} \simeq 1 + \frac{1}{2}\left(\frac{t}{k_0 a}\right)^2 + \frac{3}{8}\left(\frac{t}{k_0 a}\right)^4 + \ldots \tag{28}$$

and this results in the expression

$$\theta_{ns} \simeq \int_0^x A_n(t) A_s(t)\left[1 + \frac{1}{2}\left(\frac{t}{x}\right)^2 + \frac{3}{8}\left(\frac{t}{x}\right)^4\right] t\,dt \tag{29}$$

where

$$A_n(t) = 2\,\gamma_n^3 \frac{b_n J_0(t) - \dfrac{t}{\gamma_n} J_1(t)}{\gamma_n^4 - t^4}. \tag{30}$$

Three terms of the series (28) have been taken into account in order to ensure the convergence of integral (29) for very large values of $x = k_0 a$. If $t = \gamma_n$, then function $A_n(t)$ is an indeterminate symbol, which has the following limit

$$\lim_{t\to\gamma_n} A_n(t) = 2\gamma_n^3 \lim_{t\to\gamma_n} \frac{b_n J_0(t) - \dfrac{t}{\gamma_n} J_1(t)}{\gamma_n^4 - t^4} = \frac{1}{2} \frac{J_1^2(\gamma_n) + J_0^2(\gamma_n)}{J_0(\gamma_n)}. \tag{31}$$

Integral (29) within limits $(0, x)$ is presented in the form of a difference of integrals, i.e.

$$\int_0^x = \int_0^\infty - \int_x^\infty \tag{32}$$

The integral within limites $(0, \infty)$ is calculated from formula (A14), while the value of the integral within limits (x, ∞) can be neglected, because it is a small quantity in comparison to the value of the integral within limits $(0, \infty)$. Moreover if we take into account the characteristic equation (3) and Wronskians, (A1) and (A2), then finally we obtain

$$\theta_{ns} \simeq b_{ns} x^{-2}, \tag{33}$$

where $x = k_0 a > \gamma_n, \gamma_s$,

$$b_{ns} = 2 \frac{(\gamma_n \gamma_s)^2}{\gamma_n^4 - \gamma_s^4} \left[\gamma_n \frac{J_1(\gamma_n)}{J_0(\gamma_n)} - \gamma_s \frac{J_1(\gamma_s)}{J_0(\gamma_s)} \right] \tag{34}$$

for $n \neq s$. In order to achieve higher accuracy of calculations, the integral within limits (x, ∞) has to subtracted in expression (33). The approximate value

Table 1. Coefficients h_{ns}, α_{ns}, β_{ns}, and μ_{ns}

n, s	1, 2	1, 3	2, 3
h_{ns}	-1.7275	-1.459	-3.504
α_{ns}	$4.904 \cdot 10^{-2}$	$3.278 \cdot 10^{-2}$	$1.678 \cdot 10^{-2}$
β_{ns}	$1.232 \cdot 10^{-3}$	$5.499 \cdot 10^{-4}$	$1.412 \cdot 10^{-4}$
μ_{ns}	$3.773 \cdot 10^{-2}$	$2.599 \cdot 10^{-2}$	$1.459 \cdot 10^{-2}$

of the integral for $(k_0 a)^4 = x^4 \gg \gamma_n^4, \gamma_s^4$ is

$$\int_x^\infty \simeq \frac{33}{10} \frac{(\gamma_n \gamma_s)^2}{\pi} x^{-5}. \tag{35}$$

Values of several coefficients are gathered in Tab. 1 to facilitate numerical calculations.

Though there is a value of coefficient (34) within limits for $n = s$, but expression (33) for $n = s$ can not be used in calculations of the self-resistance. In this case an approximate formula, given in paper [8] should be applied.

5. Conclusions

Mutual acoustic interactions between vibration modes, $(0, n)$ and $(0, s)$, of a single circular plate take place for determined intervals of parameter $k_0 a$. Extreme values of the mutual impedance occur for $k_0 a$ near γ_n and γ_s. For higher modes maximal interactions occur when the linear dimensions $2a$ of the plate are comparable with the integral multiple of the length of radiated waves, $n\lambda$.

It is characteristic that acoustic interactions suddenly decay for wave lengths λ slightly differing from $2a/n$. When the wave length is decreased still, then the mutual resistance also decreases assuming negative values and within the limit for $\lambda \to 0$ it equals zero. The mutual reactance also decreases with the frequency increase of radiated waves. It assumes positive values and within the limit for $k_0 = 2\pi/\lambda \to \infty$ approaches zero.

Acoustic interactions through a fixed mode $(0, n)$ and an arbitrary different mode $(0, s)$ are the smaller, the higher the value of $n - s$. If the value of $m - s$ is fixed, then acoustic interactions decrease when higher and higher modes, $(0, n)$ and $(0, s)$, are considered.

References

[1] J. W. Detteman, *Applied complex variables*, McMillan Company, New York – London 1965.

[2] I. Malecki, *Theory of Acoustic Waves and Systems*, PWN, Warszawa 1964 (in Polish).

[3] N. W. McLachlan, *Bessel Functions for Engineers*, PWN, Warszawa 1964 (in Polish).

[4] W. Rdzanek, *Mutual acoustic impedance oi circular membranes and plates with Bessel axially-symmetric vibration velocity distributions*, Archives of Acoustics, **5**, 3, 237–250 (1980).

[5] W. Rdzanek, *Mutual and total acoustic impedance of a system of source with a variable superficial vibration velocity distribution*, Academic Publ. of the Higher Pedagogic School in Zielona Góra, Zielona Góra 1979 (in Polish).

[6] W. RDZANEK, *Acoustic interactions of a system of concentric rigg-shaped sources*, Academic Publ. of the Higher Pedagogic School in Zielona Góra, Zielona Góra 1983 (in Polish).
[7] W. RDZANEK, *Acoustic interactions of axially-symmetric Bessel modes of a cricular membrane for forced vibrations*, Scien. Scripts of the Higher Pedagogic School in Zielona Góra, XII/2, 47–56 (1983) (in Polish).
[8] W. RDZANEK, *The sound power of a circular plate for high-frequency wave radiation*, Archives of Acoustics, **3**, 4, 331–339 (1983).
[9] G. N. WATSON, *Theory of Bessel functions*, 2nd ed., University Press, University Park and London 1968.

Received on November 21, 1985; revised version on June 9, 1986.

Appendix A

The following Wronskians are known for the Bessel function $J_m(x)$, Neumann function $N_m(x)$ and the MacDonald function $K_m(x)$ [9]:

$$J_1(x)N_0(x)-J_0(x)N_1(x)=\frac{2}{\pi x}, \tag{A1}$$

$$I_1(x)K_0(x)+I_0(x)K_1(x)=\frac{1}{x}. \tag{A2}$$

The indefinite integral [9]

$$\int wJ_0(hw)J_0(lw)\,dw=\frac{w}{h^2-l^2}\{hJ_1(hw)J_0(lw)-lJ_0(hw)J_1(lw)\} \tag{A3}$$

can be applied also for complex quantities h, l.

Using the indefinite integral (A3) it can be proved that eigenfunctions

$$q_n(r)=J_0\left(\frac{r}{a}\gamma_n\right)-\frac{J_0(\gamma_n)}{I_0(\gamma_n)}I_0\left(\frac{r}{a}\gamma_n\right)$$

are orthogonal for $0\leqslant r\leqslant a$ in the sense of the Kronecker delta, i.e.

$$\int_0^a q_n(r)q_m(r)r\,dr=a^2J_0^2(\gamma_n)\delta_{nm} \tag{A4}$$

if γ_n is the n-root of the characteristic equation (3).

The following definite integrals [5] are found in expression (20):

$$A_{00}\equiv\int_0^{\pi/2}J_0^2(x\sin t)\sin t\,dt=J_0(2x)+$$

$$+\frac{\pi}{2}[J_1(2x)S_0(2x)-J_0(2x)S_1(2x)], \tag{A5}$$

$$A_{01} \equiv \int_0^{\pi/2} J_1(x\sin t) J_0(x\sin t)\sin^2 t\,dt = \frac{1}{2x}\,[A_{00}(x) - J_0(2x)] \tag{A6}$$

and

$$A_{11} \equiv \int_0^{\pi/2} J_1^2(x\sin t)\sin^3 t\,dt =$$

$$= \frac{1}{2}A_{00}(x) + \frac{3}{2}\frac{1}{(2x)^2}\,[A_{00}(x) - 2xJ_1(2x) - J_0(2x)]. \tag{A7}$$

It is convenient to introduce function

$$U(x) \equiv \frac{\pi}{2}\,[J_1(2x)S_0(2x) - J_0(2x)S_1(2x)] \tag{A8}$$

which for $x \ll 1$ can be approximated by the expression

$$U(x) \simeq \frac{2}{3}x^2\left(1 - \frac{3}{10}x^2\right) \tag{A9}$$

if we use approximate formulas for Struve and Bessel functions [3]:

$$S_0(x) \simeq \frac{2}{\pi}x\left(1 - \frac{x^2}{9}\right), \quad S_1(x) \simeq \frac{2}{3\pi}x^2\left(1 - \frac{x^2}{15}\right), \tag{A10}$$

$$J_0(x) \simeq 1 - \frac{x^2}{4}, \quad J_1(x) \simeq \frac{x}{2}\left(1 - \frac{x^2}{8}\right). \tag{A11}$$

Appendix B

The contour function (compare [9], [8])

$$\frac{1}{2\pi i}\int_c z^{\varrho-1}Z_\mu(bz)\frac{H_\nu^{(1)}(az)\,dz}{(z^4 - r^4)(z^4 - s^4)} \tag{A12}$$

where $a > b > 0$; r, s — complex numbers; Z_μ — μ-order cylindrical function; $|\mu| + |\nu| < \varrho < 10$, can be expressed in the form of a sum of residues in poles of the integrand. When $a = b$, then $\varrho < 9$.

With the application of the Jordan lemat and the Cauchy residuum theorem [1], the integration contour can be closed in the top half-plane of the complex variable z. Four poles of the integrand, for $z = r$, $z = ir$, $z = s$ and $z = is$,

are enclosed during integration. We obtain

$$\frac{1}{2\pi i}\int_0^\infty \{Z_\mu(bx)H_\nu^{(1)}(ax)-\exp(\varrho\pi i)Z_\mu[bx\exp(\pi i)]H_\nu^{(1)}[ax\exp(\pi i)]\}\times$$

$$\times\frac{x^{\varrho-1}dx}{(x^4-r^4)(x^4-s^4)}=\frac{1}{4(r^4-s^4)}\{r^{\varrho-4}Z_\mu(br)H_\nu^{(1)}(ar)-s^{\varrho-4}Z_\mu(bs)\times$$

$$\times H^{(1)}(as)+i^\varrho[r^{\varrho-4}Z_\mu(ibr)H_\nu^{(1)}(iar)-s^{\varrho-4}Z_\mu(ibs)H_\nu^{(1)}(ias)]\}. \quad \text{(A13)}$$

For a special case, when $Z_\mu=J_\mu$, $a=b=1$, taking into account relations

$$J_\mu(ix)=\exp\left(i\mu\frac{\pi}{2}\right)I_\mu(x),\quad H_\nu^{(1)}(ix)=\frac{2}{\pi}\exp\left[-i(\nu+1)\frac{\pi}{2}\right]K_\nu(x),$$

$$J_\mu[x\exp(\pi i)]=\exp(\mu\pi i)J_\mu(x),\qquad H_\nu^{(1)}[x\exp(\pi i)]=-\exp(-i\nu\pi)H_\nu^{(2)}(x),$$

$$H_\nu^{(1)}(x)=J_\nu(x)+iN_\nu(x),\qquad H_\nu^{(2)}(x)=J_\nu(x)-iN_\nu(x)$$

in place of (A13) we have

$$\int_0^\infty J_\mu(x)J_\nu(x)\frac{x^{\varrho-1}dx}{(x^4-r^4)(x^4-s^4)}=\frac{\pi}{4(r^4-s^4)}\left\{-r^{\varrho-4}J_\mu(r)H_\nu^{(1)}(r)-\right.$$

$$\left.-s^{\varrho-4}J_\mu(s)H_\nu^{(1)}(s)+\frac{2}{\pi}\cos(\varrho+\mu-\nu)\frac{\pi}{2}[r^{\varrho-4}I_\mu(r)K_\nu(r)-s^{\varrho-4}I_\mu(s)K_\nu(s)]\right\} \quad \text{(A14)}$$

for $\varrho+\mu-\nu=2n$, $n=1,2,3,\ldots$ and

$$\int_0^\infty J_\mu(x)N_\nu(x)\frac{x^{\varrho-1}dx}{(x^4-r^4)(x^4-s^4)}=\frac{\pi}{4(r^4-s^4)}\left\{r^{\varrho-4}J_\mu(r)H_\nu^{(1)}(r)-\right.$$

$$\left.-s^{\varrho-4}J_\mu(s)H_\nu^{(1)}(s)+\frac{2}{\pi}\sin(\varrho+\mu-\nu)\pi/2[r^{\varrho-4}I_\mu(r)K_\nu(r)-s^{\varrho-4}I_\mu(s)K_\nu(s)]\right\} \quad \text{(A15)}$$

for $\varrho+\mu-\nu=2n+1$, $n=0,1,2,\ldots$

ARCHIVES OF ACOUSTICS
11, 3, 253-259 (1986)

MULTI-DIMENSIONAL TRANSFER FUNCTIONS FOR A NON-DISSIPATIVE BURGERS' EQUATION

ROMAN DYBA, BRONISŁAW ŻÓŁTOGÓRSKI

Institute of Telecommunication and Acoustics, Wrocław Technical University
(50-370 Wrocław, Wybrzeże Wyspiańskiego 27)

The propagation of acoustic disturbances in a continuum medium was analyzed under the assumption that the non-dissipative Burgers' equation is a reasonable mathematical model of the phenomenon under study. Regarding the propagation as a transformation of the time dependence of the acoustic velocity in a system with an input signal and employing the Banta's solution, the non-linear Burgers-Banta system was obtained. This system was described in the form of Volterra's series; the kernels of the series being determined with the help of the method of harmonic excitations. The r-dimensional Volterra's kernels given in the paper and their Fourier transforms (transfer functions) enable the parameters and probabilistic characteristics of the output signal to be determined under the condition that the input signal is known.

1. Non-dissipative Burgers' equation

Navier-Stokes equations [1, 2] define the dynamics of a viscous gas medium with the consideration of heat conduction. These can be reduced to one equation for the potential of the acoustic velocity, with general assumptions concerning the disturbances of the medium [3]:

$$c_0^2 \nabla^2 \Phi - \frac{\partial^2 \Phi}{\partial t^2} + \left(2 + \frac{\eta'}{\eta} + \frac{\nu - 1}{Pr}\right) \nu \nabla^2 \frac{\partial \Phi}{\partial t} = 2 \nabla \frac{\partial \Phi}{\partial t} \nabla \Phi + (\gamma - 1) \frac{\partial \Phi}{\partial t} \nabla^2 \Phi \tag{1}$$

where besides typical notations, there also are:
c_0 — adiabatic sound velocity, γ — exponent of the adiabate ($= c_p/c_w$), η — first coefficient of viscosity (coefficient of dynamic viscosity), η' — second

coefficient of viscosity, ν — coefficient of kinematic viscosity ($= \eta/\varrho_0$), Pr — Prandtl number.

Applying the approximation of the theory valid for waves with a small but finite amplitude and limiting the case to a one-dimension problem, the above equation can be written in the following form:

$$\left(c_0 \frac{\partial}{\partial x} + \frac{\partial}{\partial t}\right) \frac{\partial \Phi}{\partial t} - \frac{1}{2} \delta \frac{\partial^3 \Phi}{\partial x^2 \partial t} + \frac{1}{2} (\gamma + 1) \frac{\partial \Phi}{\partial x} \frac{\partial^2 \Phi}{\partial x \partial t} = 0 \tag{2}$$

which, by integrating in terms of t and differentiating in terms of x, can be converted to the equation for acoustic velocity:

$$\frac{\partial u}{\partial t} + \left(c_0 + \frac{\gamma + 1}{2} u\right) \frac{\partial u}{\partial x} = \frac{1}{2} \delta \frac{\partial^2 u}{\partial x^2} \tag{3}$$

δ in equations (2) and (3) marks the coefficient of sound dissipation:

$$\delta = \nu \left(\frac{4}{3} + \frac{\zeta}{\eta} + \frac{\gamma - 1}{Pr}\right) \tag{4}$$

where $\zeta = \eta' + \frac{2}{3}\eta$ is the total coefficient of viscosity. The coefficient of sound dissipation represents losses in the medium due to viscosity and heat conduction.

This paper is concerned with such a case of propagation of disturbances, in which the right side of equation (3) can be neglected. Thus, equation (3) is replaced by the non-dissipative Burgers' equation:

$$\frac{\partial u}{\partial t} + \left(c_0 + \frac{\gamma + 1}{2} u\right) \frac{\partial u}{\partial x} = 0. \tag{5}$$

2. Banta's solution

The unconventional solution of equation (5) given by Banta [4], has the following form:

$$u(x, t) = \varphi + \sum_{n=1}^{\infty} (-1)^n \frac{x^n}{n!} \frac{d^{n-1}}{dt^{n-1}} [F^n(\varphi) \dot{\varphi}] \tag{6}$$

where

$$F(\varphi) = \frac{1}{c_0 + \beta \varphi}, \quad \dot{\varphi} = \frac{d}{dt} \varphi, \quad \varphi = \varphi(t) = u(0, t). \tag{6a}$$

In further considerations a slightly different expression for F will be used; applying the assumption about finite but small (with respect to c_0) acoustic velocities it can be accepted, that

$$F(\varphi) = \frac{1}{c_0+\beta\varphi} \cong \frac{1}{c_0} - \frac{\beta}{c_0^2}\varphi; \tag{6b}$$

in expressions (6a) and (6b): $\beta = (\gamma+1)/2$.

The approximation in (6b) is sufficient; e.g. if the level of acoustic pressure equals 174 dB (re $2\cdot10^{-5}$ Pa) what corresponds to the velocity of the acoustical particle of $0.1\,c_0$, the approximation error in (6b) does not exceed 1.5 % [5].

3. Application of the harmonic input method in the construction of a transfer function of a system defined by Banta's series

The phenomenon of non-linear propagation, defined by Banta's series (6), can be presented in the form of a system with an input signal $X(t) = \varphi(t) = u(0, t)$ and output signal $Y(t) = u(x, t)$ (Fig. 1) [6].

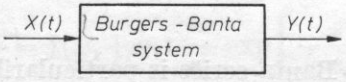

Fig. 1. Illustration of the "input – output" relations for propagation described by the Banta series

The Burgers-Banta system is a non-linear inertial system without the hysteresis effect. In a general case such a system can be described by Volterra series [7, 8]; the general form of this series is as follows:

$$Y(t) = \sum_{r=1}^{\infty} \frac{1}{r!} \int_{R^r} h_r(\tau_1, \ldots, \tau_r) \prod_{i=1}^{r} x(t-\tau_i)\, d\tau^r \tag{7}$$

where h_r are the Volterra kernels of the r-order. Their analytic form depends on the properties of the system; the integration domain R^r is the r-multiple Cartesian product of $R = \{\tau : \tau \in (-\infty, \infty)\}$ and $d\tau^r = d\tau_1 \ldots d\tau_r$.

This paper is aimed at the determination of kernels h_r and their r-dimensional Fourier transforms, i.e. r-multiple transfer functions of a system presented in Fig. 1, which is described by series (6). $h_r(t_1, \ldots, t_r)$ denotes the Volterra kernel and $\bar{h}_r(t_1, \ldots, t_r)$ denotes the kernel of the Burgers-Banta system. The harmonic input method [6, 8, 9] was used to determine the set $\{h_r\}$. In order

to apply this method effectively the series (6) should be converted to a form more convenient for further calculations. From

$$\frac{d^{n-1}}{dt^{n-1}}\left[F^m(\varphi)F'(\varphi)\dot{\varphi}\right] = \frac{1}{n+1}\frac{d^n}{dt^n}\left[F^{n+1}(\varphi)\right]$$

series (6) can be converted to

$$u(x,t) = \varphi(t) + \sum_{n=1}^{\infty}(-1)^n \frac{x^n}{(n+1)!}\frac{d^n}{dt^n}\left[F^{n+1}[\varphi(t)]\right],$$

and then using equation (6b) and taking into consideration that

$$F^{n+1}(\varphi) = \sum_{k=0}^{n+1}\binom{n+1}{k}\frac{1}{c_0^{n+1-k}}\left(-\frac{\beta}{c_0^2}\right)^k \varphi^k$$

we have

$$u(x,t) = \varphi(t) + \frac{c_0^2}{\beta x}\sum_{n=1}^{\infty}(-1)^{n+1}\frac{x^{n+1}}{(n+1)!}\frac{d^n}{dt^n}\sum_{k=0}^{n+1}\frac{1}{c_0^{n+1-k}}\left(-\frac{\beta}{c_0^2}\right)^k \varphi^k(t). \tag{8}$$

This new form of the Banta series is particularily useful in the generation of Volterra kernels with the harmonic input method. This method consists in the determination of coefficients of exponential factors of the $\exp[j(\omega_1+\ldots+\omega_r)]$ type in the input signal, under the assumption that the signal $\exp(j\omega_1 t)+\ldots$ $\ldots+\exp(j\omega_r t)$ acts at the input. As it has been proved in paper [8] these coefficients are r-dimensional transfer functions and their r-dimensional inverse Fourier transforms are Volterra kernels of the r-order. Thus, in order to determine the transfer functions of the first order (denoted by $\bar{H}_1(\omega, x)$) it was accepted that $\varphi(t) = \exp(j\omega t)$. Finding the coefficient of the $\exp(j\omega t)$ factor in series (8), $H_1(\omega, x)$ is obtained. Making the substitution in expression (8), we obtain the series:

$$u(x,t) = e^{j\omega t} + \frac{c_0^2}{\beta x}\sum_{n=1}^{\infty}(-1)^{n+1}\frac{x^{n+1}}{(n+1)!}\frac{d^n}{dt^n}\sum_{k=0}^{n+1}\binom{n+1}{k}\frac{1}{c_0^{n+1-k}}\left(-\frac{\beta}{c_0^2}\right)^k e^{j\omega t}$$

which, after differentiating, has the form:

$$u(x,t) = e^{j\omega t} + \frac{c_0^2}{\beta x}\sum_{n=1}^{\infty}(-1)^{n+1}\frac{x^{n+1}}{(n+1)!}\sum_{k=0}^{n+1}\binom{n+1}{k}\frac{1}{c_0^{n+1-k}}\left(-\frac{\beta}{c_0^2}\right)^k (jk\omega)^n e^{j\omega t}.$$

The sought coefficient can be derived from the above expression by accepting $k = 1$; then the expression for H_1 will be:

$$\bar{H}_1(\omega, x) = 1 + \frac{c_0^2}{\beta x} \sum_{n=1}^{\infty} (-1)^{n+1} \frac{x^{n+1}}{(n+1)!} (n+1) \frac{1}{c_0^n} \left(-\frac{\beta}{c_0^2}\right) (j\omega)^n =$$

$$= \exp\left(-j\frac{x}{c_0}\right) \omega,$$

hence

$$h_1(t, x) = F^{-1}\{\bar{H}_1(\omega, x)\} = F^{-1}\left\{\exp\left(-j\frac{x}{c_0}\omega\right)\right\} = \delta\left(t - \frac{x}{c_0}\right)$$

where $\delta(\cdot)$ denotes the Dirac delta. In order to obtain the transfer function of the second order we have to accept

$$\varphi(t) = e^{j\omega_1 t} + e^{j\omega_2 t}$$

and then we have to find the coefficient of the harmonic factor with a $\omega_1 + \omega_2$ pulsation in series (8) with the $\varphi(t)$ function accepted as above. The series of calculations (as above) leads to the following expression for the transfer function of the second order:

$$\bar{H}_2(\omega_1, \omega_2, x) = j(\omega_1 + \omega_2) \frac{\beta x}{c_0^2} \exp\left[-\frac{x}{c_0} j(\omega_1 + \omega_2)\right].$$

The kernel of the second order will be expressed by:

$$\bar{h}_2(t_1, t_2, x) = F_2^{-1}\left\{j(\omega_1 + \omega_2) \frac{x}{c_0^2} \exp\left[-\frac{x}{c_0} j(\omega_1 + \omega_2)\right]\right\} =$$

$$= \frac{\beta x}{c_0^2} \left(\frac{\partial}{\partial t_1} + \frac{\partial}{\partial t_2}\right) \delta\left(t_1 - \frac{x}{c_0}\right) \delta\left(t_2 - \frac{x}{c_0}\right).$$

In a general case, the following expression for the transfer function of the r-order is obtained:

$$H_r(\omega_1, \ldots, \omega_r, x) = \left(\frac{\beta x}{c_0^2}\right)^{r-1} [j(\omega_1 + \ldots + \omega_r)]^{r-1} \exp\left[-j\frac{x}{c_0}(\omega_1 + \ldots + \omega_r)\right] \tag{9}$$

hence the general form of the Volterra kernel is:

$$\bar{h}_r(t_1, \ldots, t_r, x) = F_r^{-1}[\bar{H}_r(\omega_1, \ldots \omega_r, x)] =$$

$$= \left(\frac{\beta x}{c_0^2}\right)^{r-1} \left(\frac{\partial}{\partial t_1} + \ldots + \frac{\partial}{\partial t_r}\right)^{r-1} \delta\left(t_1 - \frac{x}{c_0}\right) \ldots \delta\left(t_r - \frac{x}{c_0}\right). \tag{10}$$

The obtained expression for the general form of Volterra kernels leads to a more compact than in (6) form of the Banta series [4]. Namely, substituting (10) in (7), expressions for succeeding terms of the Volterra series are obtained. Thus, let V_r denote the r-term of series (7), i.e.

$$V_r = \frac{1}{r!} \int_{R^r} h_r(t_1, \ldots, t_r) \prod_{i=1}^{r} X(t-\tau_i)\, d\tau^r \tag{11}$$

and then in case of the Burgers-Banta series it is:

$$h_r(t_1, \ldots, t_r) = \bar{h}_r(t_1, \ldots, t_r, x), \quad X(t) = \varphi(t), \quad Y(t) = u(x, t).$$

The final result is:

$$V_1 = \int_{-\infty}^{\infty} \delta\left(\tau - \frac{x}{c_0}\right) \varphi(t-\tau)\, d\tau = \varphi\left(t - \frac{x}{c_0}\right),$$

$$V_2 = \frac{1}{2!} \frac{Bx}{c_0^2} \int_{-\infty}^{\infty} \int_{-\infty}^{\infty} \left[\delta'\left(\tau_1 - \frac{x}{c_0}\right) \delta\left(\tau_2 - \frac{x}{c_0}\right) + \delta\left(\tau_1 - \frac{x}{c_0}\right) \delta'\left(\tau_2 - \frac{x}{c_0}\right) \times \right.$$

$$\left. \times \varphi(t-\tau_1)\varphi(t-\tau_2)\, d\tau_1 d\tau_2 = \frac{\beta x}{c_0^2} \varphi\left(t - \frac{x}{c_0}\right) \dot{\varphi}\left(t - \frac{x}{c_0}\right) = \frac{1}{2!} \frac{\beta x}{c_0^2} \frac{d}{dt} \varphi^2\left(t - \frac{x}{c_0}\right), \right.$$

. . . . . .

$$V_r = \frac{1}{r!} \left(\frac{\beta x}{c_0^2}\right)^{r-1} \frac{d^{r-1}}{dt^{r-1}} \varphi^r\left(t - \frac{x}{c_0}\right).$$

Hence, a different, more compact form of the Banta series is achieved:

$$u(x, t) = \sum_{r=1}^{\infty} \left(\frac{\beta x}{c_0^2}\right)^{r-1} \frac{1}{r!} \frac{d^{r-1}}{dt^{r-1}} \varphi^r\left(t - \frac{x}{c_0}\right). \tag{12}$$

4. Conclusions

The approach applied in this paper to the description of the "input-output" relations of a Burgers-Banta system consists in treating the propagation of an intensive acoustic signal from the point of view of the analysis of non-linear changes of the signal initiating disturbances in the medium, i.e. signal $X(t) = u(0, t) = \varphi(t)$, where the signal $Y(t) = u(x, t)$ reflects these non-linear changes. Such a formulation of the problem suggests that the non-linear propagation phenomenon should be treated as a non-linear system; and the method of Volterra serieses was used, because of its versatality.

New elements of the description of lossless non-linear propagation have been achieved. A compact analytical Volterra description of the Burgers-Banta system was derived; the form of kernels (10) shows that the said system is quasi-memoryless.

Analytical forms of r-dimensional Volterra kernels and transfer functions, presented in this paper, make it possible to determine easily all parameters of the output signal, when the input signal is known. Also the construction of all probabilistic characteristics (e.g. multi-dimensional probability distributions, power spectrum density) of the output signal is possible, when the input signal is a stationary Gaussian process [7]. This can find application in investigations of non-linear propagation of intensive acoustic noises [2, 10].

References

[1] L. K. Zarembo, V. I. Timosenko, *Nieliniejnaja akustika*, Izd. Moskovskovo Universiteta, Moskva 1984, pp. 6–23.

[2] C. A. Vasil'eva, A. A. Karabutov, E. A. Łapsin, C. V. Rudenko, *Vzajmodiejstvie odnomiernych voln v sredach bez dispersji*, Izd. Moskovskovo Universiteta, Moskva 1983, p. 20.

[3] D. G. Crighton, *Model equations of non-linear acoustics*, Ann. Rev. Fluid Mech., **11**, 11–13 (1979).

[4] E. D. Banta, *Lossless propagation of one-dimensional finite amplitude sound waves*, Journal of Math. Analysis and Appl., **10**, 166–173 (1965).

[5] L. Bjorno, *Non-linear acoustics*; [in:] Acoustics and Vibration Progress, vol. 2, ed.: R. W. Stephens, H. G. Leventhall, printed: Chapman and Hall, London 1976, p. 140.

[6] R. Dyba, A. Gabor, M. Głowacki, J. Szymbor, B. Żółtogórski, *Non-linear transformations of signals — application in the description of non-linear phenomena in hydrodynamics and electrotechnics*, ed.: Institute of Telecommunication and Acoustics of the Technical University of Wrocław, Series: Raporty, Wrocław 1980, pp. 80–85 (in Polish).

[7] K. A. Pupkov, V. I. Kapalin, A. S. Juscenko, *Funkcjonal'nyje riady v teorii nieliniejnych sistem*, Izd. Nauka, Moskva 1976, pp. 85–100, 234.

[8] E. Bedrosian, S. O. Rice, *The output properties of Volterra systems* (non-linear systems with memory) driven by harmonic and Gaussian inputs, Proc. of the IEEE, **59**, 12 1688–1707 (1971).

[9] R. Dyba, B. Żółtogórski, *Non-dissipative Burgers' equation — review of methods of spectral analysis*, Proc. of the 9th Int. Symp. on Non-linear Acoustics, Leeds 1981, p. 23.

[10] R. Dyba, B. Żółtogórski, *Lagrangian boundary condition and non-linear propagation as causes of Gaussian noise spectrum deformation*, Journal of Sound and Vibr., **81**, 2, 239–253 (1982).

Received on December 27, 1985; revised version on May 29, 1986.

ARCHIVES OF ACOUSTICS
11, 3, 261-285 (1986)

CALCULATION OF THE ACOUSTICAL FIELD OF A SEMI-INFINITE CYLINDRICAL WAVE-GUIDE BY MEANS OF THE GREEN FUNCTION EXPRESSED IN CYLINDRICAL COORDINATES

ANNA SNAKOWSKA, ROMAN WYRZYKOWSKI

Institute of Physics, Higher Pedagogic School
(35–959 Rzeszów, ul. Rejtana 16a)

The exact solution to the problem of the acoustic wave propagation is presented for a half-infinite cylindrical wave-guide with rigid walls, i.e., with taking into account the diffraction phenomena on the open end of wave-guide. The problem was solved by means of the theory of acoustic field without sources and the use is made of the Green's function method in the cylindrical space co-ordinates, leading to two integral equations which are solvable with the help of the Wiener-Hopf method.

The wave number considered was taken to be a complex quantity, and the reduced forms of the final formulae are presented for the limiting case of real wave number.

Notations

$f(\overline{u})$ — directivity factor,
$f_m(z)$ — function of apparent sources,
$F_m(w)$ — Fourier transform of functions of apparent sources,
$g_m(z)$ — source function,
$\tilde{G}(\varrho, \varrho', w)$ — Fourier transform of Green function,
k — constant,
$l_m(z)$ — nucleus of the integral equation,
$L(w)$ — Fourier transform of the nucleus of the integral equation,
$L_+(w), L_-(w)$ — factors,
l, m — integers, indexes of wave mode,
N — order of the highest acceptable mode,
w — partial wave number,

v — radial wave number,
$S(w)$ — function determining factors L_+, L_-,
$X(w)$, $Y(w)$ — real and imaginary part of function $S(w)$,
γ_m — radial wave number of mode numbered m,
ε — imaginary part of wave numbered k,
η — imaginary part of variable w,
μ_m — m root of the Bessel function $J_1(z)$,
$\Psi(z)$ — jump of the potential on the wall of the wave-guide,
$\Omega(v)$ — function equaling $\operatorname{tg}^{-1} \dfrac{N_1(v)}{J_1(v)} + \dfrac{\pi}{2}$.

Other notations used in this paper are typical and have not been included in the above list.

1. Introduction

The determination of a wave-guide acoustic field consists from the mathematical point of view in the solution of a wave equation with given boundary conditions, generally applied to the normal component of the vibrational velocity on the walls. Such solutions are known only for a few cases, where the boundary conditions are accepted on highly symmetrical planes (e.g. infinite wave-guides). In other cases the symmetry of vibrating systems is corrected by supplementing them with infinite acoustic baffles. However, only few problems have an exact solution.

From among papers concerned with theoretical and experimental acoustics in the field of phenomena taking place in cylindrically symmetrical wave-guides, the fundamental work of Rayleigh should be mentioned [1]. Rayleigh calculated the quantity called the "correction for the open end", which is the measure of the phase shift of a plane wave due to the reflection at the wave-guide orfice supplied additionally with an infinite rigid acoustic baffle. The method of separation of variables, applied to the wave equation expressed in cylindrical coordinates [2], gives a solution, which points out that not only a plane wave can propagate in the wave-guide, but also higher wave modes can occur. They appear above certain limit frequencies, depending on the pipe radius. It is by intuition evident that the same modes can also occur in a half-infinite wave-guide and that their generation can be related to diffraction effects taking place at the orfice. This proves that the Rayleigh method applied in certain cases especially with waves shorter than the doubled pipe radius can give completely erroneous results.

LEVIN'S and SCHWINGER'S, and WAJNSZTEJN'S papers published in the 40-fies have contributed in particular to significant progress in the mathematic theory of vibrations in a pipe. The first two scientists [3] have achieved an exact solution of the wave equation with boundary conditions characteristic for a semi-infinite cylindrical pipe with perfectly rigid walls, under an assumption

that only a plane wave propagates in the direction of the orfice and in the reverse direction. Of course, this limits the practical application of the results to waves not shorter than the pipe radius, when the generation of higher Bessel modes is impossible. WAJNSZTEJN, on the other hand, in his works [4, 5] gave an exact solution to the problem of electromagnetic wave propagation in a flat and cylindrical wave-guide, and then on the analogy of electric waves (in a flat wave-guide), or magnetic waves (in a cylindrical wave-guide) and acoustic waves, he established an expression for the acoustic potential, postulating, also by analogy, such a form of the jump of the potential on the wall of the wave-guide, which would result in integral equations identical with equations obtained for electromagnetic waves.

This paper presents a method of obtaining an exact solution to this problem with the sole application of the acoustic field theory, for a region without sources, including constraints of the mathematical solution resulting from its physical interpretation as the potential. The theory of Green functions expressed in cylindrical coordinates has been applied.

2. Formulation of the problem in the form of an integral equation

Our analysis will concentrate on the acoustic field inside a cylindrical wave-guide stretching from $z = 0$ to ∞, with its axis of symmetry coinciding with the z-axis. The wall of the wave-guide is described by the equation of the side surface of a semi-infinite cylinder with a radius a (Fig. 1):

$$\sum = \{(\varrho, \varphi, z): \varrho = a, z \geqslant 0\}. \tag{1}$$

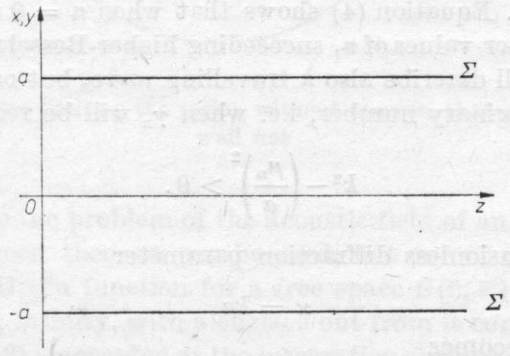

Fig. 1. Geometry of the system — semi-infinite cylindrical wave-guide with radius a and the axis of symmetry coinciding with the z-axis of the coordinate system

Let us consider a case when the wave-guide is axially excited (the velocity distribution is independent from the angular variable) to vibrate with a determinate circular frequency w. The expression for the acoustic potential inside

an infinite wave-guide, obtained from the wave equation, is

$$\Delta\Phi(\bar{r}, t) = \frac{1}{c^2}\frac{\partial^2\Phi(\bar{r}, t)}{\partial t^2} \tag{2}$$

with the condition of the decay of the radial component of the vibration velocity on the surface of an infinite wave-guide

$$\left.\frac{\partial\Phi(\bar{r}, t)}{\partial\varrho}\right|_{\varrho=a} = 0, \quad -\infty < z < +\infty. \tag{3}$$

Considering only harmonic vibrations and assuming that the time dependence of the potential is expressed by factor $\exp(-i\omega t)$, we obtain the following solution [2], which satisfies physical conditions of the potential:

$$\Phi_n(\varrho, z) = A_n \frac{J_0\left(\frac{\mu_n}{a}\varrho\right)}{J_0(\mu_n)} \cdot e^{-i\gamma_n z} \tag{4}$$

where γ_n is the radial wave number related to the vave numbered k, by the following relationship

$$\gamma_n = \sqrt{k^2 - \left(\frac{\mu_n}{a}\right)^2} \tag{5}$$

and μ_n is the n root of the Bessel function $J_1(x)$. The $J_0(\mu_n)$ factor, which appeared in the denominator in (4) is a standarizer, so constant A denotes the amplitude. Index n numbers successive allowed wave modes. Of course, in a general case, the potential of an incident wave can be a superposition of the potentials of individual modes. Equation (4) shows that when $n = 0$ a plane wave is obtained, while for other values of n, succeeding higher Bessel modes occur. Moreover, formula (4) will describe also a travelling wave, but only when the exponent will be an imaginary number, i.e. when γ_n will be real, that is when

$$k^2 - \left(\frac{\mu_n}{a}\right)^2 > 0. \tag{6}$$

Introducing a dimensionless diffraction parameter

$$\varkappa = ka, \tag{7}$$

the condition (6) becomes

$$\varkappa > \mu_n. \tag{8}$$

Denoting by N the greatest integer, so

$$\mu_N < \varkappa \leqslant \mu_{N+1} \tag{9}$$

then N determines the order of the highest Bessel mode which can propagate in the wave-guide without loss, with an assigned diffraction parameter $\varkappa$.

In order to determine the acoustic field of a semi-infinite wave-guide, the wave equation (2) has to be solved with a boundary condition of the decay of the normal component of the vibration velocity on the wave-guide surface, i.e. only for $z \geqslant 0$:

$$\left.\frac{\partial \Phi(\bar{r}, t)}{\partial \varrho}\right|_{\varrho=a} = 0, \quad z \geqslant 0. \tag{10}$$

An assumption is made that the sound wave, which propagates towards the open end, has a potential expressed by formula (4), i.e. it is a single wave mode. It undergoes diffraction at the orfice — part of the energy is radiated outside, and part returns to the wave-guide as a reflected wave. We postulate that it can consist of all Bessel modes, which can propagate in the given wave-guide. Therefore, the solution of the diffraction problem lies in the determination of complex amplitudes of modes in a wave returning from the open end.

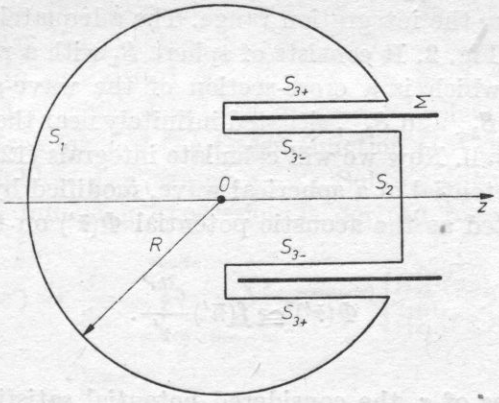

Fig. 2. Integration surface limiting the region without sources; that is with the wave-guide wall out

In order to solve the problem of the acoustic field of an investigated wave-guide the second Green theorem can be used, but one of the scalar functions is substituted by a Green function for a free space $G(\bar{r}, \bar{r}')$ and a sphere with a radius approaching infinity, with a surface out from it comprising the wall of the wave-guide (Fig. 2) is accepted as the integration surface. The Green function $G(\bar{r}, \bar{r}')$ satisfies the following differential equation

$$(\Delta + k^2) G(\bar{r}, \bar{r}') = -\delta(\bar{r} - \bar{r}') \tag{11}$$

where the function on the right side is the δ Dirac distribution. Using the mentioned above theorem and including the fact that the spatial part of the expres-

sion for the potential fulfills the Helmholtz differential equation, it can be written

$$\Phi(\bar{r}) = \oint_S [G(\bar{r}, \bar{r}')\bar{n}'\nabla'\Phi(\bar{r}') - \Phi(\bar{r}')\bar{n}'\nabla'G(\bar{r}, \bar{r}')]d\sigma', \tag{12}$$

The "prim" mark at the deloperator means, that the differentiation is done in respect to variables marked "prim", so $\bar{n}'$ is the unit vector normal to the $d\sigma$ surface element. If we want to use the form of the Green function for a free space

$$G(\bar{r}, \bar{r}') = \frac{1}{4\pi} \frac{e^{ik|\bar{r}-\bar{r}'|}}{|\bar{r}-\bar{r}'|} \tag{13}$$

then there should be no sources in the range limited by surface S. The surface of the wave-guide with apparent sources related to the potential discontinuity has been cut out from the integration range. The adequately chosen integration surface is shown in Fig. 2. It consists of sphere S_1 with a radius R approaching infinity, circle S_2, which is a cross-section of the wave-guide at $z = R$ and cylindrical surfaces, S_{3+} and S_{3-}, situated infinitely near the inner and outer side of the wave-guide wall. Now we will calculate integrals (12) on individual parts of surface S. The potential of a spherical wave, modified by a directivity factor $f(n')$, can be accepted as the acoustic potential $\Phi(\bar{r}')$ on the surface S_1

$$\Phi(\bar{r}') \cong f(\bar{n}') \frac{e^{ikr'}}{r'}. \tag{14}$$

For great values of r, the considered potential satisfies the Sommerfeld's radiation and finity conditions; the Green function fulfills the so-called sharpened Sommerfeld's radiation and finity conditions; the (12) integral on the surface of sphere S_1 vanishes, what has been proved among others by RUBINOWICZ [6]. The integral on surface S_2 tends to zero for $R \to \infty$ due to the finite value of the potential, finite integration surface and the decrease of the Green function with inverse proportion to distance. Thus, the value of potential $\Phi(\bar{r})$ will be determined only by an integral on surfaces S_{3+} and S_{3-}. Considering that the side surface of the cylinder satisfies the boundary condition (10) of the decay of the normal component of the vibration velocity, and that $\bar{n}'\nabla' = \partial/\partial\varrho$ for elements of the surface S_{3+}, and $\bar{n}'\nabla' = -\partial/\partial\varrho$ for elements of the surface S_{3-}, the expression (12), which determines the acoustic potential, can be written in the form

$$\Phi(\bar{r}) = 2\pi a \int_0^\infty \Psi(z') \frac{\partial}{\partial\varrho'} G(\bar{r}, \bar{r}')\Big|_{\varrho'=a} dz' \tag{15}$$

where the function $\Psi(z')$ determines the jump of the potential on the surface of the wave-guide

$$\Psi(z') = \Phi(\varrho', z')|_{\varrho' \to a_+} - \Phi(\varrho', z')|_{\varrho' \to a_-}. \tag{16}$$

The analysis of expression (15) shows that the acoustic potential in an arbitrary point of the field is univocally defined by the jump (discontinuity) of the potential on the surface of the wave-guide. The application of this form allows the notation of the boundary condition (10) in the form of a homogeneous integral equation

$$\int_0^\infty \Psi(z') \frac{\partial}{\partial \varrho} \frac{\partial}{\partial \varrho'} G(\bar{r}, \bar{r}')\Big|_{\substack{\varrho'=a \\ \varrho=a}} dz' = 0; \quad z \geqslant 0. \tag{17}$$

Thus, the calculation of the acoustic potential of a semi-infinite cylindrical wave-guide has been reduced to the determination of the value of the jump of the potential $\Psi(z')$ on the wave-guide surface, i.e. to the solution of integral equation (17). Because the problem is cylindrically symmetric, then the Green function expressed in cylindrical coordinates can be applied, i.e. the Green function for a cylinder, which has been discussed in detail in papers [2], [7]. It results from the free form of the Green function (13) that this is a function of the following variables $(\varrho, \varrho', \varphi - \varphi', z - z')$. Solving equation (11) in cylindrical coordinates, the following expression is derived for the Green function:

$$G(\varrho, \varrho', \varphi - \varphi', z - z') = \frac{i}{8\pi} \int_{-\infty+i\eta}^{\infty+i\eta} \sum_{m=-\infty}^{\infty} e^{im(\varphi-\varphi')} \begin{Bmatrix} H_m^{(1)}(v\varrho) J_m(v\varrho') \\ H_m^{(1)}(v\varrho') J_m(v\varrho) \end{Bmatrix} e^{iw(z-z')} dw, \quad \begin{matrix} \varrho > \varrho' \\ \varrho < \varrho' \end{matrix} \tag{18}$$

This is the Green function for a cylinder. It has the form of an inverse Fourier transform, while the integration path is a line parallel to $\mathrm{Re}\, w$, and coefficient η satisfies the inequality

$$-\mathrm{Im}\, k < \eta < \mathrm{Im}\, k. \tag{19}$$

When the excitation is axial (the case under investigation), then the infinite series under the integral is reduced to one term for $m = 0$. Then we obtain

$$G(\varrho, \varrho', z - z') = \frac{i}{8\pi} \int_{-\infty+i\eta}^{\infty+i\eta} \begin{Bmatrix} H_0^{(1)}(v\varrho) J_0(v\varrho') \\ H_0^{(1)}(v\varrho') J_0(v\varrho) \end{Bmatrix} e^{iw(z-z')} dw, \quad \begin{matrix} \varrho > \varrho' \\ \varrho < \varrho' \end{matrix} \tag{20}$$

where v is the radial wave number

$$v = \sqrt{k^2 - w^2}. \tag{21}$$

The form of the obtained Green function differs in dependence on whether the point of the field lies inside ($\varrho < \varrho'$) or outside ($\varrho > \varrho'$) the wave-guide. This occurs because from among a family of solutions of equation (11) we have to chose those, which fulfill the physical conditions of the problem. Both solutions are symmetrical with respect to the change from ϱ to ϱ', what corresponds to the change of location of the source and the observation point. The expression in braces describes the propagation of cylindrical waves along the radial coordinate ϱ.

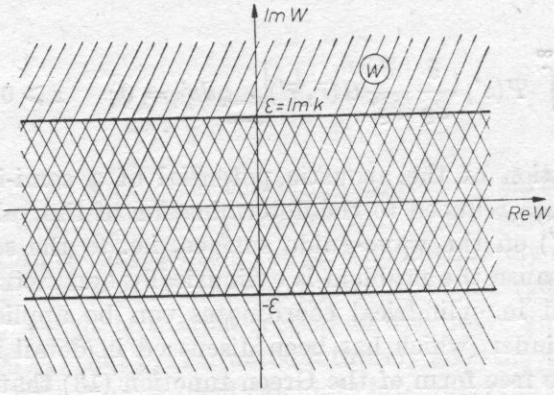

Fig. 3. Analyticity regions of Fourier transforms, $L(w)$ and $F_l(w)$. Common analyticity region $-\varepsilon < \mathrm{Im} < \varepsilon$.

Using expression (20) in the equation describing the potential (15) and the boundary condition (17), two integral equation are obtained

$$\Phi(\varrho, z) = \frac{ai}{4} \int_0^\infty \Psi(z')\,dz' \int_{-\infty+i\eta}^{\infty+i\eta} v \begin{Bmatrix} H_0^{(1)}(v\varrho) J_1(va) \\ H_1^{(1)}(va) J_0(v\varrho) \end{Bmatrix} e^{iw(z-z')}\,dw, \qquad \begin{matrix} \varrho > a \\ \varrho < a \end{matrix}, \tag{22}$$

$$\int_0^\infty \Psi(z')\,dz' \int_{-\infty+i\eta}^{\infty+i\eta} v^2 H_1^{(1)}(va) J_1(va)\, e^{iw(z-z')}\,dw = 0, \qquad z \geqslant 0. \tag{23}$$

The acoustic potential can be found by solving the second equation, i.e. fining the function $\Psi(z')$. The problem of solving a wave equation with a boundary condition of the decay of the normal derivative on the side surface of a semi-infinite cylinder has been reduced to the problem of solving a pair of integral equations, (22) and (23).

3. The determination of source functions on the surface of a wave-guide

The jump of the potential on the surface of the wave-guide can be accepted as the occurrence of apparent sources on this surface. The function describing sources on the surface of the wave-guide is marked $g(z)$. When a single allowed

wave mode (e.g. 1-st) propagates in the wave-guide, then this function can be expressed as a sum

$$g_l(z) = f_l(z) + \Phi_l(a, z) \tag{24}$$

where $f_l(z)$ determines apparent sources, which appear on the surface of the wave-guide due to diffraction, and $\Phi_l(a, z)$ is the value of the potential of the wave inciding on the wave-guide wall. For $z < 0$ sources do not occur, therefore

$$g_l(z) = 0, \quad z < 0. \tag{25}$$

It results from the above discussion that the function of sources equals the sought value of the potential jump on the surface of the wave-guide and zero on its extension

$$g_l(z) = \begin{cases} \Psi(z), & z \geqslant 0, \\ 0 \quad , & z < 0. \end{cases} \tag{26}$$

Therefore, the integration range can be widened onto the interval $(-\infty, +\infty)$, and then expressions (22) and (23) will have a form convenient for further calculations. The boundary condition, in particular, will have the form of a convolution, so it will be simple to find its Fourier transform. Moreover, if we denote

$$l(z-z') = \frac{1}{2\pi} \int_{-\infty+i\eta}^{\infty+i\eta} e^{iw(z-z')} v^2 H_1^{(1)}(va) J_1(va)\, dw \tag{27}$$

then the boundary condition for a l wave mode reaching the open end will be

$$\int_{-\infty}^{\infty} g_l(z') l(z-z')\, dz' = 0, \quad z \geqslant 0, \tag{28}$$

while the expression for the acoustic potential will equal

$$\Phi_l(\varrho, z) = \frac{ai}{4} \int_{-\infty}^{\infty} g_l(z') \int_{-\infty+i\eta}^{\infty+i\eta} v \begin{cases} H_0^{(1)}(v\varrho) J_1(va) \\ H_1^{(1)}(va) J_0(v\varrho) \end{cases} e^{iw(z-z')} dw, \quad \begin{matrix} \varrho > a \\ \varrho < a \end{matrix} \tag{29}$$

The function of sources is equal to

$$g_l(z) = f_l(z) + A_l e^{-i\gamma_l z} \tag{30}$$

because the form of the second term in expression (24) is accepted as explicit.

Equation (28) is an equation with a nucleus with a translated argument. It can be solved with the factorization method, which consists in the distribution of the Fourier transform (if it exists) of the investigated equation onto the product of analytical functions (factors), which do not have zeroes respecti-

vely in the upper and lower half-plane of the complex variable w. The upper half-plane will be noted by $\{w: \mathrm{Im}\, w > -\mathrm{Im}\, k\}$, and the lower by $\{w: \mathrm{Im}\, w < \mathrm{Im}\, k\}$. It should be noted that these half-planes have a common part, denoted by expression $\{w: -\mathrm{Im}\, k < w < \mathrm{Im}\, k\}$.

As it has been previously stated, expression (28) presents a convolution, so its Fourier transform can be easily found. Expression (27) has the form of an inverse transform, so the transform will be

$$L(w) = v^2 H_1(va) J_1(va). \tag{31}$$

Certain conditions have to be satisfied by both functions in order for the transform to exist. The analysis of the function of sources proves that $f_l(z)$ as a diffraction term, must tend to zero for $z \to \infty$, so it has a Fourier transform

$$F_l(w) = \int_{-\infty}^{\infty} f_l(z) e^{iwz} dz \tag{32}$$

while if $\mathrm{Im}\, k > 0$, then $\mathrm{Im}\, \gamma_l > 0$, and thus for $z \to \infty$ the second term in expression (30) approaches infinity. At the same time it results from transform $L(w)$ that

$$L(\gamma_n) = 0 \tag{33}$$

so set $\left\{\gamma_n = \sqrt{k^2 - \left(\frac{\mu_n}{a}\right)^2}\right\}$ is the set of roots of equation (31). Taking all that was up to now said into consideration we obtain the following form of the Fourier transform of the boundary condition

$$\int_{-\infty}^{\infty} e^{-iwz} dz \int_{-\infty}^{\infty} g_l(z') l(z - z') dz' = F_l(w) L(w). \tag{34}$$

The last equality is true if both transforms $F(w)$ and $L(w)$ have a common analyticity range. This range is the zone of the complex plane w, defined by equality $-\mathrm{Im}\, k < \mathrm{Im}\, w < \mathrm{Im}\, k$. Now, additional conditions, which the transform of the function of apparent sources, $F_l(w)$, must satisfy will be determined. The function of sources $g_l(z)$ equals zero when $z < 0$, therefore

$$f_l(z) = -A_l e^{-i\gamma_l z} \quad z < 0. \tag{35}$$

This equality will be satisfied if the transform $F_l(w)$ will have a first order pole with the residuum equal to $\frac{A_l}{i}$ in point $w = -\gamma_l$, and furthermore it will uniformly tend to zero on the lower half-plane, for $|w| \to \infty$. Then

$$\frac{1}{2\pi} \int_{-\infty + i\eta}^{\infty + i\eta} F_l(w) e^{iwz} dw + A_l e^{-i\gamma_l z} = 0, \quad z < 0. \tag{36}$$

The physical interpretation of this equation is as follows: for $z < 0$, i.e. on the extension of the wave-guide surface, the potential is continuous.

The boundary condition will be noted with the use of Fourier transform. The inverse Fourier transform of expression (34) is

$$\int_{-\infty}^{\infty} g_l(z')l(z-z')dz' = \int_{-\infty}^{\infty} F_l(w)L(w)e^{iwz}dw \tag{37}$$

hence the boundary condition (28) becomes

$$\int_{-\infty}^{\infty} F_l(w)L(w)e^{iwz}dw = 0, \quad z > 0. \tag{38}$$

This equation will be satisfied when the product of functions $F_l(w)$ and $L(w)$ is an analytic function in the upper half-plane and tends uniformly to zero on the infinite semicircle on the half-plane.

Both equations, (37) and (38), can be written in the form of homogeneous equations

$$\int_C F_l(w)e^{iwz}dw = 0, \qquad z < 0 \tag{39}$$

$$\int_C F_l(w)L(w)e^{iwz}dw = 0, \qquad z > 0 \tag{40}$$

where C is the integration contour, consisting of a line parallel to the real axis (it can be the axis itself in particular) and a loop around point $w = -\gamma_l$ (Fig. 4).

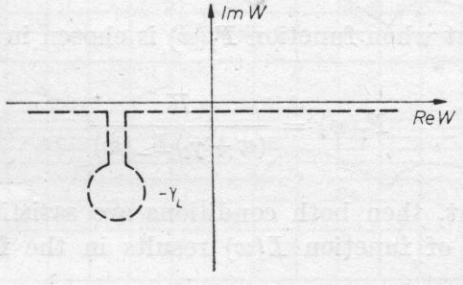

Fig. 4. Integration contour C in the plane of the complex variable w. Consists of a line parallel to the real axis and a loop around point $w = \gamma_l$

It follows from this paragraph that the condition of continuity of the potential on the extension of the wave-guide surface (36) and the condition of decay of the normal component of the vibration velocity on its wall (38) are fulfilled, when

1. Function $F_l(w)$ is analytic in the lower half-plane, $\mathrm{Im}\, w < \mathrm{Im}\, k$, excluding the point $w = -\gamma_l$, where it has a first order pole with a residuum equal to A_l/i, and it tends to zero on this half-plane for $|w| \to \infty$.

2. Product $F_l(w) \cdot L(w)$ is an analytical function in the upper half-plane, $\mathrm{Im}\, w > -\mathrm{Im}\, k$, and it uniformly tends to zero for $|w| \to \infty$ in this range.

Thus, the problem of the acoustic field of a semi-infinite cylindrical waveguide can be solved by determining function $F_l(w)$, which satisfies conditions (24) and (25), i.e. by solving the pair of integral equations (36) and (38) or (39) and (40).

Integral equations derived in this paragraph are identical with WAJNSZTEJN's equations for electromagnetic waves [5]. Therefore, his methods and results can be applied in further considerations.

4. Application of the Wiener-Hopf method in solving obtained integral equations

As it has been mentioned in the preceeding paragraph, the integral form (28) of the boundary condition (10) is a Wiener-Hopf type equation, so it can be solved with the factorization method. In this paper only a short outline of the solution will be presented, because of the applied complicated calculation methods [11].

An assumption is made at present that the distribution of function $L(w)$ onto analytical factors, respectively in the upper and lower half-plane of the complex variable w is known

$$L(w) = L_+(w) L_-(w). \tag{41}$$

It can be seen that when function $F_l(w)$ is chosen in the form

$$F_l(w) = \frac{K}{(w+\gamma_l) L_-(w)} \tag{42}$$

where K is a constant, then both conditions are satisfied.

The factorization of function $L(w)$ results in the following expressions

$$L_+(w) = (k+w)\left(H_1^{(1)}(va) J_1(va) \prod_{i=1}^{N} \frac{\gamma_i + w}{\gamma_i - w}\right)^{1/2} e^{S(w)/2} \tag{43}$$

$$L_-(w) = (k-w)\left(H_1^{(1)}(va) J_1(va) \prod_{i=1}^{N} \frac{\gamma_i - w}{\gamma_i + w}\right)^{1/2} e^{-S(w)/2} \tag{44}$$

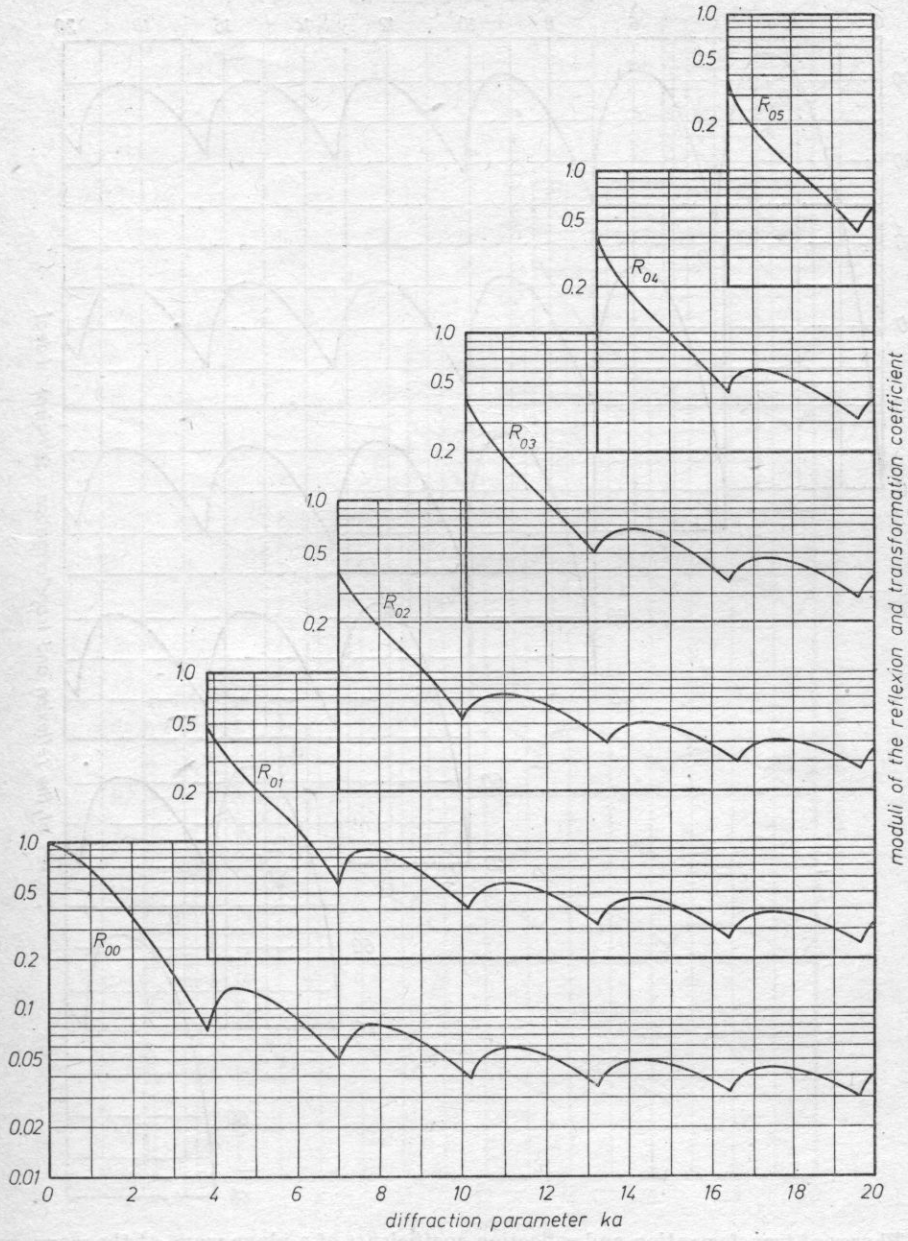

Fig. 5. Moduli of transformation and reflection coefficients of a plane wave at the wave-guide orfice in terms of the diffraction parameter *ka*

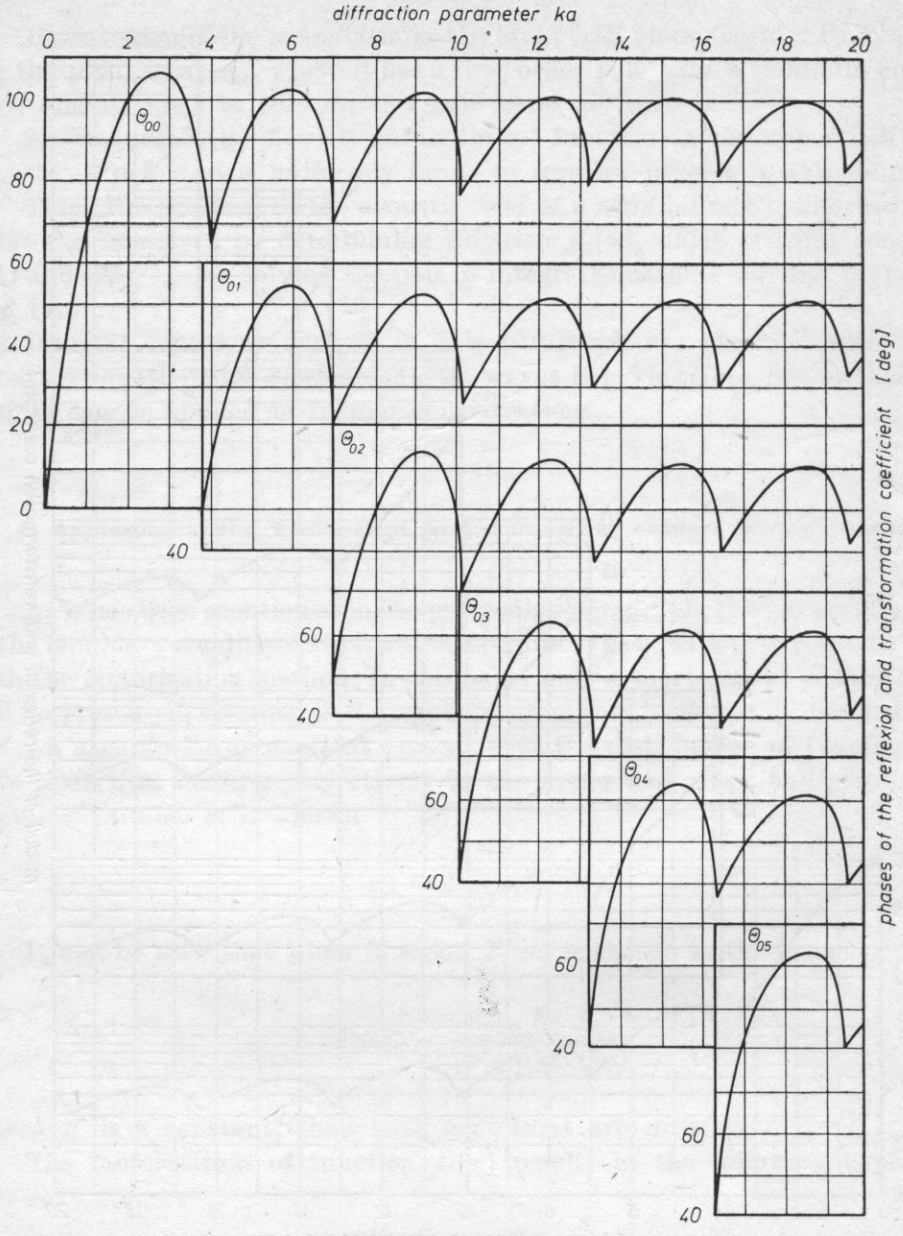

Fig. 6. Phases of transformation and reflection coefficients of a plane wave at the wave-guide orfice in terms of the diffraction parameter *ka*

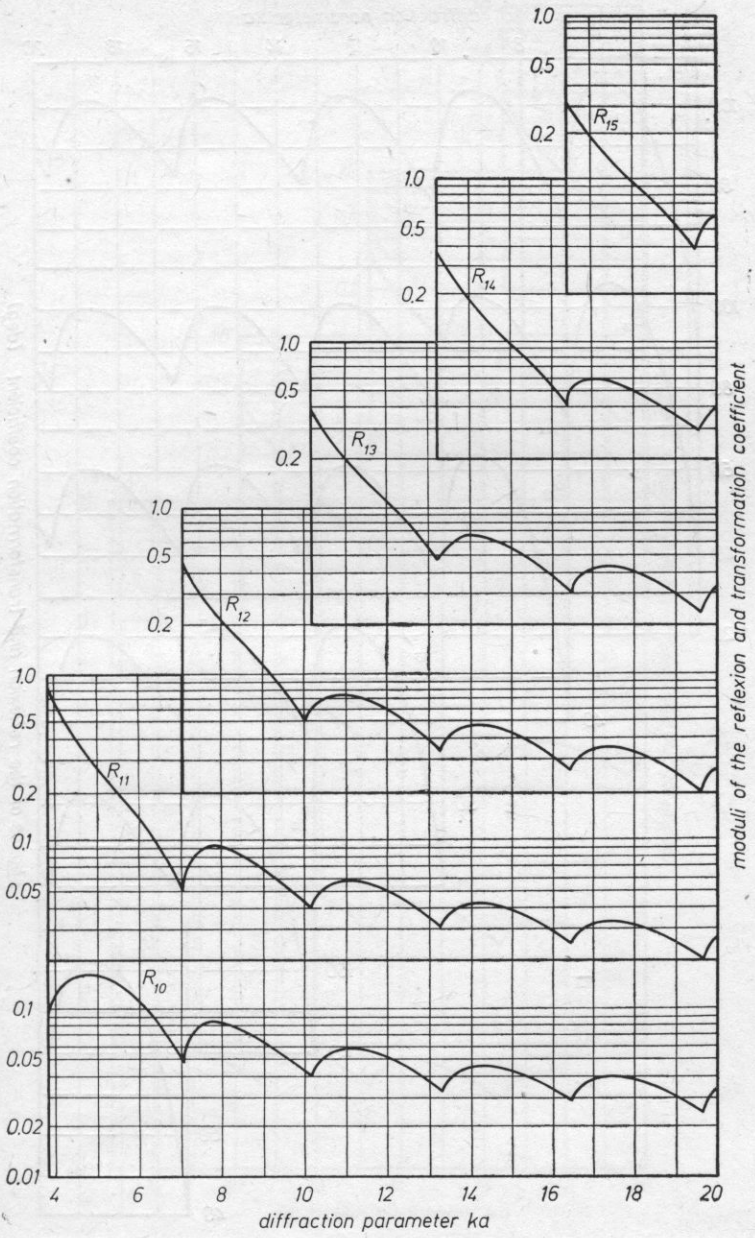

Fig. 7. Moduli of transformation and reflection coefficients of the first Bessel mode in terms of the diffraction parameter ka. This mode appears when the diffraction parameter ka exceeds the first zero of the Bessel function $J_1(z)$, $(ka > 3.83)$

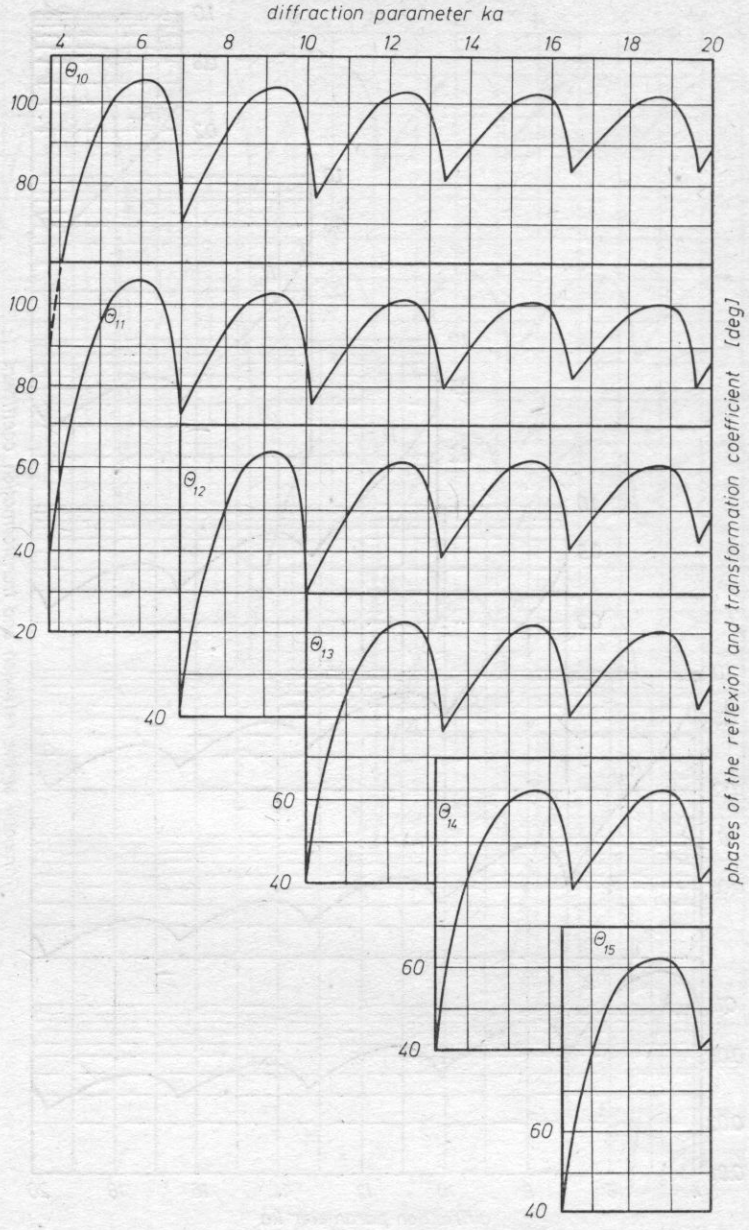

Fig. 8. Phases of transformation and reflection coefficients of the first Bessel mode in terms of the diffraction coefficient *ka*

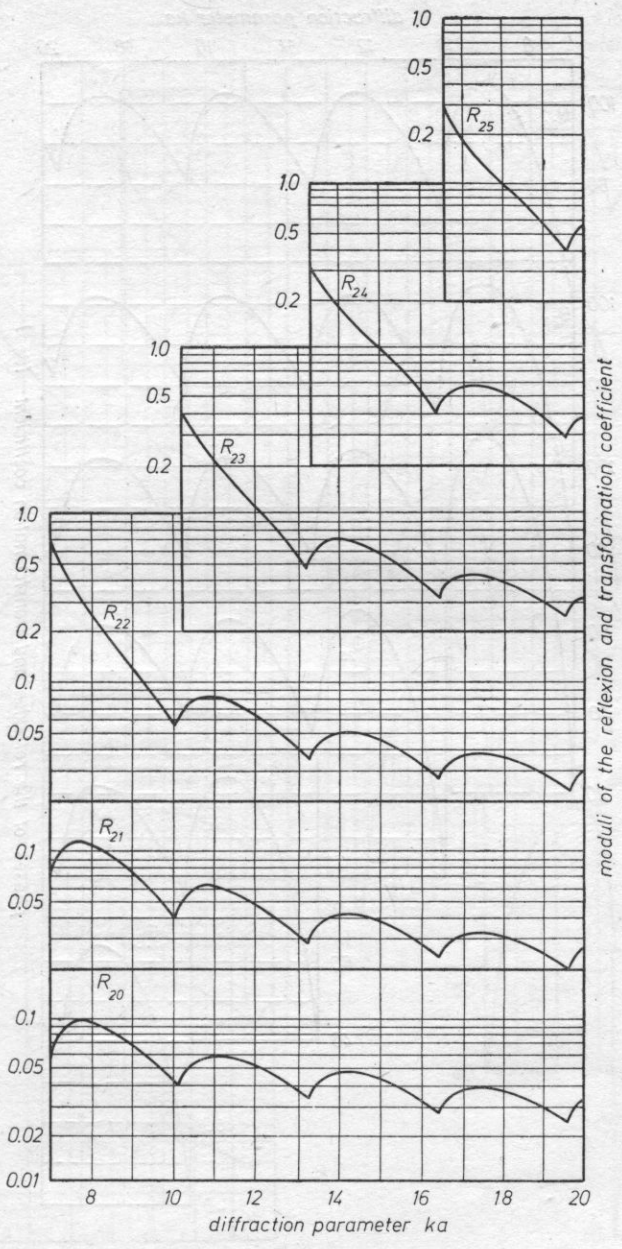

Fig. 9. Moduli of transformation and reflection coefficients of the second Bessel mode in terms of the diffraction parameter ka. This mode appears when the diffraction parameter ka exceeds the second zero of the Bessel function $J_1(z)$, $(ka > 7.01)$

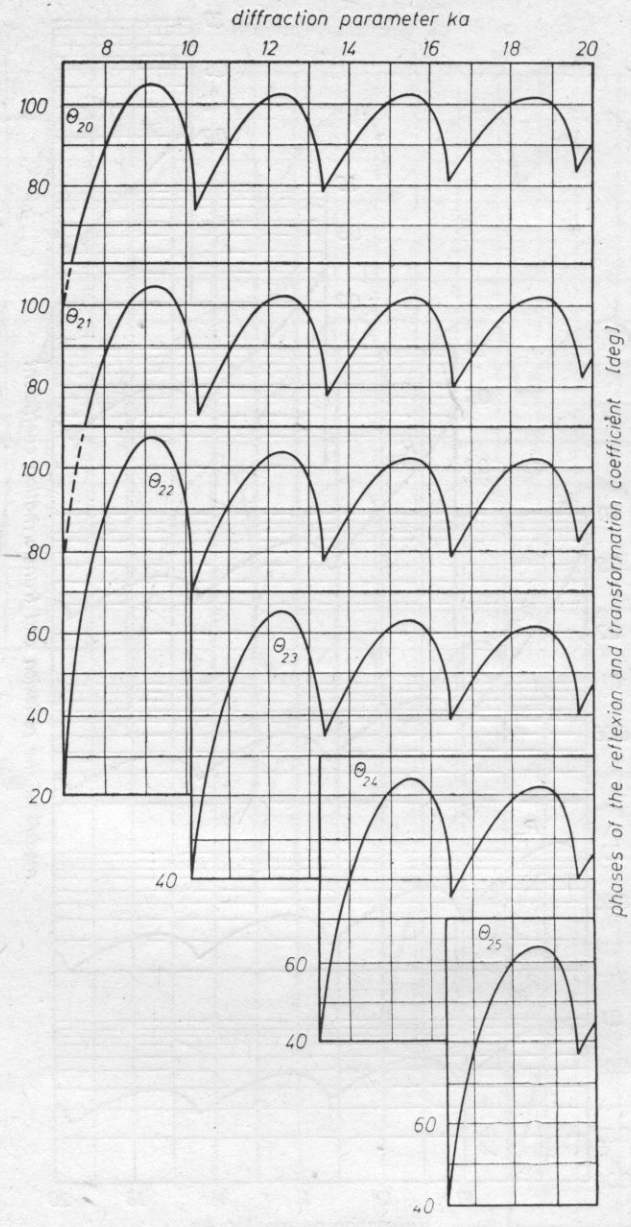

Fig. 10. Phases of transformation and reflection coefficients of the second Bessel mode in terms of the diffraction parameter *ka*

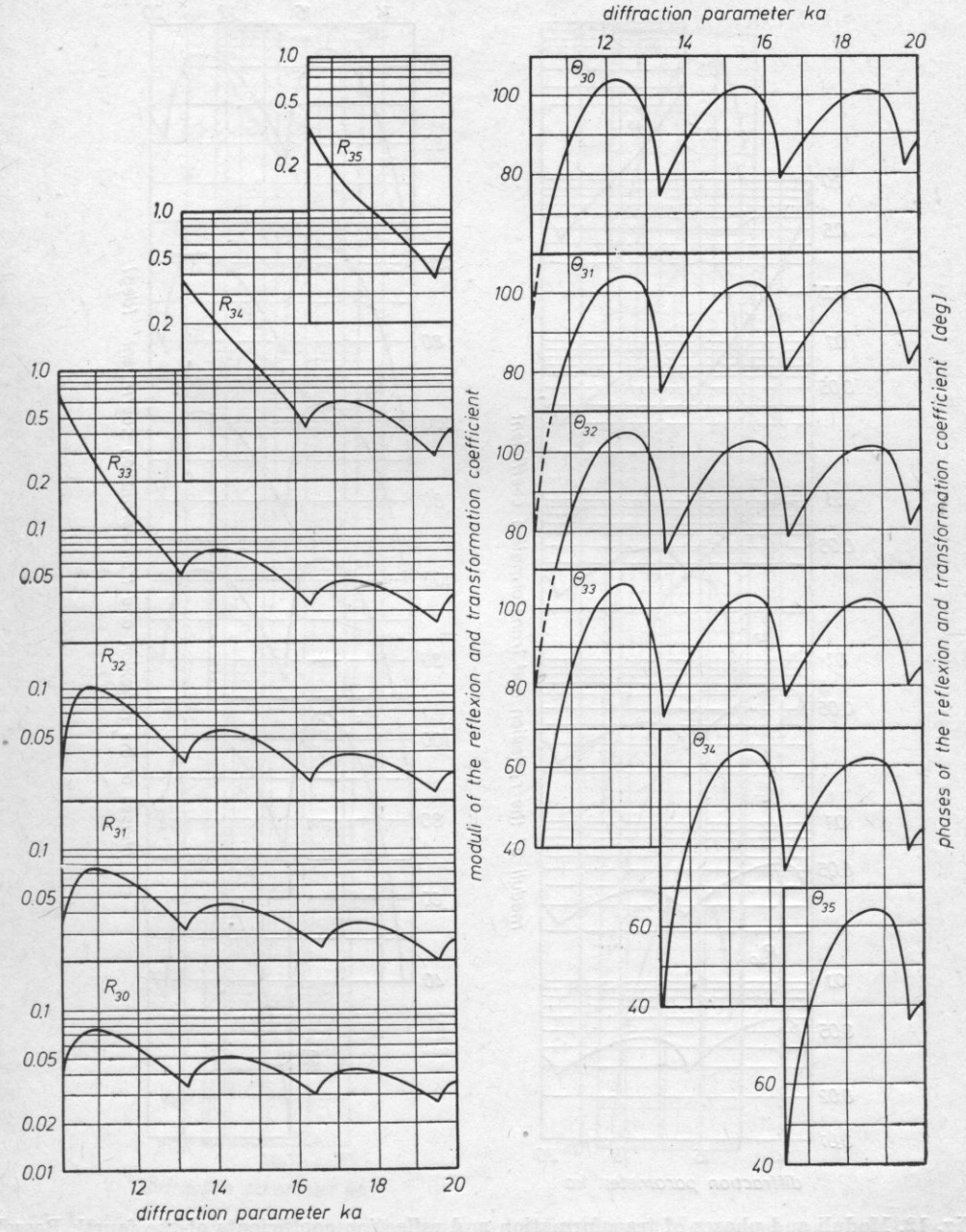

Fig. 11. Moduli and phases of transformation and reflection coefficients of the third Bessel mode in terms of the diffraction parameter ka. This mode appears when the diffraction parameter ka exceeds the third zero of the Bessel function $J_1(z)$, $(ka > 10.17)$

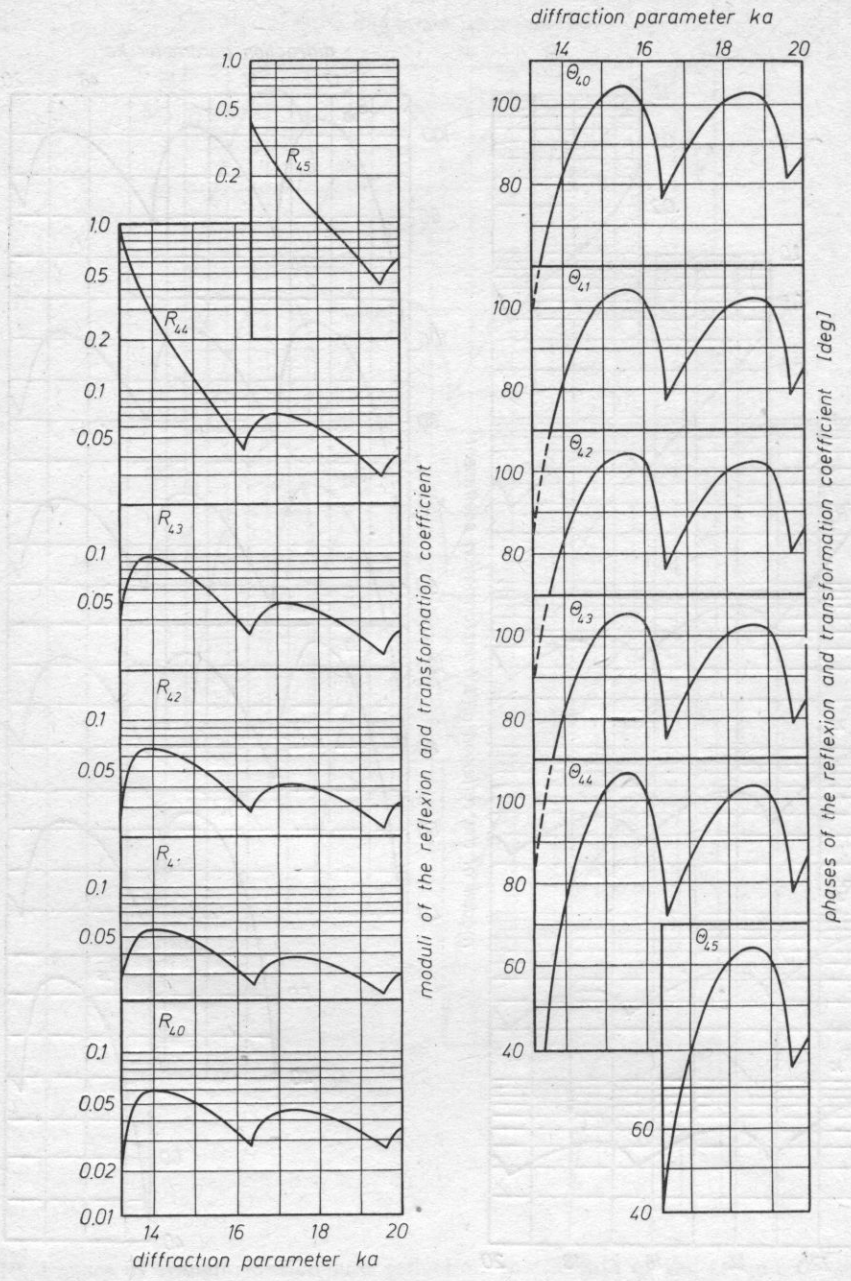

Fig. 12. Moduli and phases of transformation and reflection coefficients of the fourth Bessel mode in terms of the diffraction parameter ka. This mode appears when the diffraction parameter ka exceeds the fourth zero of the Bessel function $J_1(z)$, $(ka > 13.32)$

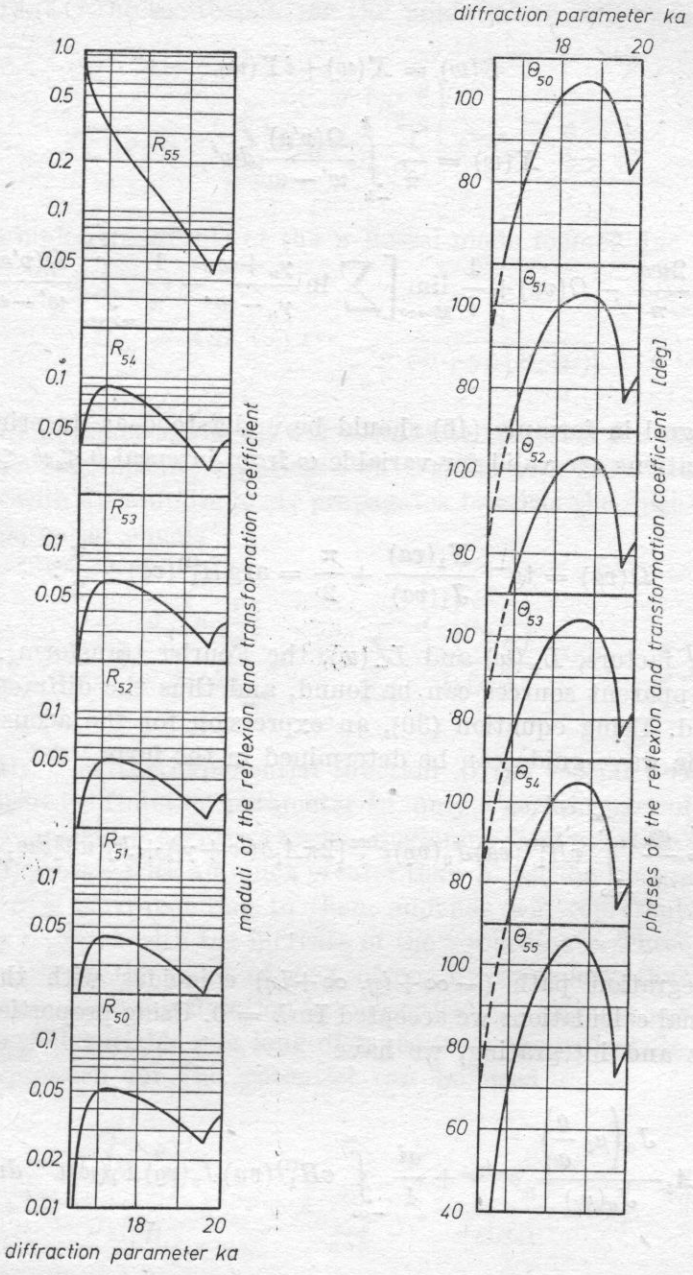

Fig. 13. Moduli and phases of transformation and reflection coefficients of the fifth Bessel mode in terms of the diffraction parameter ka. This mode appears when the diffraction parameter ka exceeds the fifth zero of the Bessel function $J_1(z)$, $(ka > 16.47)$

where

$$S(w) = X(w) + iY(w) \tag{45}$$

$$X(w) = \frac{1}{\pi} \int_{-k}^{k} \frac{\Omega(v'a)}{w'-w}\, dw', \tag{46}$$

$$Y(w) = \frac{2wa}{\pi} - \Omega(va) + \frac{1}{i} \lim_{M\to\infty} \left[\sum \ln \frac{\gamma_n + w}{\gamma_n - w} - \frac{1}{\pi} \int_{-\gamma_M}^{\gamma_M} \frac{\Omega(v'a)}{w'-w}\, dw' \right]. \tag{47}$$

The integral in formula (46) should be understood as its principal value. Two last equations are valid for variable w from interval $0 \leqslant w \leqslant k$. Function $\Omega(va)$ equals

$$\Omega(va) = \operatorname{tg}^{-1} \frac{N_1(va)}{J_1(va)} + \frac{\pi}{2} = \arg H_1^{(1)}(va) + \frac{\pi}{2}. \tag{48}$$

Knowing factors, $L_+(w)$ and $L_-(w)$, the Fourier transform $F_l(w)$ of the function of apparent sources can be found, and thus the diffraction problem can be solved. Using equation (30), an expression for the acoustic potential (31) inside the wave-guide can be determined in the form

$$\Phi_l(\varrho, z) = \frac{ai}{4} \int_{-\infty}^{\infty} vH_1^{(1)}(va) J_0(v\varrho) e^{iwz} [2\pi A_l \delta(w+\gamma_l) + F_l(w)]\, dw, \qquad \begin{matrix} \varrho > a \\ z > 0 \end{matrix}. \tag{49}$$

The integration path $(-\infty + i\eta,\ \infty + i\eta)$ coincides with the real axis, because in final calculations we accepted $\operatorname{Im} k = 0$. Using properties of cylindrical functions and integrating, we have

$$\Phi_l(\varrho, z) = A_l \frac{J_0\left(\mu_l \frac{\varrho}{a}\right)}{J_0(\mu_l)} e^{-i\gamma_l z} + \frac{ai}{4} \int_{-\infty}^{\infty} vH_1^{(1)}(va) J_0(v\varrho)\, F_l(w) e^{iwz}\, dw, \qquad \begin{matrix} \varrho > a \\ z > 0 \end{matrix}. \tag{50}$$

The first term describes the potential of the incident wave; thus it can be accepted that the second term describes the reflected and transformed waves, which are generated due to diffraction at the open end. The improper integral in equation (50) can be calculated from the theory of residue, remembering that variable v is an elemental variable, so the integrand is not unique. From

formulae (41)–(44) the expression for the potential of reflected waves is

$$\Phi_l^{\mathrm{ref}}(\varrho, z) = \sum_{n=0}^{\infty} B_{l,n} \frac{J_0\left(\mu_n \frac{\varrho}{a}\right)}{J_0(\mu_n)} e^{i\gamma_n z}, \quad \begin{matrix} \varrho < a \\ z > 0 \end{matrix}. \tag{51}$$

$B_{l,n}$ is the complex amplitude of the n Bessel mode formed due to diffraction at the open end

$$B_{l,n} = A_l L_+(\gamma_l)\, \mathrm{res}_{w=\gamma_n} \frac{1}{(w+\gamma_l)\left(L_-(w)\right)}. \tag{52}$$

Summarizing, once again we will write the expression for the acoustic potential inside a semi-infinite cylindrical wave-guide with rigid walls, when a 1-st Bessel mode with an amplitude A_1 propagates towards the open end. In such a case the potential equals

$$\Phi_l(\varrho, z) = A_l \frac{J_0\left(\mu_l \frac{\varrho}{a}\right)}{J_0(\mu_l)} e^{-\gamma_l z} + \sum_{n=0}^{\infty} \frac{J_0\left(\mu_n \frac{\varrho}{a}\right)}{J_0(\mu_n)} e^{i\gamma_n z}, \quad \begin{matrix} \varrho < a \\ z > 0 \end{matrix}. \tag{53}$$

The analysis of the exponential function in the second term shows that for an established diffraction parameter ka, only a certain part of the terms of the sum will represent progressive waves. Beginning from a certain N, so $\mu_N < ka \leqslant \mu_{N+1}$, coefficients γ with an index greater than N will be imaginary numbers and in that case corresponding to them addends will represent disturbances exponentially damped with the increase of the z coordinate. These disturbances are not waves from the point of view of energy transport, thus they do not have to be taken into consideration in energetical calculations as well as in case of great values of variable z (a long distance from the orfice). In this case the following expression for the potential can be used

$$\Phi_l(\varrho, z) = A_l \frac{J_0\left(\mu_l \frac{\varrho}{a}\right)}{J_0(\mu_l)} e^{-i\gamma_l z} + A_l \sum_{n=0}^{\infty} R_{l,n} \frac{J_0\left(\mu_n \frac{\varrho}{a}\right)}{J_0(\mu_n)} e^{i\gamma_n z}, \quad \begin{matrix} \varrho < a \\ z > 0 \end{matrix}. \tag{54}$$

$R_{l,n}$ is a complex transformation coefficient and it is equal to the ratio of the amplitude of the induced mode and the amplitude of the incitent mode

$$R_{l,n} = \frac{B_{l,n}}{A_l}. \tag{55}$$

For $l = n$ it is simply a reflection coefficient. Diagrams present moduli and phases of these coefficients, with the diffraction parameter ka, varying from 0 to 20.

5. Conclusions

To recapitulate, effects taking place at the end of the wave-guide are as follows: one of the Bessel modes, which is allowed from the point of view of the diffraction parameter ka, propagates towards the orfice. In undergoes diffraction at the orfice — part of the energy is radiated outside, the rest returns to the wave-guide in the form of allowed wave modes — higher, lower and also the mode of the same order as the incident wave. In order to determine the acoustic field inside the wave-guide in such a case, N complex reflection and transformation coefficients have to be established. The number of these coefficients has to equal the number of modes which can propagate in the wave-guide at an assigned diffraction parameter. Furthermore, if we include that the incident wave can be a superposition of all allowed modes, then the number of coefficients, describing the field, increases to N^2. This may complicate the univocal interpretation of the results. This is a view shared by many authors occupied with this problem. They consider that the Wiener-Hopf method applied to diffraction problems is mathematically very complicated and the interpretation of the results is difficult due to their complicated form [8, 9]. This statement is only partly true, because the mathematical description of the theory is indeed difficult (it is not presented in this paper, because only final formulae have been used in paragraph 4), but the interpretation of the results can be carried out with the application of the analysis of energetic quantities, such as impedance for example [10].

Thus the problem of the acoustic field of a cylindrical wave-guide is important from the cognitive point of view, because it is one of the fundamental diffraction problems, as well as from the practical point of view, because elements which can be approximated by a long cylindrical pipe without a baffle, occur frequently in acoustic systems.

References

[1] LORD RAYLEIGH, *Theory of Sound*, MacMillan, London 1940.
[2] W. RDZANEK, R. WYRZYKOWSKI, *Acoustic field of a cylinder*, WSP, Rzeszów 1975 (in Polish).
[3] H. LEVINE, J. SCHWINGER, *On the Radiation of Sound from an Unflanged Circular Pipe*, Phys. Rev., **73**, 4, 383–406 (1948).
[4] L. A. WAJNSZTEJN, ZTF, **18**, 10, 1543 (1948).

[5] L. A. WAJNSZTEJN, *The theory of diffraction and factorization methods*, Sowietskoje Radio, Moscow 1966 (in Russian).

[6] A. RUBINOWICZ, *A Sharpened Formulation of Sommerfeld's Radiation Conditions for Green's Function of the Helmholtz Equation*, Rep. Math. Phys., **2**, 2, 93–98 (1971).

[7] E. SKUDRZYK, *The Foundations of Acoustics*, Springer Verlag, Wien-New York 1971.

[8] G. F. HOMICZ, J. A. LORDI, *A Note on the Radiational Directivity Patterns of Duct Acoustic Modes*, J. Sound Vib., **41**, 3, 283–290 (1975).

[9] Y. ANDO, T. KOIZUMI, *Sound Radiation from a Semi-Infinite Circular Pipe Having an Arbitrary Profile of Orfice*, JASA, **59**, 5, 1033–1039 (1976).

[10] A. SNAKOWSKA, *Impedance of an orfice of a cylindrical pipe without a baffle for a plane wave inciding onto the orfice*, Archiwum Akustyki, **13**, 3, 223–234 (1978) (in Polish).

[11] P. M. MORSE, H. FESHBACH, *Methods of Theoretical Physics*, McGraw-Hill, New York 1961.

Received on October 26, 1984; revised version on March 20, 1986.

ARCHIVES OF ACOUSTICS
11, 3, 287-298 (1986)

ULTRASONIC ECHO METHOD IN DETECTION OF BREAST CALCIFICATIONS. TRANSIENT ANALYSIS

LESZEK FILIPCZYŃSKI, TAMARA KUJAWSKA, GRAŻYNA ŁYPACEWICZ

Department of Ultrasonics, Institute of Fundamental Technological Research, Polish Academy of Sciences
(00-049 Warsaw, ul. Świętokrzyska 21)

The detectability of calcifications in women breast by means of the ultrasonic echo method was estimated on the basis of the transient analysis of the ultrasonic pulse reflection. Two calcification models in the form of a rigid and an elastic sphere were considered.

Echoes obtained at tissue inhomogeneities form an interference background which masks echoes from small calcifications. The level of the tissue interference background was determined on the basis of measurements in 100 femal breasts and it was shown that the obtained experimental results are probable from the theoretical point of view.

As the result of the performed analysis and experiments the author concluded that microcalcifications are not detectable by the ultrasonic echo method. The radii of calcifications which can be found at the frequency of 5 MHz are equal to 0.6 mm or 1.6 mm depending on the maximum sampling error assumed for a single measurement of the tissue interference background.

1. Introduction

The detection of microcalcifications is of basic significance in the early diagnosis of breast tumors. The reactions occurring in breast tissue cells causing calcifications in the case of tumors appear already at the very early stage of their development. In view of this the question of possibilites of detecting small calcifications by the ultrasonic method becomes one of essential significance. Two versions of this method, the echo and the shadow techniques are of interest [2].

In both cases examinations involve short ultrasonic pulses at frequencies usually contained between 3 and 5 MHz.

In previous papers [1], [2] the problem of calcification detection by means of the echo method was investigated on the basis of the steady-state analysis. The purpose of this paper is to extend the analysis of transient phenomena and to discuss in detail the obtained experimental results.

2. Assumptions

It is assumed for simplification that the calcifications are rigid or elastic sphereswith the radius a. The longitudinal wave velocity in the calcification and its density are assumed similarly to those for bone tissue, to be, respectively, $c_L = 3.2.$ km/s and $\varrho = 2.23$ g/cm^3 [14]. The literature contains no information on the velocity of transverse waves in bone tissue, therefore the value of Poisson ratio $v = 0.2$ will be assumed. In follows from Table 1 that this assumption

Table 1. Poisson's ratio v for various materials and the value assumed for the calcification

Material	v	Material	v
Lead	0.44	Bismuth	0.33
Gold	0.42	Nickel	0.31
Platinum	0.39	Cadmium	0.30
Silver	0.38	Steel	0.28
Brass	0.35	Glass (crown)	0.27
Perspex	0.35	Zinc	0.25
Tungsten	0.35	Glass (flint)	0.24
Copper	0.35	Porcelain	0.23
Constantan	0.33	Calcification	0.2
Ice	0.33	Fused quartz	0.17
Tin	0.33	Berylium	0.05

is most probably, when this value is compared with those of other materials. The wave velocity and the attenuation coefficient of the breast tissue is assumed to be $c_L = 1.5$ km/s and $a = 1.1$ dB/cm MHz, respectively. It is also assumed that pulse of a plane ultrasonic wave, composed of two high frequency 5 MHz periods, is incident on the spherical calcification.

To analyse the detection ability of the echo method with a typical ultrasonograph we assume its sensitivity to be 10 μV, the transmitter pulse voltage: 250 V and overall transducing losses (double piezoelectric transducing) equal to $T = -15$ dB.

3. The reflection of ultrasonic pulses from rigid and elastic spheres

The transient analysis of the ultrasonic pulse reflection enables us to find the smallest calcification size which is potentially detectable with a typical ultrasonograph (scanner). In our computations we applied the procedure as

presented by RUDGERS [11] and HICKLING [7] for pulse reflections from rigid and elastic spheres, respectively.

The acoustic pressure p_i of a plane continuous wave, travelling in the x direction, incident on the sphere, has the form

$$p_i = p_{i0} \exp[j(\omega t - kx)] \quad \text{or} \quad p_i = p_{i0} \exp[jk(ct - x)] \tag{1a, b}$$

where p_{i0} denotes the pressure amplitude, $\omega = 2\pi f$, f — frequency, t — time, $k = \omega/c$, c — wave velocity in the soft tissue.

The acoustic pressure p_s of the wave reflected from the sphere can be expressed as

$$p_s = p_{i0} \sum_{m=0}^{\infty} (2m+1)(-j)^m c_m h_m^{(2)}(kr) P_m(\cos\theta) \exp(j\omega t) \tag{2}$$

where m denotes natural number, $j = \sqrt{-1}$, $h_m^{(2)}(kr)$ — spherical Hankel function of second kind $P_m(\cos\theta)$ — Legendre polynominal, c_m — scatternig coefficient of the m-th partial wave, θ — azimuth. For the backward reflection $\theta = 180°$, $P_m(\cos\theta) = (-1)^m$. The function $h_m^{(2)}(kr)$ can be represented by the assymptotic expression (for $kr \gg 1$)

$$h_m^{(2)}(kr) = \frac{1}{kr} \exp\left[-j\left(kr - \frac{m+1}{2}\pi\right)\right]. \tag{3}$$

Thus, Eq. (2) becomes

$$p_{s0} = p_{i0} \frac{a}{2r} f_\infty(ka) \tag{4}$$

where

$$f_\infty(ka) = \frac{2j}{ka} \sum_{m=0}^{\infty} (2m+1)(-1)^m c_m(ka) \tag{5}$$

when $r \gg a$ [1], [7], [12]. p_{s0} denotes the pressure amplitude of the reflected wave.

Figs. 1 and 2 show the far field form function (for backward reflection) [7] $f_\infty(ka)$ which was computed Eq. (5). For computations of c_m formulae of HASEGAWA [6] were applied. The diagrams of the far field form function presented in Figs. 5 and 1 in the papers [1] and [2], respectively, are incorrect due to an error in the computing program.

In the case of a rigid sphere, the longitudinal and transverse wave velocities in the sphere tend to infinity. It can then be shown that Eq. (5) takes a much simpler form as $c_m = -j_m'(ka)/h_m^{(2)'}(ka)$, where $j_m'(ka)$ and $h_m^{(2)'}(ka)$ denote derivatives of spherical Bassel and Hankel functions with respect to the argument.

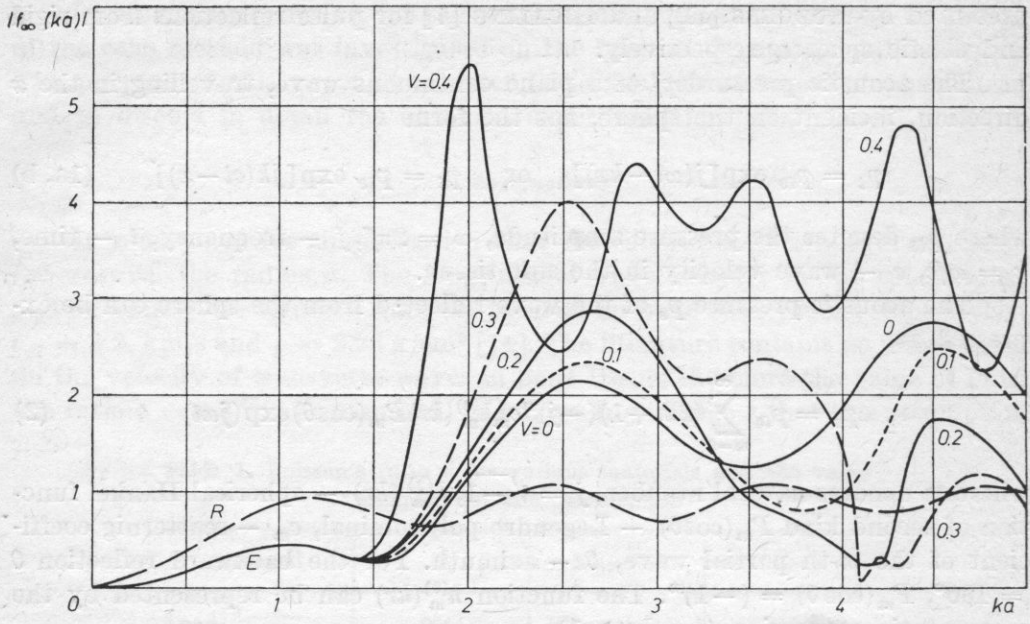

Fig. 1. Modulus of the far field form function $f_\infty(ka)$ (backward reflection) calculated for rigid (R) and elastic (E) spheres under consideration, v — Poisson's ratio

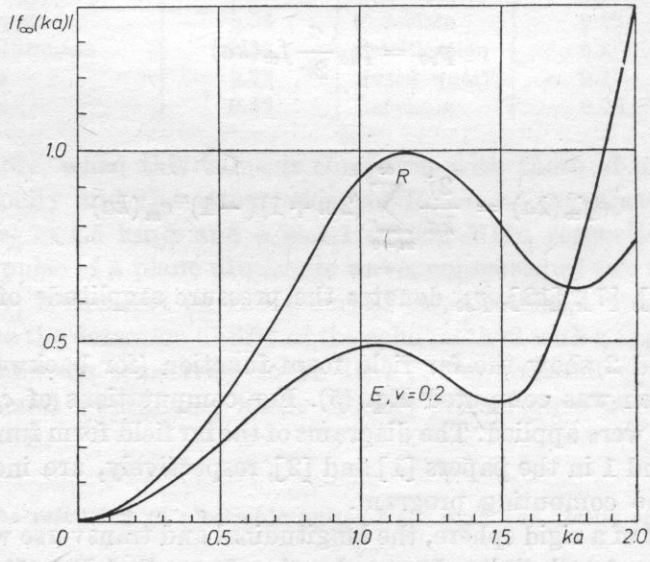

Fig. 2. Modulus of the function $f_\infty(ka)$ as in Fig. 1 but calculated for small arguments of ka ($v = 0{,}2$)

It follows from Eqs. (1a, b) that the acoustic pressure varies as a function of two variables, t and r. It is convenient to introduce one dimensionless variable in the form

$$\tau = (ct - r)/a \tag{6}$$

then Eq. (1b) becomes

$$p_i = p_{i0} \exp(jka\tau). \tag{7}$$

The last expression is valid for steady-state. In the case of transients the incident wave pulse can be represented in the form [11]

$$p_i = p_{i0} \prod (\tau/l - 1/2) \sin k_0 a\tau \tag{8}$$

where

$$\prod = \begin{cases} 1 \text{ when } |x| \leqslant 1/2, \\ 0 \text{ when } |x| > 1/2 \end{cases}$$

and $l = 2\pi b/k_0 a$ is the dimensionless pulse duration, b — number of high frequency periods, equals 2 in our case, k_0 — wave number corresponding to the carrier frequency of the incident wave pulse.

The incident wave pulse can be represented in the frequency domain as a function of a. However, in view of the form of Eqs. (7), (8), it will be given in a more general form, as a function of the dimensionless variable $\omega a/c = ka$. By using the inverse Fourier transform [8] the pulse reflected from the sphere can be represented in the form

$$p_s(\tau) = \frac{p_{i0}}{2\pi} \int_{-\infty}^{+\infty} \frac{a}{2r} f_\infty(ka) G_i(ka) \exp(jka\tau)\, d(ka) \tag{9}$$

where $G_i(ka)$ represents the spectrum of the incident pulse in the domain of ka, expressed as the Fourier transform of $p_i(\tau)$

$$G_i(ka) = \int_{-\infty}^{+\infty} p_i(\tau) \exp(-jka\tau)\, d\tau. \tag{10}$$

In Eq. (9), each monochromatic component of the incident pulse spectrum $G_i(ka)$ is weighted by the function $(a/2r)\, f_\infty(ka)$ [12] which represents the reflection spectral characteristics of the sphere.

Fig. 3 shows the reflected pulse shape computed as the real component from Eqs. (9), (10), (5), (8) for $k_0 a = 2.5$ ($f = 5$ MHz, $a = 0.12$ mm). Its relative amplitude is equal to 2.2, while the one of the reflected continuous wave, obtained directly from Fig. 1. equals 2.7. For $k_0 a = 1$ transient and steady-state analysis do not show any difference in the relative amplitude of the reflected wave being equal to 0.45.

The reflected pulse (Fig. 3) starts at $\tau = -2$, as this point corresponds to the pulse reflection from the anterior sphere surface ($r = a$) which takes place in the time $t = -a/c$. For our time coordinate starts at the instant in which the incident wave arrives at the sphere center, i.e., $t = 0$ for $r = 0$.

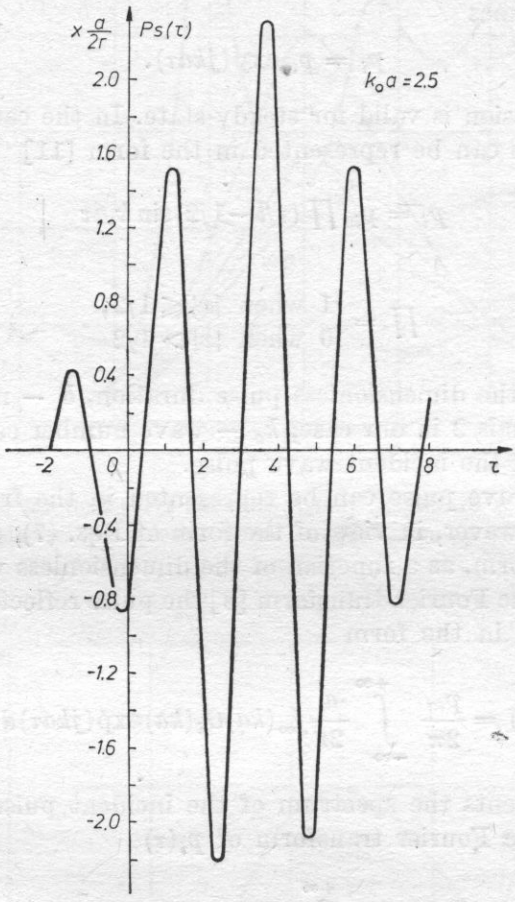

Fig. 3. Ultrasonic pulses reflected from elastic sphere under consideration for $k_0a = 2.5$

The frequency bandwidth of the incident wave pulse (between first zeros) falls within the interval (0.5–1.5) $\omega_0 = (0.5–1.5)\ k_0a$, where ω_0 denotes the angular carrier frequency of the pulse. It follows hence, that in the formation of integral (9) averaging of the function $f_\infty(ka)$ will occur over a large range of ka (see Fig. 1). In the case elastic sphere the function $f_\infty(ka)$ shows many peaks which correspond to many resonances occurring in the sphere. FLAX et al. [3] have shown that the scattering by elastic sphere is the superposition of the scattering by a rigid sphere and a number of resonances arising in the sphere. These resonances differ in character, since they correspond to different wave types, including also transverse waves, surface waves, of the "whispering gallery" type and so on.

Therefore, in the case of calcifications with irregular shapes and corrugated surfaces, one should expect that a number of resonances will not occur at all an average value of the function $f_\infty(ka)$ could, approximately, be taken as 1 for higher values of $k_0 a$. This approximation signifies in practice that the calcification model of the rigid sphere is accepted in this case.

4. Determination of the tissue interference background level

Many echoes obtained at the boundary of fat, fibre and gland tissues and on their inhomogeneities form a tissue interference background which may mask echoes from small calcifications. To determine the tissue interference background level, measurements were performed in 100 femal normal breasts of 50 women 21–54 years old at a depth of $r = 4$ cm by means of an echoscope with a non-focused ultrasonic beam of 5 MHz frequency (transducer radius $a_t = 2.5$ mm). The level of the tissue interference background was found $D = 27$ dB higher than the electronic noise level of the echoscope. The standard deviation of a single measurement was equal to $\sigma = 8$ dB. The electronic noise level was equal to 10 μV corresponding to the level $N = -148$ dB in respect to the transmitter signal of 240 V (in pulse), assumed as the reference level of 0 dB. Thus the overall electrical dynamics of the echoscope equated $W = 148$ dB.

The measurement idea is illustrated in Fig. 4. Taking into account transducing losses $T = -15$ dB, attenuation losses $A = \alpha \cdot 2r$ [cm]$\cdot f$[MHz] $= 44$ dB diffraction losses of the beam equal to 4 dB (not shown in Fig. 4) and the measured level D, one obtains the remaining value of the overall electrical dynamics equal to $\Delta W = 58$ dB. This value is crucial for the detection ability of calcifications.

To show that the obtained experimental results is probable from the theoretical point of view, we introduced a hypothetic reflector formed by the surface of the half-space H (Fig. 4) with characteristic acoustic impedance $\varrho' c' = \varrho c + \Delta\varrho c$. It can be assumed that tissue interference echoes result from the reflections of the ultrasonic beam when it is incident perpediculary at the plane surface of the reflector H. Different breast tissues may have irregular boundaries, however, highest echoes will be received from these surface elements of tissue boundaries, which are plane perpendicular to the ultrasonic beam axis.

If we assume that the plane reflecting surface element of the tissue boundary has a form of a disc with the diameter d, then the echo signal S_E can be expressed by the formula

$$S_E = \left(\frac{d}{D_b}\right) \delta_q S_T \quad \text{for } d \leqslant D_b \tag{11}$$

where D_b denotes the ultrasonic beam diameter, S_T — transmitting signal, q — reflection coefficient equal to

$$q = (\varrho' c' - \varrho c)/(\varrho' c' + \varrho c) \cong \Delta\varrho c / 2\varrho c. \tag{12}$$

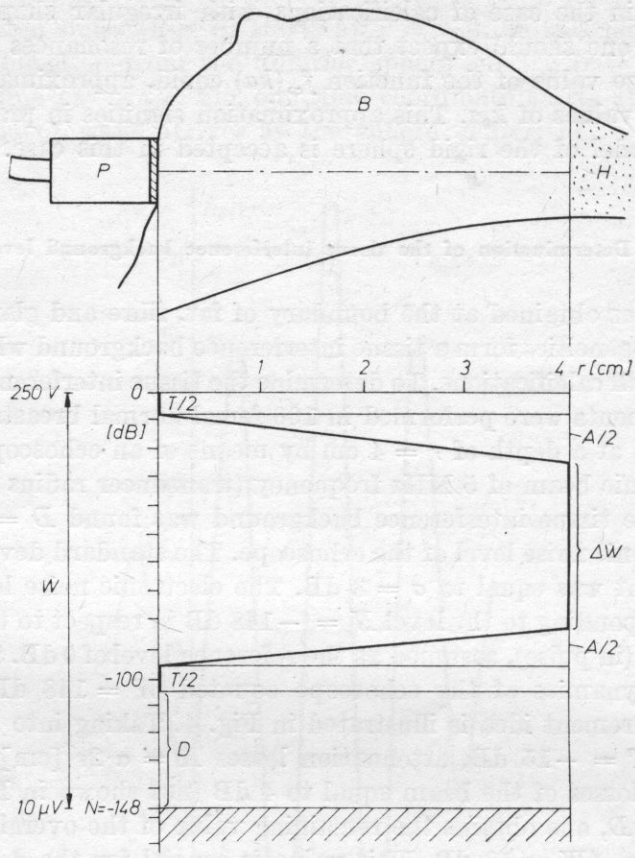

Fig. 4. The idea of the experimental determination of the tissue interference background level in womans breast: P — ultrasonic probe, B — breast, H — hypothetic reflector, O — level of the transmitting signal, T — transducing losses, A — attenuation losses in breast tissues, N — electronic noise level, W — electrical dynamics of the ultrasonograph, D — difference between the levels of the tissue interference background and the electronic noise, r — distance from the probe (depth)

The coefficient $\delta = \delta(r/l_0, d/D_b)$, depending on undulations in the ultrasonic field, can be found from the diagram determined experimentally by KRAUTKRÄMER [9], [10]. Its value tends to 1 for $r/l_0 \to 0$, where r is the distance between the reflector and the transducer, $l_0 = a_i^2/\lambda$ is the near field length. Eq. (11) is a generalized formula which for $q = 1$ was given and experimentally verified by KRAUTKRÄMER [9], [10]. For instance, in the case under consideration $D_b = 5$ mm, $d = 1$ mm, $r = 40$ mm, $l_0 = 21$ mm. For $r/l_0 = 2$ and $d/D_b = 0.2$ the coefficient $\delta = 1.8 - 5$ dB [10]. If one assumes for breast tissues $\Delta\varrho c/\varrho c = 5\,\%$ then Eqs. (13) and (14) give

$$S_E/S_T = 0.0018 = -55 \text{ dB}. \tag{13}$$

In this way we have shown that a small plane surface element of the tissue boundary, with the diameter of $d = 1$ mm, gives in uor case a maximum echo signal which is 55 dB lower than the transmitting signal S_T, incident at our hypothetic reflector. It means, that the resulting value $-\Delta W = S_E/S_T = -58$ dB obtained in measurements of the tissue interference background, seems to be most probable.

Now, equating ΔW to the ratio P_{s0}/P_{i0} one obtains from Eq. (4) the relation

$$\Delta W = \frac{a_m}{2r} f_\infty(ka_m) \tag{14}$$

where a_m denotes the radius of the calcification which given an echo on the level of the tissue interference background.

Table 2

r [cm]	R		$E(v = 0.2)$		R		R	
	a_m [mm]	ka	a_m [mm]	ka	$a_{2\sigma}$ [mm]	ka	$a_{3\sigma}$ [mm]	ka
2	0.09	1.9	0.085	1.77	0.4	8.5	1.0	21
4	0.1	2.25	0.09	1.9	0.6	13	1.6	34
6	0.11	2.25	0.09	1.93	0.7	14	1.7	35

If we assume that this level depends on the distance r according to the diagram of KRAUTKRÄMER [9] then ΔW for $r = 2$ cm is 4 dB greater and for $r = 6$ cm is 5 dB smaller than that one determined experimentally for the distance $r = 4$ cm. In this way one can find a_m from Eq. (14) for various values of r. Results of the calculations are shown in Table 2 for rigid and elastic spherical models of calcifications. The far field form function $f_\infty(ka)$ presented in Figs. 1 and 2 was applied in these computations.

It seems reasonable to assume the maximum error of single measurement of the tissue interference background to be 2σ or even 3σ. Then, according to the theory of error estimation [8] in the first case 97.72 % of all the values of $D = 27$ dB are smaller than $D+2\sigma = 43$ dB; the last value corresponding to $\Delta W = -42$ dB; in calcification detection to be certain, we assumed these limiting values in our calculations, thus determining the overestimated radius $a_{2\sigma}$ of the calcification which gives echoes higher by $2\sigma = 16$ dB (6.5 times) than the mean level of the tissue interference background. This seems to be necessary as in the case of small calcifications only the echo amplitude and no additional information e.g., on the shape, can be obtained. For the maximum error of 3σ one obtains the above values equal to 99.86 % and $\Delta W = -34$ dB, respectively.

Fig. 5 shows ultrasonic pulses reflected from elastic spherical calcifications, computed from Eqs. (9), (10), (5) and (8) for $k_0a = 5$ and 10. Their relative amplitudes are equal to 0.7 and 0.8, while those ones for the reflected continuous wave would be 1 (for $f_\infty(ka) = 1$). Thus the far field form function $f_\infty(ka)$ can be for $ka = 5$ or 10 approximated by the value of 1 giving an error in amplitude of 2 and 3 dB, respectively which can be neglected in our estimations. However, it is interesting to notice a great distortion of the shape of these reflected pulses.

5. Conclusions

Microcalcifications in the breast can not be detected with the ultrasonic echo method. The detectability is restricted by the tissue heterogeneities which constitute the background of tissue interference signals. The level of these signals was determined experimentally in 100 femal breasts. Assuming rigid and elastic spherical models, the radius of calcification which gives the same signal level was estimated to be $a_m = 0.1$ at the distance $r = 4$ cm and at the frequency of 5 MHz (standard deviation $\sigma = 8$ dB). This value does not depend distinctly on the distance $r = 2$–6 cm. For maximum sampling error 2σ and 3σ, assumed for a single measurement of the tissue interference background, the radii of detectable calcifications are equal to $a_{2\sigma} = 0.6$ mm and $a_{3\sigma} = 1.6$ mm, respectively.

a)

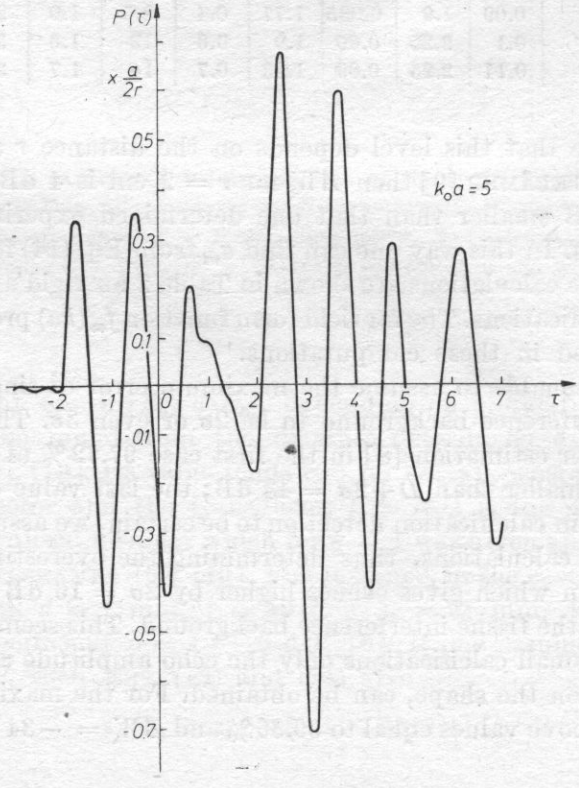

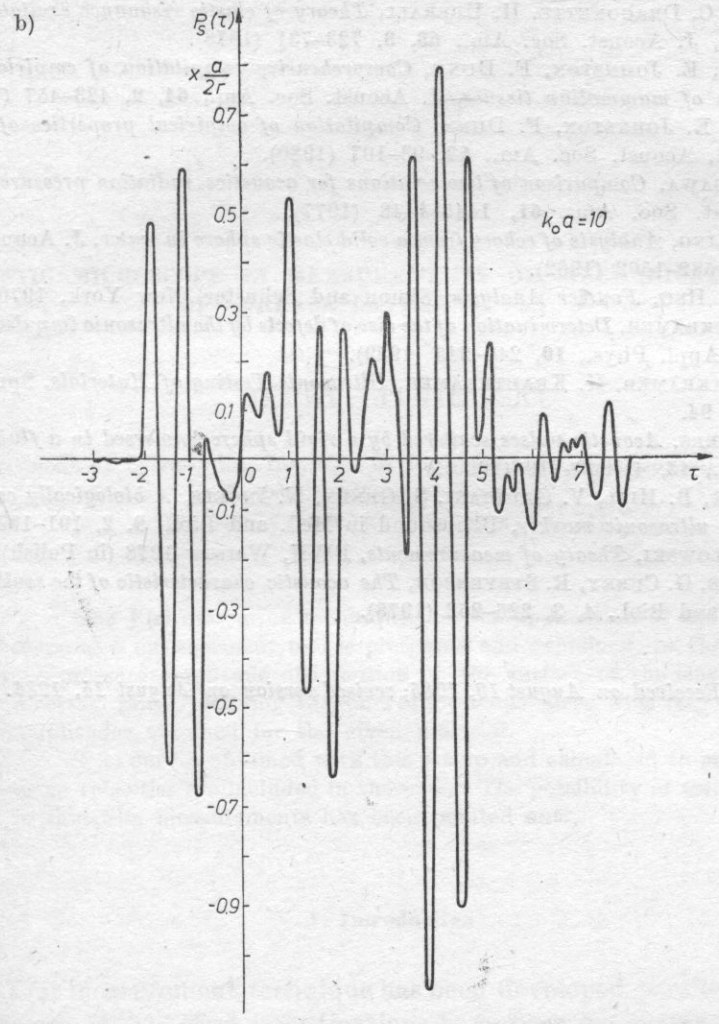

Fig. 5. Ultrasonic pulses reflected from elastic spheres under considerations for $k_0a = 5$ (a) and $k_0a = 10$ (b)

Both, rigid and elastic models give similar estimation results of calcification size. Therefore, it seems to be useful to apply the rigid spherical calcification model, in further research, as it is much simpler for computation than the elastic one.

References

[1] L. Filipczyński, *Detectability of calcifications in breast tissues by the ultrasonic echo method*, Archives of Acoustics, **8**, 3, 203–220 (1983).

[2] L. Filipczyński, G. Łypacewicz, *Estimation of calcification detectability in breast tissues by means of the ultrasonic echo and shadow method*, Archives of Acoustics, **9**, 1–2, 41–50 (1984).

[3] L. FLAX, C. DRAGONETTE, H. UBERALL, *Theory of elastic resonance excitation by sound scattering*, J. Acoust. Soc. Am., **63**, 3, 723–731 (1978).

[4] S. GROSS, E. JOHNSTON, F. DUNN, *Comprehensive compilation of empirical ultrasonic properties of mammalian tissues*, J. Acoust. Soc. Am., **64**, 2, 423–457 (1978).

[5] J. GOSS, E. JOHNSTON, F. DUNN, *Compilation of empirical properties of mammalian tissues*, J. Acoust. Soc. Am., **68**, 93–107 (1980).

[6] T. HASEGAWA, *Comparison of two solutions for acoustics radiation pressure on a sphere*, J. Acoust. Soc. Am., **61**, 1445–1448 (1977).

[7] R. HICKLING, *Analysis of echoes from a solid elastic sphere in water*, J. Acoust. Soc. Am., **34**, 10, 1582–1592 (1962).

[8] P. HWEI HSU, *Fourier Analysis*, Simon and Schuster, New York, 1970, p. 74.

[9] J. KRAUTKRÄMER, *Determination of the size of defects by the ultrasonic impulse echo method*, Brit. J. Appl. Phys., **10**, 240–245 (1959).

[10] J. KRAUTKRÄMER, H. KRAUTKRÄMER, *Ultrasonic Testing of Materials*, Springer, Berlin 1983, p. 94.

[11] A. RUDGERS, *Acoustic pulses scattered by a rigid sphere immersed in a fluid*, J. Acoust. Soc. Am., **45**, 4, 900–919 (1969).

[12] R. STERN, B. HILL, V. GAUDIANI, S. GREEN, N. INGELS, *A biologically compatible implantable ultrasonic marker*, Ultrasound in Med. and Biol., **9**, 2, 191–199 (1983).

[13] H. SZYDŁOWSKI, *Theory of measurements*, PWN, Warsaw 1978 (in Polish).

[14] D. WHITE, G. CURRY, R. STEVENSON, *The acoustic characteristic of the scull*, Ultrasound in Med. and Biol., **4**, 3, 225–252 (1978).

Received on August 19, 1985; revised version on August 15, 1986.

ARCHIVES OF ACOUSTICS
11, 3, 299-312 (1986)

AN ACOUSTIC MICROSCOPE IN MEASUREMENTS OF MECHANICAL PROPERTIES OF SURFACE LAYERS — $V(z)$

JERZY LITNIEWSKI

Department of Ultrasonics, Institute of Fundamental Technological Research,
Polish Academy of Sciences
(00-049 Warsaw, ul. Świętokrzyska 21)

The $V(z)$ measuring technique, i.e. the application of the acoustic microscope as a measurement tool is presented and explained. In the measurements, the pressure amplitude distribution on the surface of the lens is controlled in a certain range, enabling $V(z)$ curves to be optimized with respect to oscillation amplitudes obtained for the given material.

$V(z)$ curves obtained with this set-up and calculated from them Rayleigh wave velocities are included in the paper. The possibility of using such a set-up in thin film measurements has been pointed out.

1. Introduction

The $V(z)$ measurement technique has been developed parallely with acoustic microscopy [1, 2]. First investigations have been conducted independently by A. ATALAR at the university in Stanford and R. G. WILSON in Hughes [3, 4]. This technique applies the acoustic microscope which acts in reflection mode.

A strongly focused beam of ultrasounds (frequency 20 MHz — 100 GHz) is reflected from a sample located in the focal plane, returns to the piezoelectronic transducer and induces an electric signal, which controls the brightness of the spot on the screen [5, 6]. The sample is scanned in the XY plane and the location of the focal point on the sample is correlated with the position of the spot on the screen.

If we stop XY scanning and the distance along the Z-axis will be changed, i.e. the distance between the sample and the lens, then the voltage on the transducer proves to depend strongly on this distance. Graphs of voltage in terms of the lenssample distance have been called $V(z)$ curves. The $V(z)$ curve for a dis-

tance z, between the focal point of the lens and the radius of curvature of the lens seems particularily interesting. In this range, the oscillation period of $V(z)$ curves is velocity-dependent and the amplitude is dependent on the attenuation of Rayleigh waves, which can propagate on the surface of the sample. Therefore, $V(z)$ curves are called "acoustic material signature", because they univocally characterize the investigated material.

Leading research centres conduct work on the utilization of the $V(z)$ technique in many fields of science, such as:

- measurements of velocity and attenuation of surface waves [7, 8, 9],
- film thickness measurements [10, 11],
- crystal acoustic anisotropy investigations [12],
- detection of subsurface cracks [13],
- measurements of rates of surface hardening [14],
- investigations of the influence of heat treatment on the surface [14],
- measurements of residual stress patterns [15],
- determination of surface distribution of the coefficient of reflection [16, 17],
- acoustic parameter distribution measurements in living cells [18].

Theoretical and experimental research of the process of forming of $V(z)$ curves can lead to the interpretation of images obtained in the acoustic microscope. However, although acoustic microscope technology is highly advanced and microscope images of various materials and biologic samples are being obtained, this problem has not been solved yet.

In our case the lens is located in the near field of the transducer, what through frequency tuning of the sending-receiving transducer enables changes of the pressure amplitude distribution on the lens surface, and thus the optimization of the $V(z)$ curve in terms of the oscillation amplitude.

2. Physical interpretation of the $V(z)$ curve forming effect

W. PARMON and H. L. BERTONI have given the simplest physical interpretation of $V(z)$ forming on basis of the approximation of "geometric acoustics". From among rays reflected directly from the investigated surface (located outside the focal point) only rays near the axis of the system can reach the transducer. At the same time, waves inciding onto the sample under an angle close to the Rayleigh angle induce a *LRW* surface wave (*Leaky Rayleigh Wave*), which propagates on the sample surface and radiates a longitudinal wave under the Rayleigh angle, θ_R, into the liquid. After passing through the lens a part of these waves reach the transducer. The interference of the directly reflected wave and the wave induced by the surface wave occurs on the surface of the transducer. Changes of the distance, z, give rise to a change in the path and phase of the wave, what leads to the oscillations of the $V(z)$ function. The

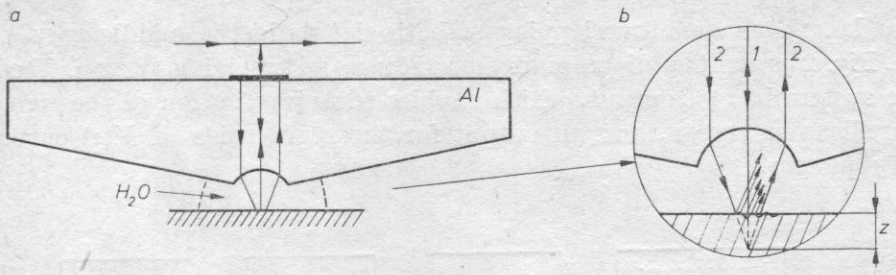

Fig. 1. a) Diagram of the acoustic part of the system for obtaining $V(z)$ curves; b) Diagram of waves composing $V(z)$, i.e. wave directly reflected and wave from *LRW*

oscillation period of the $V(z)$ can be determined on the basis of the given above interpretation. According to the denotation in Fig. 1, the phases of both ray beams can be expressed as follows:

$$\Phi_1 = \Phi_r - \frac{4\pi z}{\lambda_w}, \quad \Phi_2 = \Phi_f - \frac{4\pi z}{\lambda_w \cos\theta_R} + \frac{4\pi z \operatorname{tg}\theta_R}{\lambda_r} + \pi \tag{1}$$

where Φ_f – ray phase for $z = 0$, θ_R – Rayleigh angle $\left(\sin\theta_R = \frac{\lambda_w}{\lambda_R}\right)$, λ_R – Rayleigh wave length, λ_w – wave length in water.

The phase of the wave radiated into water was increased by π according to [20]. The phase difference is:

$$\Phi_1 - \Phi_2 = \frac{4\pi(1-\cos\theta_R)z}{\lambda_R \sin\theta_R} + \pi. \tag{2}$$

The minimum of the $V(z)$ curve is obtained when the phase difference is equal to the π odd multiply. Thus, the calculated $V(z)$ period is:

$$\Delta z = \frac{\lambda_R}{\sin\theta_R}\left(\frac{1+\cos\theta_R}{2}\right). \tag{3}$$

This result is in very good concurrence with experiment.

3. The set-up for obtaining $V(z)$ curves

The experimental set-up built at the Department of Ultrasonics of the IFTR operates in the 30–40 MHz frequency range. Differences in time in which the signal directly reflected from the sample and the signal coming from *LRW* reach the transducer can be derived from eq. (2) for this system. This difference equals 0.2 μs for the reflection from an aluminium sample at a frequency of 36 MHz. Hence, sending pulses of a 1 μs length were used in measurements, because

such a length ensured overlapping of both signals in the middle part of the pulse. Fig. 2 presents a diagram of the sending and receiving system. The electronic system has an output, which enables the visualization of the signal on the oscilloscope screen, and an output for the registration of $V(z)$ curves on the xy plotter.

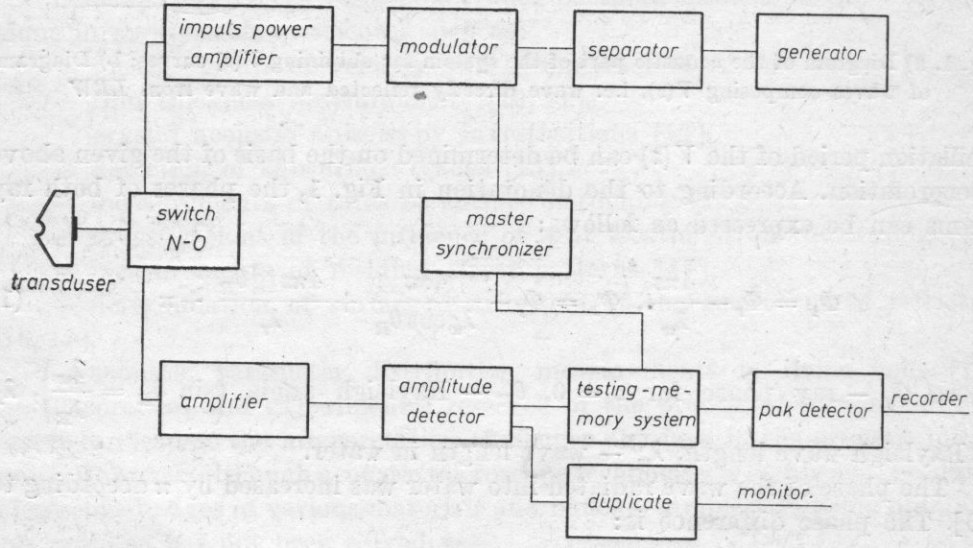

Fig. 2. Diagram of the electronic part of the system for obtaining $V(z)$ curves

The lens with the radius of the spherical cap of 3 mm, was made from aluminium, for which the measured coefficient of damping of a longitudinal wave in this frequency range does not exceed 0.12 dB/cm. Geometrical dimensions of the lens and the whole cylinder were chosen in such a manner that interfering signals reflected from the cylinder walls reached the transducer in a longer time than the signal reflected from the sample. The transducer has a 3 mm radius and the distance between the lens and the transducer equals 22.5 mm. Thus, the lens is situated in the near field of the transducer. When the distance z is changed, then the measured signal moves in a range free from acoustic noise, determined by signals generated by the first and second reflection from the surface of the lens.

The area between the lens and the sample was filled with water. The diameter of the focal point formed by such a system theoretically equals 1.8 wave lengths in water (about 74 μm). The mechanical system ensures sample movement in three directions with the accuracy of setting of 0.01 mm, and the regulation of the inclination of the sample with regard to the axis of the system with the accuracy of 0.5 min.

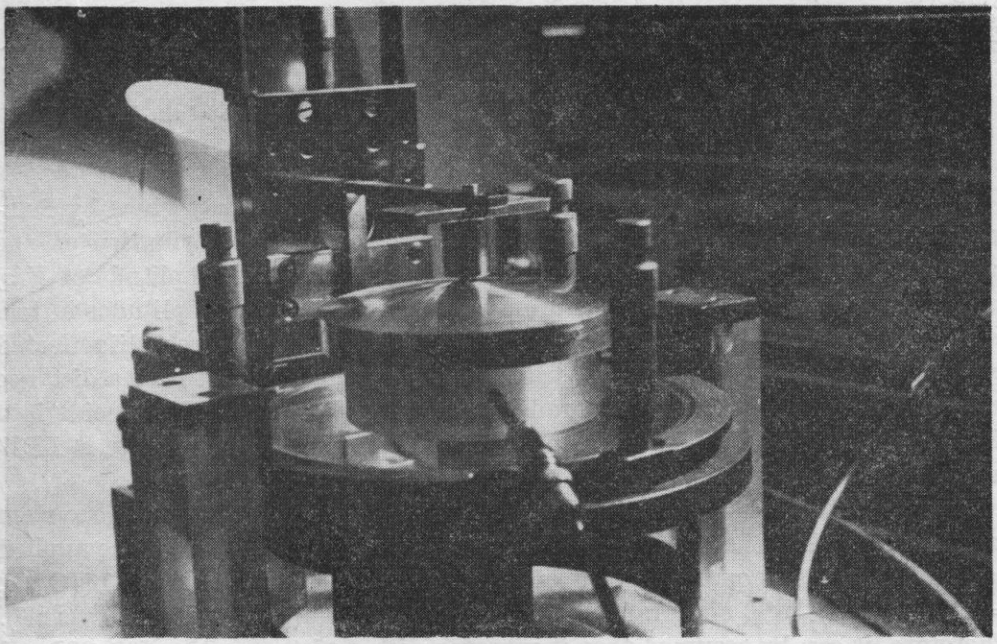

Fig. 3. Photograph of the set-up for obtaining $V(z)$ curves, built at the Department of Ultrasonics IFTR

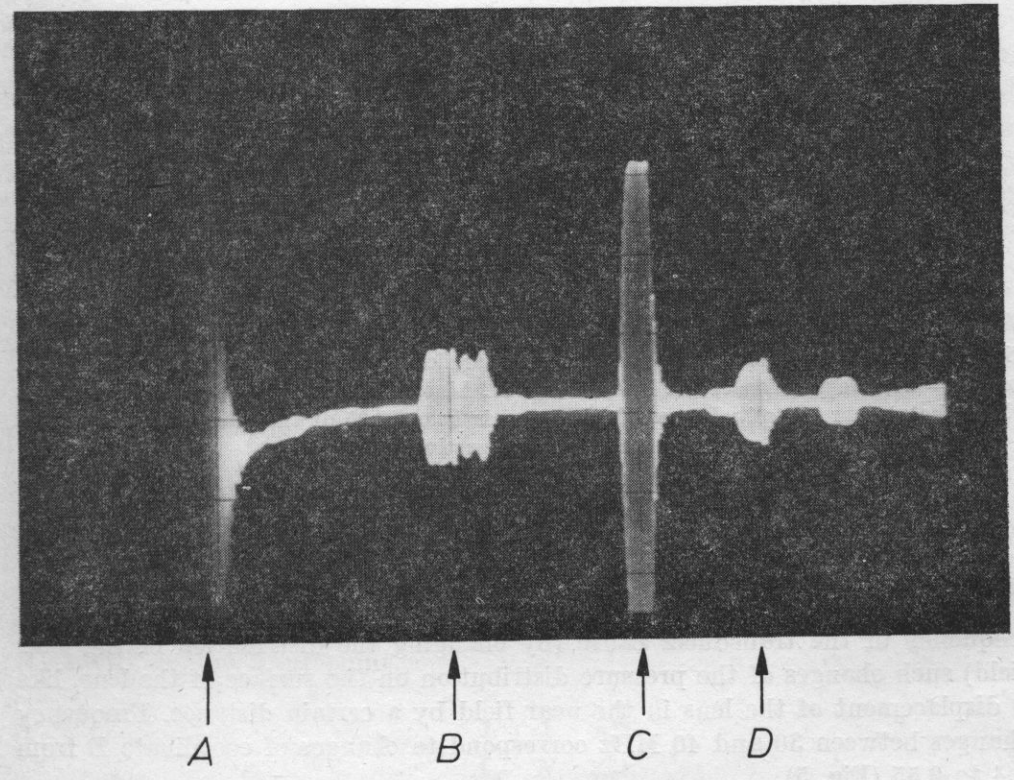

Fig. 4. Photograph of the oscilloscope screen. High frequency signals, from the left: A — sending signal, B — reflection from the lens surface, C — signal reflected from the sample, D — second reflection from the lens surface

4. The influence of the pressure amplitude distribution on the surface of the lens on the oscillation amplitude of $V(z)$ curves

The interpretation of the process of forming of $V(z)$ curves given by PARMON, BERTONI [19] suggests, that the pressure amplitude distribution on the surface of the lens should decisively influence the oscillation amplitude of $V(z)$ curves. Especially, it should depend on the ratio of pressure amplitudes in two regions of the lens — the region near the axis of the system, where radii reflected from the sample directly reach the transducer, and the region at such a distance from the axis of the system, that radii after going through the lens incide into the sample under an angle close to the Rayleigh angle and generate a *LRW* surface wave.

In order to investigate this relationship the spherical surface of the system lens was located in the near field of the transducer. The thickness of the applied here transducer is equal to 1/120 of its diameter. It is made from $LiJO_3$ ($\varrho_c = 18.5 \cdot 10^6$ kg/s m^2) and radiates into aluminium ($\varrho_c = 17.3 \cdot 10^6$ kg/s m^2). Therefore, it can be assumed that it vibrates with a piston motion [22, 23] and thus calculation results from ZEMANEK'S paper [26] can be applied in this case.

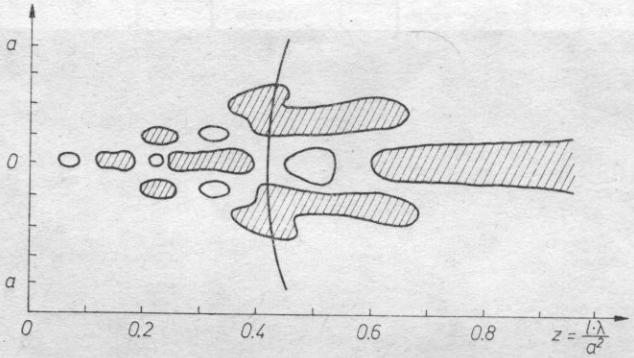

Fig. 5. Pressure amplitude distribution in the near field of the transducer with a radius a, for $a/\lambda = 20$; the position of the lens is denoted. Lined and not lined regions mark places where the pressure amplitude exceeds 0.85 and is below 0.35 of the maximal value of the amplitude, respectively

Fig. 5 presents the theoretical pressure amplitude distribution for a transducer vibrating with a piston motion and with a radius a, and a lens situated in this field [26]. Coordinate $D (D = l\lambda/a^2)$ depends on the product of the wave length λ and the distance from the transducer, l. Hence, changes of the operating frequency of the transducer cause (by changing the distribution of the near field) such changes of the pressure distribution on the surface of the lens, like a displacement of the lens in the near field by a certain distance. Frequency changes between 30 and 40 MHz correspond to changes of coordinate D from 0.4 to 0.55 (Fig. 5).

Phase changes in the pressure distribution on the surface of the lens, due to changes of the operating frequency of the transducer, do not influence the oscillation amplitude of the $V(z)$ curve, because possible additional phase shifts between the wave reflected directly from the sample and the wave from the *LRW* add up with the phase difference generated during the formation of the $V(z)$ curve (2) and thus the $V(z)$ curve is only shifted along the Z-axis without a change in its shape.

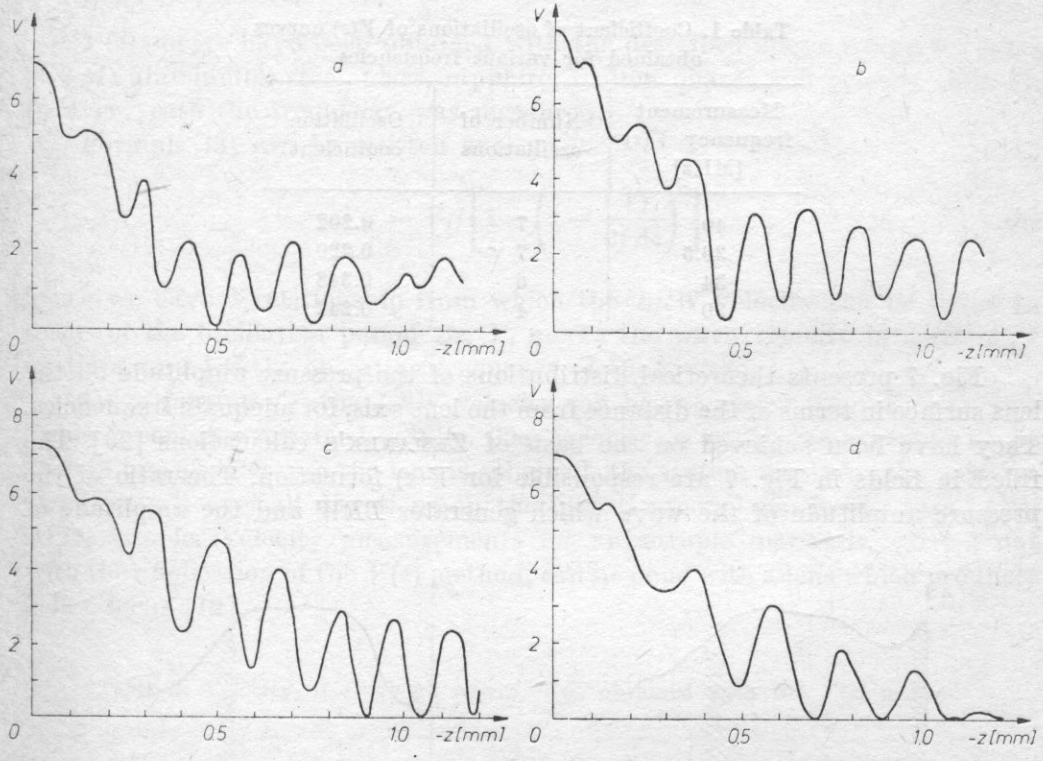

Fig. 6. $V(z)$ curves for an aluminium sample obtained for various frequencies: a) 40 MHz, b) 36.5 MHz, c) 34 MHz, d) 30 MHz

Measurements were performed for four frequencies (30, 34, 36.5, 40 MHz). Fig. 6 presents $V(z)$ curves for an aluminium sample. The coefficient determining the degree of oscillation of the $V(z)$ curve (WO — coefficient of oscillations) has been calculated for every curve. It is defined as the ratio of the mean oscillation amplitude of $V(z)$ to the value of the signal received when the sample is exactly in the focal point.

$$WO = \frac{1}{A_0} \cdot \frac{1}{N} \cdot \sum_{i=1}^{N} A_i \tag{4}$$

where: N — quantity of oscillations, A_i — amplitude of the i-th oscillation, A_0 — amplitude of the voltage from the transducer for a sample in the focal point.

Calculated WO values are given in Table 1.

This coefficient has the maximal value at the frequency of 34 MHz and hence the distribution of the pressure amplitude in this frequency range is optimal for the formation of a $V(z)$ curve.

Table 1. Coefficient of oscillations of $V(z)$ curves obtained for various frequencies

Measurement frequency $V(z)$ [MHz]	Number of oscillations	Oscillation coefficient
40	7	0.202
36.5	7	0.220
34	6	0.348
30	4	0.242

Fig. 7 presents theoretical distributions of the pressure amplitude on the lens surface in terms of the distance from the lens axis, for adequate frequencies. They have been achieved on the basis of ZEMANEK'S calculations [26]. The filled in fields in Fig. 7 are responsible for $V(z)$ formation. The ratio of the pressure amplitude of the wave which generates LRW and the amplitude of

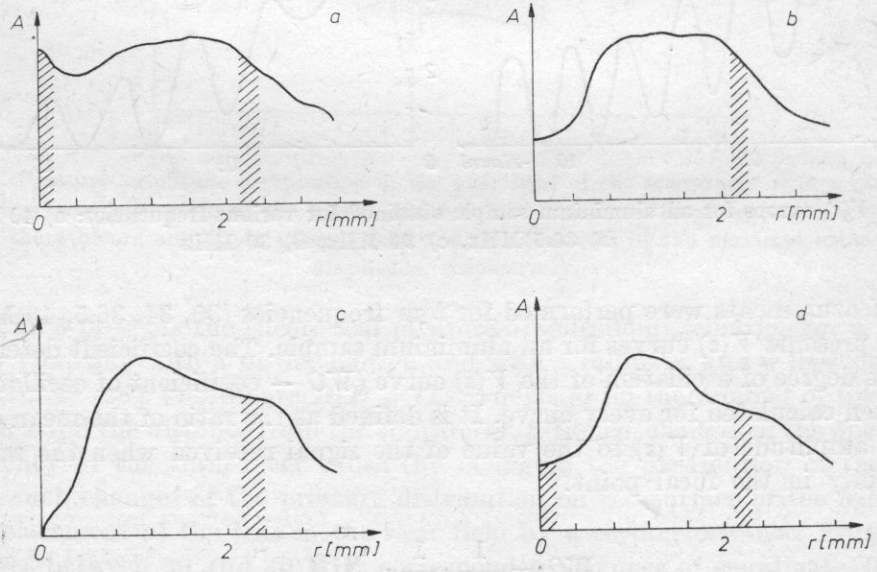

Fig. 7. Distributions of pressure amplitude (A) on the surface of the lens in terms of distance (r) from the axis of the lens, calculated for various frequencies: a) 40 MHz, b) 36.5 MHz, c) 34 MHz, d) 30 MHz

the wave which propagates along the axis is greatest for the frequency of 34 MHz. Because also the maximal oscillation amplitude of $V(z)$ is obtained for this frequency, then such conditions ensure an optimal ratio of the $V(z)$ components, i.e. the wave from the *LRW* and wave reflected directly from the sample.

5. Measurement of surface waves velocities with the $V(z)$ method

$V(z)$ curves have been obtained with the described above set-up for samples of: aluminium, steel, glass, sapphire, molten quartz and perspex (Fig. 8). In every case the frequency was measured.

Formula (3) can be written as:

$$V_R = V_l / \left[1 - \left(1 - \frac{V_l}{2f\Delta z}\right)^2\right]^{1/2} \tag{5}$$

hence we have a relationship from which the *LRW* velocity can be found in terms of the oscillation period Δz. V_l marks the wave velocity in a coupling medium, and f is the operating frequency of the system.

Using formula (5) the *LRW* velocity can be calculated from $V(z)$ curves. Table 2 contains obtained results. The velocity in water was accepted at $V_l = 1.48$ mm/μs. Because the lens is spherical, the system measures the velocity V_r, averaged over all directions on the investigated plane, in the case of an Al_2O_3 sample. Velocity measurements for anisotropic materials, carried out with the application of the $V(z)$ method, can be done with a lens which produces a line-focus [12].

Table 2. Velocity of Rayleigh waves, V_R, obtained with the $V(z)$ method

Material	Number of oscillations	Period of $V(z)$ [10^{-3} m]	V_R calculated [10^3m s^{-1}]	Measurement accuracy [%]
Aluminium (37.1 MHz)	5	0.150	2.97	3.4
Steel (NC 10) (37.1 MHz)	6	0.158	3.04	2.6
Glass (crown) (37.1 MHz)	4	0.180	3.23	3.1
Molten quartz (33.3 MHz)	3	0.214	3.36	1.5
Al_2O_3C (34.1 MHz)	2	0.535	5.25	4.2
Perspex (35.6 MHz)	3	0.137	2.82	4.3

Interesting results have been obtained for the perspex sample. In this case *LRW* generation does not occur, because the velocity of Rayleigh waves is lower in perspex than in water. So here the lateral wave, which propagates on the water-perspex interface with the velocity of a longitudinal wave in perspex, is responsible for the generation of $V(z)$ curves [24].

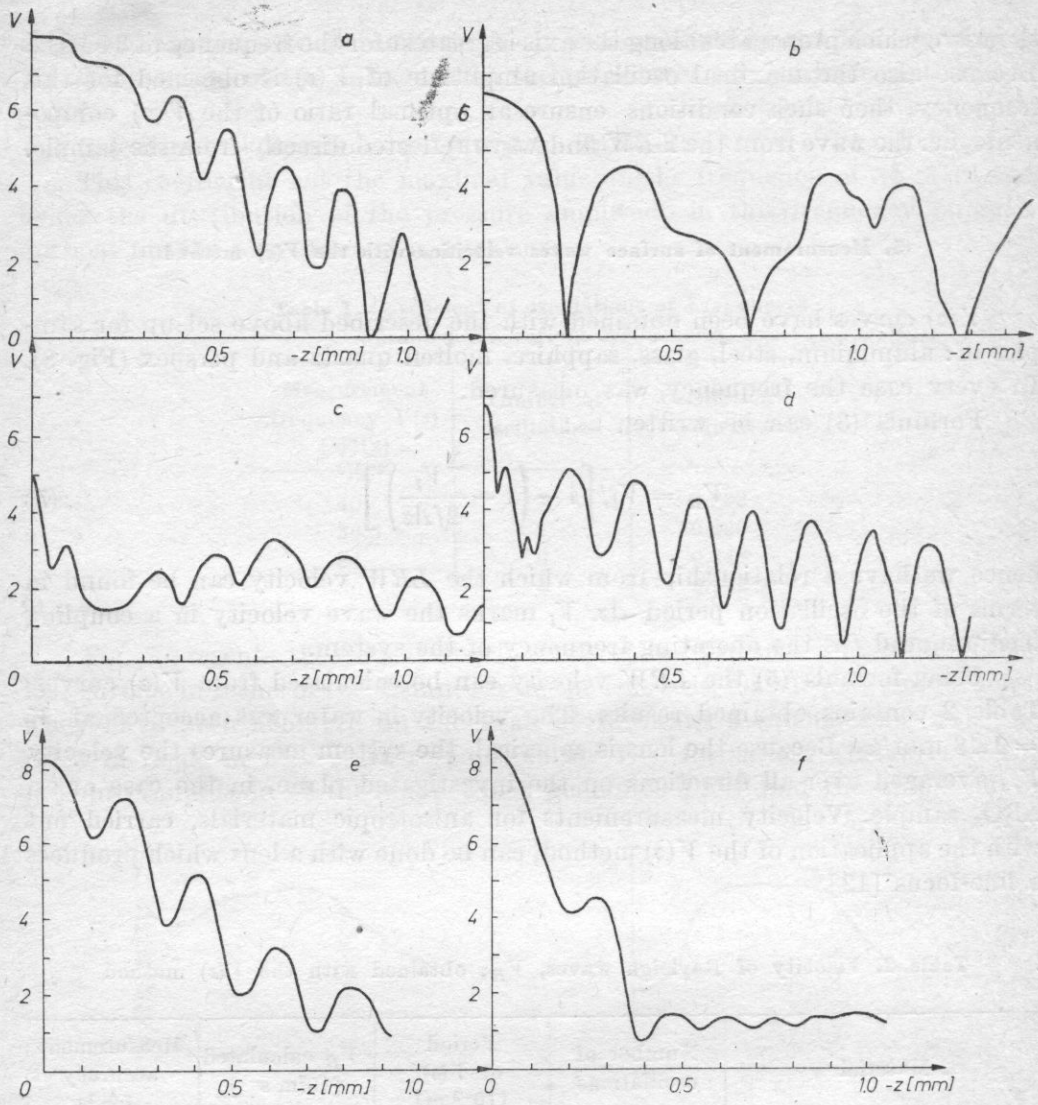

Fig. 8. $V(z)$ curves obtained for a) aluminium, b) Al_2O_3, c) crown-glass, d) steel — NC10, e) molten quartz, f) perspex

The accuracy of obtained results depends mainly on the error in determining the period Δz. An inaccuracy of ± 5 μm in measuring Δz causes a velocity error of 0.1 mm/μs. Additional disturbances are introduced by low-amplitude oscillations, with a period equal to 0.5 wave lengths in water, which overlap $V(z)$. Measuring errors can also result from inaccuracies in setting the sample perpendicularily in respect to the axis of the system.

Very accurate velocity measurements can be done with the application of the numerical technique in finding the oscillation period of $V(z)$, by determining the spectrum of the $V(z)$ function [25].

6. Film thickness measurement with the $V(z)$ method

The $V(z)$ technique also can find application in indirect measurements of the thickness of thin films [10]. To this end the dispersion curve of a surface wave in the film has to be found. Having the relationship between film thickness and surface wave velocity, the film thickness can be determined from velocity measurements.

The following experiment confirms the applicability of the $V(z)$ technique and the built set-up to velocity measurements of surface waves in terms of film thickness.

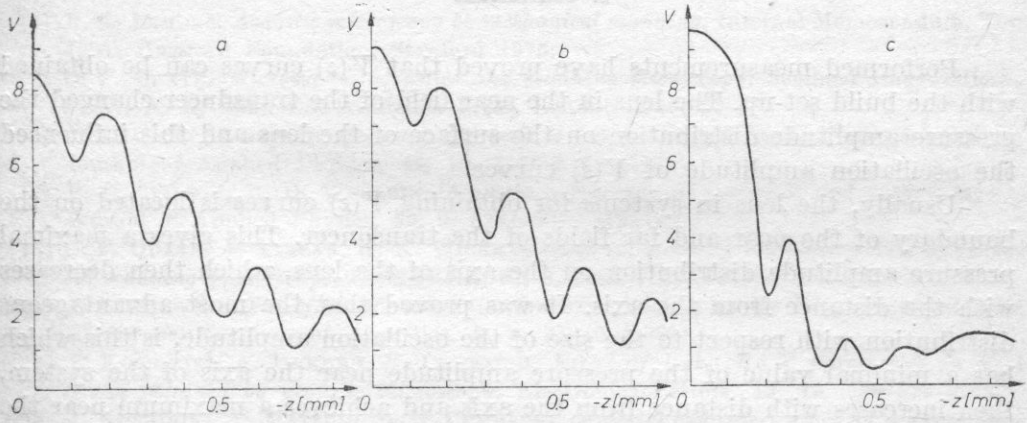

Fig. 9. $V(z)$ curves obtained for a molten quartz sample with a gold film: a) sample of pure molten quartz, b) sample with a 0.2 μm gold film, c) sample with a 0.8 μm gold film

A sample of molten quartz has been covered in two places with a gold film of a 0.2 μm and 0.8 μm thickness (this is 0.002 λ_0 and 0.008 λ_0, respectively, where λ_0 is the length of a Rayleigh wave on the surface of molten quartz). $V(z)$ curves have been obtained for these covered areas and for pure molten quartz. The measurement frequency was optimized and set at 33.3 MHz. The oscillation period of $V(z)$ curves decreased with the increase of thickness. This corresponds to a decrease of the surface wave velocity. The measured oscillation period was used in the calculation of the Rayleigh wave velocity. Table 3 presents the results in terms of film thickness.

A relatively high velocity decrease ($\simeq 5\%$) for a very thin layer of gold (0.002 λ_0) indicates high sensitivity of the method in film thickness measurements. The velocity measuring error for a quartz sample equals about 1.5%. Therefore, the application of this set-up and method should make it possible to observe a gold layer of a 0.0006 λ_0 thickness. This leads to a conclusion that a system with the lens situated in the near field of the transducer is more sensitive than a system with the lens on the boundary of the far and near field [10].

Table 3. Measurement results of *LRW* velocities on a molten quartz sample with a gold film

Gold film thickness $[10^{-6}\ \mathrm{m}(\lambda_0)]$	Oscillation period $[10^{-3}\ \mathrm{m}]$	Calculated velocity $[10^3\ \mathrm{m\ s^{-1}}]$
0	0.214	3.36
0.2 (0.002)	0.192	3.19 95%
0.8 (0.008)	0.163	2.96 88%

7. Conclusions

Performed measurements have proved that $V(z)$ curves can be obtained with the build set-up. The lens in the near field of the transducer changed the pressure amplitude distribution on the surface of the lens and this influenced the oscillation amplitude of $V(z)$ curves.

Usually, the lens in systems for obtaining $V(z)$ curves is located on the boundary of the near and far fields of the transducer. This gives a maximal pressure amplitude distribution on the axis of the lens, which then decreases with the distance from the axis. It was proved that the most advantageous distribution with respect to the size of the oscillation amplitude, is this which has a minimal value of the pressure amplitude near the axis of the system, then increases with distance from the axis and achieves a maximum near the part of the lens which refracts the wave in such a manner that it incides onto the sample under the Rayleigh angle. It seems that an adequate choice of the pressure distribution on the lens can lead to "better" $V(z)$ curves, i.e. curves which allow more accurate velocity measurements or observations of velocity changes on the surface of materials strongly damping to Rayleigh waves.

The measuring accuracy can be increased still by increasing the accuracy of reading of the oscillation period Δz and by obtaining a precisely perpendicular position of the investigated surface in respect to the lens axis.

The greatest advantage of measurements conducted with the $V(z)$ method are results averaged over scarcely ten to twenty wave lengths. Due to this maps of velocity distribution of Rayleigh waves on a given surface can be made.

$V(z)$ curves are sensitive to changes of velocity and damping of surface waves and this causes changes of frequency or oscillation amplitude. Also faults in the investigated material, which interact with the propagating surface wave, should influence $V(z)$ curves. Therefore, the $V(z)$ method is particularily useful in investigations of surface layers of materials.

Acknowledgement

The first in Poland microscope system for ultrasonic investigations by the $V(z)$ method was built at the Department of Ultrasonics IFTR-PAS. This was possible thanks to Prof. L. Filipczyński and Dr. J. Zieniuk as well as Dr. A. Latuszek. The author would also like to thank Doc. S. Turczyński and M. Sc. K. Stypuła for their help in building the electronic part of the system.

References

[1] R. A. Lemons, *Acoustic microscopy by mechanical scanning*, Internal Memorandum, The J. A. Hartford Foundation, Stanford 1975.

[2] C. F. Quate, *Microwaves, acoustics and scanning microscopy*, Scanned Image Microscopy, E. A. Ash., Ed. Academic Press, London 1980, 23–55.

[3] A. Atalar, *An angular spectrum approach to contrast in reflection acoustic microscopy*, Journal of Applied Physics, **49**, 10, 5130–5139 (1978).

[4] R. G. Wilson, R. D. Weglein, *Acoustic microscopy of materials and surface layers*, Journal of Applied Physics, **55**, 9, 3261–3275 (1984).

[5] C. F. Quate, A. Atalar, H. K. Wickramasinghe, *Acoustic microscopy with mechanical scanning — a review*, Proc. IEEE, **67**, 8, 1092–1113 (1979).

[6] J. Litniewski, *The effect of modulation transfer function on the image in an acoustic microscope*, Archives of Acoustics, **8**, 1, 31–40 (1983).

[7] J. Kushibiki, A. Ohkubo, N. Chubachi, *Effect of leaky SAW parameters on $V(z)$ curves obtained by acoustic microscopy*, Electronics Letters, **18**, 15, 668–670 (1982).

[8] J. Kushibiki, Y. Matsumoto, N. Chubachi, *Material characterization by acoustic line-focus beam*, Acoustical Imaging, 13, Plenum Press, N. York 1983, 193–202.

[9] A. A. Kulakov, A. I. Morozov, *Peculiarities of SAW velocity measurements by acoustic microscope*, Proc. of The First Soviet-West Germany International Symposium on Microscope Photometry and Acoustic Microscopy in Science, Moscow 1985, 80–84.

[10] R. Weglein, *Acoustic microscopy applied to SAW dispersion and film thickness measurement*, IEEE Trans. Sonics Ultrason., **SU-27**, 2, 82–86 (1980).

[11] R. Weglein, *Non-destructive film thickness measurement on industrial diamond*, Electronics Letters, **18**, 23, 1003–1004 (1982).

[12] J. Kushibiki, A. Ohkubo, N. Chubachi, *Material characterization by acoustic microscope with line-focus beam*, Acoustical Imaging, 12, Plenum Press, N. York 1982, 101–111.

[13] M. G. Soumekh, G. A. D. Briggs, C. Ilett, *Detection of surfacebreaking cracks in the acoustic microscope*, Acoustical Imaging, 13, Plenum Press, N. York 1983, 119–128.

[14] K. Yamanaka, Y. Enomoto, Y. Tsuya, *Application of scanning acoustic microscope to the study of fracture and wear*, Acoustical Imaging, 12, Plenum Press, N. York 1982, 79–87.

[15] K. Liang, B. T. Khuri-Yakub, S. D. Bennett, G. S. Kino, *Phase measurements in acoustic microscopy*, Proc. Ultrasonics Symposium, Atlanta 1983, **2**, 591–604.

[16] J. A. Hildebrand, K. Liang, S. D. Bennett, *Fourier transform approach to materials characterization with the acoustic microscope*, Journal of Applied Physics, **54**, 12, 70 16–7019 (1983).

[17] K. K. LIANG, G. S. KINO, B. T. KHURI-YAKUB, *Material characterization by the inversion of V(z)*, IEEE Trans. on Sonics and Ultrasonics, **SU-32**, 2, 213–224 (1985).

[18] J. A. HILDEBRAND, D. RUGER, R. N. JOHNSTON, C. F. QUATE, *Acoustic microscopy of living cells*, Proc. Nat. Acad. Sci. USA, **78**, 3, 1656–1660 (1981).

[19] W. PARMON, H. L. BERTONI, *Ray interpretation of the material signature in the acoustic microscope*, Electronics Letters, **15**, 21, 684–689 (1979).

[20] H. L. BERTONI, T. TAMIR, *Unified theory of Rayleigh-angle phenomena for acoustic beams at liquid-solid interfaces*, Applied Physics, 2, 157–172 (1973).

[21] R. WEGLEIN, *A model for predicting acoustic material signature*, Appl. Phys. Lett. **34**, 3, 179–181 (1979).

[22] G. ŁYPACEWICZ, L. FILIPCZYŃSKI, *Measurement method and experimental study of ceramic transducer vibrations*, Acustica, **25**, 1971.

[23] D. BELINCOURT, D. CURRAN, H. JAFFE, *Piezoelectric and piezomagnetic materials and their function in transducers*, Physical Acoustics, Academic Press, vol. 1, part A, New York 1964.

[24] L. M. BREKHOVSKIKH, *Waves in Layered Media*, Academic Press, New York 1960.

[25] J. KUSHIBIKI, N. CHUBACHI, K. HORRI, *Velocity measurement of multiple leaky waves on germanium by line-focus-beam acoustic microscope using FFT*, Electronics Letters, **19**, 11, 404–405 (1983).

[26] J. ZEMANEK, *Beam Behaviour within the Near Field of a Vibrating Piston*, JASA, **49**, 1. 181–191 (1971).

Received on Febraury 5, 1986; revised version on May 25, 1986.

ARCHIVES OF ACOUSTICS
11, 3, 313-324 (1986)

DETERMINATION OF AVERAGE LENGTHS OF CONCENTRATION WAVES AND OF THE DIFFUSION COEFFICIENT OF THE CRITICAL N-AMYLIC ALCOHOL-NITROMETHANE MIXTURE*

MIKOŁAJ ŁABOWSKI, TOMASZ HORNOWSKI

Institute of Acoustics, A. Mickiewicz University
(60-769 Poznań, ul. Matejki 48/49)

The kinetics of concentration fluctuations in the critical *n*-amylic alcohol-nitromethane mixture have been analysed in this paper. Average lengths of concentration waves and the diffusion coefficient for investigated mixtures have been established on the basis of results obtained previously by the authors from estimations of the average relaxation time of concentration fluctuations and the radius of their correlation.

1. Introduction

The structure of various liquid mixtures and their molecular micsibility has not been hitherto sufficiently explained. Various methods are being applied in this problem, but optic and acoustic methods prove to be the most useful. The method of molecular light scattering proved very effective in explaining: the state of short-range order in liquids, liquid molecular micsibility and the influence of various factors on the micsibility. Molecular light scattering is caused by non-homogeneities of the dispersion medium. These non-homogeneities in mixtures are: density, concentration and orientation fluctuations of anisotropic molecules.

A strong increase of the absorption of acoustic waves in mixtures in the direct nearness of the critical point, an intensity increase of the central component in the fine structure of Rayleigh light scattering and a strong decrease of

* This work was performed within the framework of problem CPBR 02.03/2.3.

the diffusion coefficient are all caused by an increase of concentration fluctuations and an increase of its radius of correlation when approaching the critical point.

This paper presents the analysis of the kinetics of concentration fluctuations in an investigated mixture, carried out on the basis of earlier acoustic and optic measurements. Values of the following parameters have been established: average relaxation time of concentration fluctuations, average length of concentration waves, diffusion coefficient.

2. Thermodynamic fluctuations

The fluctuation of an arbitrary thermodynamic quantity is an instantaneous departure of this quantity from its average value. Density and concentration fluctuations in mixtures are important from the point of view of molecular acoustics. For example, in a volume of 10^{-24} m^3 and at a temperature of $T = 20°$C, the density fluctuation for an acetone-nitromethane mixture (concentration $x = 0.5$) is $\delta_\varrho = 1.7\ 10^{-3}$, while the concentration fluctuation is $\delta_x = 1.7 \cdot 10^{-2}$, i.e. 10 times greater. The average value of concentration fluctuations in critical mixtures near the phase transition point, i.e. in the $|T - T_k| \leqslant 1$–$2°$ temperature range, is several hundred times greater than density fluctuations. Therefore, the investigation of properties of critical mixtures can be limited only to concentration fluctuations.

Concentration fluctuations and their characteristic dynamic properties influence the optic and acoustic properties of critical mixtures. According to the thermodynamic theory of fluctuations, the average value of concentration fluctuations in a two-component mixture with the concentration of the components, x_1 and x_2, respectively, is expressed by formula [1]

$$\langle(\Delta x_2)^2\rangle_V = \frac{x_1}{N\left(\dfrac{\partial \ln p_2}{\partial x_2}\right)_{p,T}} \tag{1}$$

where $N = N_1 + N_2$ is the number of particles of the mixture in volume V, p_2 is the partial pressure of the saturated vapour of component "2", i.e. vapour in thermodynamic equilibrium with the mixture. The above formula is valid only for systems in thermodynamic conditions far from critical. It was derived under an assumption that fluctuations in neighbouring volume elements are independent. On the basis of the effect of light scattering near the critical point L. S. ORNSTEIN and F. ZERNIKE [2] as the first assumed that fluctuations in neighbouring volume elements are interdependent, so a correlation between them exists.

Spatial correlation — radial correlation function

If dV_1 and dV_2 denote two small volume elements of a liquid, distant from each other by a distance r, then the probability dW_1 that particle "1" is contained in volume element dV_1 is

$$dW_1 = dV_1/V. \tag{2}$$

Whereas the probability dW_2 that particle "2" is contained in volume element dV_2 is

$$dW_2 = dV_2/V. \tag{3}$$

If positions of particles would be totally independent from each other, then the probability dW_{12} that particle "1" is contained in element dV_1 and particle "2" in element dV_2 would be expressed by formula

$$dW_{12} = \frac{dV_1}{V}\frac{dV_2}{V}. \tag{4}$$

Instead, if we assume that there is a certain correlation between positions of particles, then equation (4) should be written as

$$dW_{12} = g(r)\frac{dV_1}{V}\frac{dV_2}{V}. \tag{5}$$

The function $g(r)$, which describes the correlation, does not depend on the direction of vector $\vec{r}$ and is called the radial function of the distribution of particles. When $r \to \infty$, then $g(r) \to 1$ and edition (5) changes into equation (4).

Because function $g(r)$ is related to probability dW_{12}, it can be considered as the averaged statistic characteristic of the structure of the liquid. The application of the radial distribution function, $g(r)$, allows the determination of the relative frequency of occurrence of various intermolecular distances in the liquid, when the thermodynamic parameters, namely density, temperature and concentration, are given.

The radial distribution function of atoms for simple liquids can be determined on the basis of data obtained from the scattering of X-rays, neutrons or electrons. The relationship between the radial distribution function and distance r usually has a shape as in Fig. 1; r_0 is the radius of the atom. Function $g(r)$ has several maxima and minima; their value tends to 1 with the increase of r. Far from the critical point, function $g(r)$ reaches 1 already for distances equal to 4–5 atom diameters. There is a "long tail" near the critical point, shown at the right side in Fig. 1.

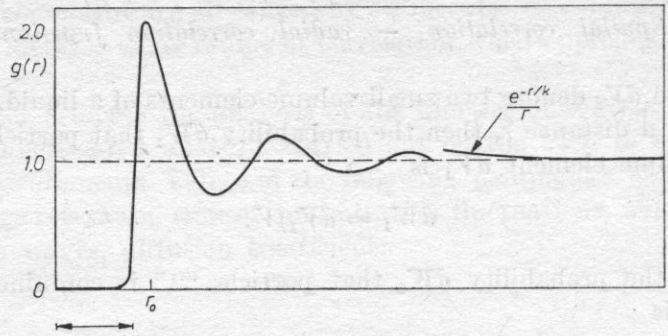

Fig. 1. Radial correlation function for a liquid [3]

Taking advantage of the idea of a correlation between density fluctuations in a liquid in critical conditions, ORNSTEIN and ZERNIKE [2] derived a formula describing the intensity of scattered light near the critical point (critical opalescence). Due to the existance of the correlation there is an asymmetry of scattering (dependence of the intensity of scattered light on the scattering angle), which can be used in the experimental determination of the radius of density (or concentration) fluctuations correlation [4]. Also on the basis of the above correlation, ARCOVITO, FALOCI, ROBERTI and MISTURA [3] proposed a simple explanation of the diffusion effect near the critical point in liquids. According to them, when there is a correlation between density fluctuations with a radius of correlation ξ, then we can imagine that a diffusion process of droplets, which have a radius of the same order as ξ, takes place in the liquid. Of course the atoms "evaporate" and "settle" on the surface of the droplets all the time. In obedience to the Stokes law the mobility of a sphere with a radius ξ is described by expression $(6\pi\eta_s\xi)^{-1}$, while in accordance with Einstein's expression the relationship between mobility and diffusion coefficient has the following form: $D = (k_B t) \times$ (*mobility*). Hence, the diffusion coefficient can be drived from the following expression:

$$D = k_B T / 6\pi\eta_s \xi. \tag{6}$$

Further theoretical considerations, carried out on the basis of the mode coupling theory developed by KAWASAKI [5], and KADANOFF and SWIFT [6], have resulted in an expression for the diffusion coefficient in a hydrodynamic range, which differs from the one presented above only by a constant factor of 1.05.

3. Kinetics of fluctuations

Mixtures with developed concentration fluctuations resemble disperse systems with very small non-homogeneities. They differ from ordinary disperse systems by the fact that concentration fluctuations are unstable. These fluctua-

tions are formed and disappear very quickly. Average lifetimes of concentration fluctuations are inversely proportional to the diffusion coefficient of the mixture. It was experimentally proved [1] that for mixtures with positive departures from the ideal and in thermodynamic conditions distant from critical, relaxation times can be contained in the range 10^{-5}–10^{-11} s. Moving towards the critical point average lifetimes of concentration fluctuations approach infinity.

Kinetics of fluctuations are closely related to the process of propagation of an acoustic wave in critical mixtures. When an acoustic wave propagates in a mixture, the pressure and temperature change periodically. This effect influences the average value of concentration fluctuations and their distribution function, because the average amplitude of concentration fluctuations is p- and T-dependent. The fluctuation distribution attains the equilibrium value with a certain delay, which depends on the diffusion coefficient D.

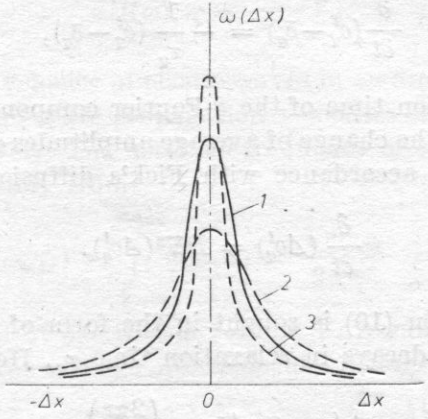

Fig. 2. Example of possible changes in the distribution of concentration fluctuations due to an acoustic wave *1* — distribution in equilibrium; *2* — distribution at reduced pressure; *3* — distribution at increased pressure

A part of the energy of the acoustic wave causes a change in the distribution of concentration fluctuations and then is transformed into heat. The process is irreversible, so acoustic waves are absorbed. When the frequency of acoustic vibrations is sufficiently increased, then the change of the distribution of concentration fluctuations will not occur during one wave period and the fluctuation-induced absorption is not observed. A case in which the distribution function of concentration fluctuations is changed by an acoustic wave is illustrated in Fig. 2.

Let $|\Delta x(r)| = x(r) - \bar{x}$ represent concentration fluctuations. Expanding the distribution of fluctuations into a Fourier series (formal operation introduced by Einstein), we have

$$|\Delta x(r)| = \sum_q \bar{c}_q e^{i\vec{q}\,\vec{r}}. \tag{7}$$

Harmonic components of this spectrum are represented by concentration waves with wave vector $\vec{q}$ and amplitude $\bar{c}_q$. In the state of thermodynamic equilibrium the average amplitude of the Fourier component with wave vector $\vec{q}$, equals

$$\bar{c}_q = f(V, T, x). \tag{8}$$

The distribution function of concentration fluctuations in the field of an acoustic wave differs from the distribution in equlibrium. Therefore, average amplitudes of concentration waves assume new values c_q^t. After the acoustic wave has passed through the mixture, the system will change in the direction of the initial state and $c_q^t \to \bar{c}_q$. According to ONSAGER'S hypothesis it can be accepted that the change of $\bar{c}_q$ in terms of time is subject to the macroscopic law of irreversible processes, so

$$\frac{\partial}{\partial t}(c_q^t - \bar{c}_q) = -\frac{1}{\tau_q}(c_q^t - \bar{c}_q), \tag{9}$$

where τ_q is the relaxation time of the q-Fourier component. Let us assume, as it is usually done, that the change of average amplitudes of concentration waves $\Delta c_q^t = c_q^t - \bar{c}_q$ occurs in accordance with Fick's diffusion equation [7]

$$\frac{\partial}{\partial t}(\Delta c_q^t) = D\nabla^2(\Delta c_q^t). \tag{10}$$

The solution of equation (10) is sought in the form of a concentration wave with length Λ_q, which decays in relaxation time τ_q. Hence we have

$$\Delta c_q^t = Ce^{-t/\tau_q}\cos\left(\frac{2\pi r}{\Lambda_q}\right). \tag{11}$$

Substituting solution (11) in equation (10), we achieve the following relationship between the q-concentration wave and its relaxation time τ_q:

$$\frac{1}{\tau_q} = 4\pi^2 D/\Lambda_q^2. \tag{12}$$

An analogical relationship can be written for a concentration wave, which has an amplitude decaying in relaxation time τ_a. This is the average relaxation time of concentration fluctuations, defined by the following formula [8]:

$$\tau_a = \frac{\int_0^\infty \tau H(\tau)\, d(\ln\tau)}{\int_0^\infty H(\tau)\, d(\ln\tau)} \tag{13}$$

where function $H(\tau)$ is the density of the relaxation time spectrum. $H(\tau)d\tau$ describes the contribution of all Maxwell mechanisms, which have their relaxation times in an interval from τ to $\tau+d\tau$. Function $H(\tau)$ can be determined as the global module per unit interval of the logarithm of relaxation times $(\ln\tau)$.

Concentration waves, hitherto considered only as a result of a formal expansion of concentration fluctuations into a Fourier series, correspond to density waves in mixtures; and these — according to MANDELSZTAM [9] — are elastic Debye waves. Taking advantage of this analogy and basing on Debye'a considerations we can estimate the smallest possible length of a concentration wave. If we consider a crystal as a continuum, then its normal vibrations can be determined from the elasticity theory with adequate boundary conditions. The total number of normal vibrations with frequencies contained in an interval from ω to $\omega+d\omega$, is equal to

$$dD(\omega) = \frac{3\omega^2 d\omega}{2\pi^2 v^2} V, \tag{14}$$

where v is the average velocity of elastic waves in an amorphic solid body when $3/v^3 = 2/v_t^3 + 1/v_l^3$; v_t and v_l are propagation velocities of a transverse and longitudinal wave, respectively. The maximal frequency of elastic vibrations can be determined approximately from

$$D(\omega_{\max}) = \int_0^{\omega_{\max}} dD(\omega) = \frac{V\omega_{\max}}{2\pi^2 v^3} = 3N \tag{15}$$

where N is the number of particles in volume V. Assuming that $d^3 = V/Nd$ is the lattice constant or the average intermolecular distance in liquids, we have [9]

$$\omega_{\max} = \frac{2\pi v}{d}\left(\frac{3}{4\pi}\right)^{1/3}, \quad \Lambda_{\min} = \left(\frac{4\pi}{3}\right)^{1/3} d. \tag{16}$$

The maximal frequency of elastic Debye waves, $\omega_{\max} = 10^{14}$ Hz, and their minimal wave length, $\Lambda_{\min} = 1.5$ Å, can be estimated from formula (16). All $3N$ elastic waves propagate in the medium in all directions forming a complex, spatial "lattice" of optical non-homogeneities. However, if a parallel light beam, characterized by wave vector k, incides onto such a medium and scattered light is observed in the direction determined by wave vector $\boldsymbol{k}'$, then the maximal intensity of the scattered light will be observed only when wave vectors $\boldsymbol{k}$, $\boldsymbol{k}'$ and $\boldsymbol{q}$ satisfy Bragg's condition [9]. In such a case $|\boldsymbol{q}|$ is described by formula

$$|\vec{q}| = \frac{4\pi n}{\lambda}\sin\frac{\vartheta}{2}. \tag{17}$$

It results from equation (17) that if we use He-Ne laser light with wave length $\lambda = 6328$ Å, then the minimal length of the concentration wave, which

can be examined in scattered light will equal approximately 2000 Å (scattering angle equal to 180°). As it will be proved further on, the average length of a concentration wave in critical mixtures will be by 1–2 orders of magnitude shorter.

The Debye approximation of the description of lattice waves [10] assumes that the spectrum of lattice vibrations $D(\omega)$ has a rather specific form. Namely, it is accepted that $D(\omega)$ is proportional to ω^2 near $\omega = 0$, where the material behaves like a continuous elastic medium, and quickly decreases to zero for frequency $\omega_{\max}$. Such a form of function $D(\omega)$ is not justifiable for solids [10], but can considerably well describe the situation in liquids. It has been experimentally and theoretically proved that the spectrum of lattice waves in solids spreads over a considerably wide frequency range and has sharp maxima corresponding to modes with various polarizations and velocities. In low viscosity liquids generally only longitudinal waves occur and they propagate with the same velocity in all directions. Therefore, the spectrum of lattice waves should not exhibit such maxima in liquids. Furthermore, many similarities can be noted between the character of function $D(\omega)$, proposed by Debye, and the distribution function of relaxation times, presented in paper [8]. In this paper we also have a sharp maximum for shorter times and a graduate decrease of the value of the distribution function for longer times.

4. Determination of the average length of a concentration wave in a critical *n*-amylic alcohol-nitromethane mixture

The determination of the spectrum of concentration waves in a series of critical mixtures would supply valuable information concerning the kinetics of concentration fluctuations and widen the knowledge of such phenomena and effects as light scattering or propagation of acoustic waves in such media. Yet this is a rather complex problem for solids and a very complex one for liquids with their random character of particle motion. Most formulations of the spectrum of concentration waves in liquid media have the character of qualitative predictions rather than exact empirical or theoretical solutions.

On the basis of the above mentioned analogy between concentration waves and, density and elastic Debye waves, it can be found that the determination of the spectrum of concentration waves is tantamount to the determination of the spectrum of normal vibrations. In a solid body the problem is reduced to the solution of the following system of 3 N equations [10]:

$$\sum_{s'j'} \{G^{jj'}_{ss'}(q) - \omega^2 M_s \delta_{ss'} \delta_{jj'}\} U^{j'}_{sq} = 0 \tag{18}$$

where $U_{s,q}$ are lattice deflections with a time factor $\exp(i\omega t)$; $G_{s,s'}(q)$ is the tensor describing interatomic interactions; M_s is the mass of the s-atom. The solution of these equations for a dense network of wave vectors q gives values ω_q

from every interval $d\omega_q$. As it has been mentioned previously the situation is more complex in liquids, which are random media, and the determination of the distribution of Debye waves is still to be done. Of course the determination of the average length of concentration waves is not tantamount to the determination of the spectrum of these waves. Yet all the same it leads to several inferences concerning the behaviour of such a spectrum in terms of temperature and concentration of the mixture.

In order to establish the average length of concentration waves according to formula (12) we have to know the average relaxation time of concentration fluctuations and the diffusion constant of the mixture. Relaxation times, τ_a, in the critical *n*-amylic alcohol-nitromethane mixture have been determined with the application of the method described in papers [8, 11] for various concentrations and for two temperatures. Values of diffusion coefficients for these temperatures and concentrations have been calculated from formula (6). The radius of correlation, ξ for this mixture has been determined by the authors previously with the utilization of the effect of Rayleigh light scattering [4, 12]. Values of the radius of correlation for chosen concentrations and temperatures were calculated from [13]:

$$\xi = \xi_1[|T-T_k| + d(x-x_k)^3]^{-0.6}. \tag{19}$$

Final calculation results are presented in Table 1.

Table 1

Concentration of n-$C_5H_{11}OH$ [mole fraction]	T [K]	ξ [10^{-10} m]	$D \cdot 10^3$ [$m^2 s^{-1}$]	A_a [10^{-2}m]	τ_a [s]
0.1	302.35	6.1	39.2	$2.5 \cdot 10^{-6}$	$4.05 \cdot 10^{-10}$
	313.15	4.0	74.3	$3.8 \cdot 10^{-6}$	$5.03 \cdot 10^{-10}$
0.3	302.35	18.5	7.4	$1.1 \cdot 10^{-5}$	$4.04 \cdot 10^{-8}$
	313.15	5.5	31.2	$6.7 \cdot 10^{-6}$	$3.60 \cdot 10^{-9}$
0.385	302.35	20.4	5.7	$2.2 \cdot 10^{-5}$	$2.23 \cdot 10^{-7}$
	313.15	5.6	26.3	$4.4 \cdot 10^{-6}$	$1.91 \cdot 10^{-9}$
0.5	302.35	16.4	5.9	$9.6 \cdot 10^{-6}$	$3.99 \cdot 10^{-8}$
	313.15	5.4	22.9	$3.4 \cdot 10^{-6}$	$1.34 \cdot 10^{-9}$

Figs. 3 and 4 illustrate D and τ_a in terms of concentration in a critical *n*-amylic alcohol-nitromethane mixture for two temperatures: 29.2 and 40°C. In accordance to the theory, the average relaxation time of concentration fluctuations increases when approaching the critical point, while the diffusion coefficient decreases. Figs. 5 and 6 present the relationship between the average length of concentration waves and the concentration of the mixture for the same

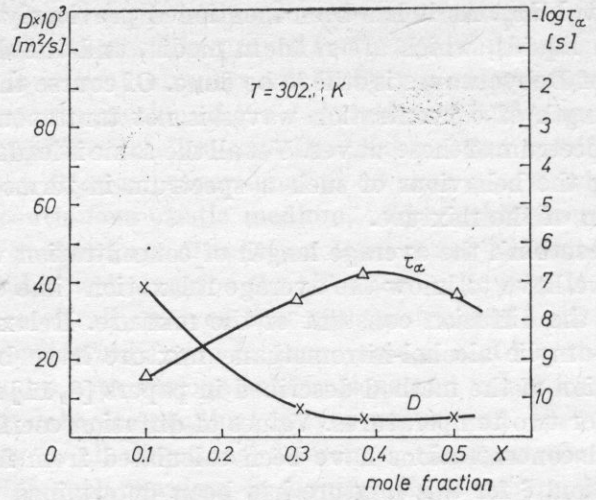

Fig. 3. D and τ_α in terms of concentration in the critical n-amylic alcohol-nitromethane mixture at temperature $T = 302.35$ K

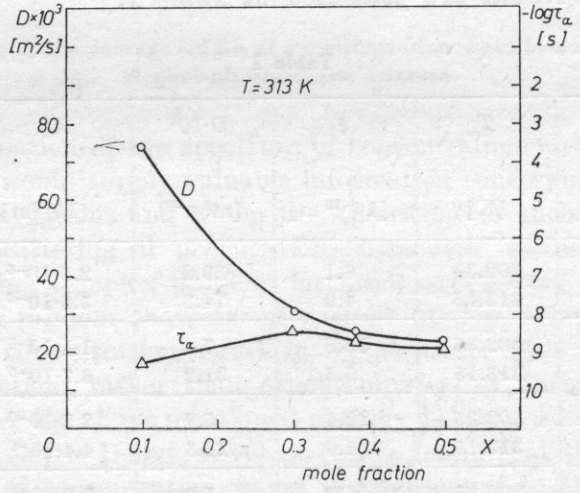

Fig. 4. D and τ_α in terms of concentration in the critical n-amylic alcohol-nitromethane mixture at temperature $T = 313.15$ K

two temperatures. As it can be seen, the average length of concentration waves increases by one order of magnitude, when conditions of the mixture approach critical conditions. This indicates that the spectrum of concentration waves moves towards lower frequencies.

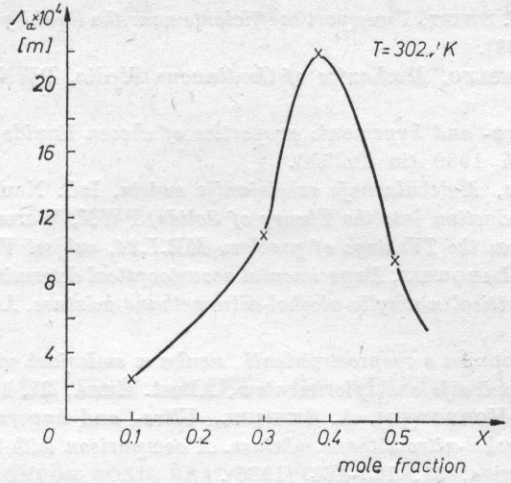

Fig. 5. The average length of concentration waves in terms of concentration in the critical *n*-amylic alcohol-nitromethane mixture at temperature $T = 302.35$ K

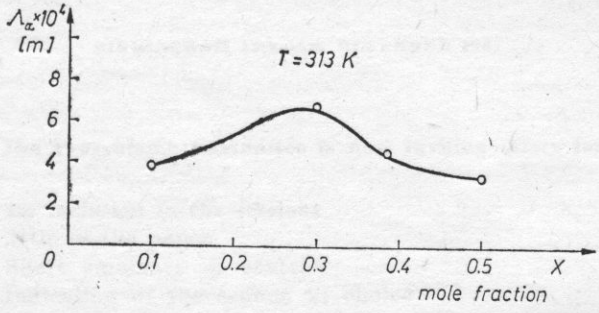

Fig. 6. The average length of concentration waves in terms of concentration in the critical *n*-amylic alcohol-nitromethane mixture at temperature $T = 313.15$ K

References

[1] M. I. Szachparonow, *Wwiedienije w sowriemiennuju tieoriju rastworow*, Izd. "Wysszaja Szkoła", 1976.

[2] M. A. Leontowicz, *Statistic Physics*, PWN, Warszawa 1957 (in Polish).

[3] H. L. Swinney, *Kriticzeskije jawlenije w żidkostjach*, in: Spiektroskopija opticzeskogo smieszenija i korrielacja fotonow, ed. H. Z. Cumnins and E. R. Pike, Izd. Mir, Moskwa 1978.

[4] T. Hornowski, M. Łabowski, *Experimental determination of the radius of correlation of concentration fluctuations in the critical n-amylic alcohol-nitromethane mixture*, Proc. XXXII OSA, 179–182, Kraków 1985 (in Polish).

[5] K. Kawasaki, *Sound attenuation and dispersion near the liquid-gas critical point*, Phys. Rev., 1A, 1750 (1970).

[6] L. P. KADANOFF, J. SWIFT, *Transport coefficients near the liquid-gas critical point*, Phys. Rev., 166, 89 (1968).

[7] L. LANDAU, E. LIFSZYC, *Mechanics of Continuous Media*, PWN, Warszawa 1958 (in Polish).

[8] M. ŁABOWSKI, *Ultra- and hypersonic properties of chosen liquids and critical mixtures*, Ed. UAM, Poznań 1980 (in Polish).

[9] I. L. FABIELINSKIJ, *Molekularnoje rassiejanije swieta*, Izd. Nauka, Moskwa 1965.

[10] J. M. ZIMAN, *Introduction into the Theory of Solids*, PWN, Warszawa 1977 (in Polish).

[11] *Scientific report from the IV stage of problem MR.I.24, subject VI.4* (in Polish).

[12] T. HORNOWSKI, M. ŁABOWSKI, *Experimental acoustooptical determination of some physical parameters of the critical n-amylic alcohol-nitromethane mixture*, Acta Physica Polonica, A69/4 (in print).

[13] I. A. CZABAN, *K woprosu o rasprostranienii zwuka w smiesjach wblizi kriticzeskoj toczki rassłaiwanija. Srawnienije s ekspierimentom*, Akust. Żurn., **21**, 1, 286–293 (1975).

[14] M. ŁABOWSKI, T. HORNOWSKI, A. SKUMIEL, *Ultra- and hypersonic properties of the critical n-amylic alcohol-nitromethane mixture. A comparison with the theories of Fixman and Chaban*, Acustica, **57**, 175–184 (1985).

Received on December 12, 1985; revised version on May 28, 1986.

C H R O N I C L E

BRITISH SOCIETY OF AUDIOLOGY

HARVEST HOUSE, 62 LONDON ROAD, READING, BERKSHIRE RG1 5AS. TELEPHONE READING 0734 861345.

21st ANNIVERSARY INTERNATIONAL CONFERENCE

BIRMINGHAM 13th-16th DECEMBER 1987

The Programme Committee is now inviting offers for

1. **Papers-Suitable for inclusion in the sessions**
   With: (a) Title of the paper
   (b) Short summary of content
   (c) Indication of the session of choice
2. **Commercial Exhibitions**
   Indicating: (a) Approximate size
   (b) Character exhibit
   (c) Indication of associated services required

Those intending to provide such participation, please reply as soon as possible to:

NC BLAND FRCS
Conference Organiser
BSA 21st Anniversary Conference
Centre for the Hearing Impaired
Western Road
Birmingham B18 7QQ
England
Tel: 021-554 3801

for early evaluation and decision

3. **Posters, displays, audio-visual, film or tape material, non-commercial exhibits**
   Indicating: (a) Title
   (b) Size of space required, and special requirements
   (c) Format

To:

DR B C MOORE
Department of Experimental Psychology
Downing Street, Cambridge CB2 3EB Tel: 0223 333550

INSTITUTE OF NOISE CONTROL ENGINEERING

Post Office Box 3206 Arlington Branch
Poughkeepsie, NY 12603, U.S.A.

FOR IMMEDIATE RELEASE:

THE INTER-NOISE 86 PROCEEDINGS ARE AVAILABLE

INTER-NOISE 86, the 15th International Conference on Noise Control Engineering, was held at the Massachusetts Institute of Technology on 1986 July 21-23. The meeting was sponsored jointly by the School of Engineering at MIT and the Institute of Noise Control Engineering. Five hundred and twenty-five delegates from 36 different countries attended INTER-NOISE 86.

The Proceedings of INTER-NOISE 86 have been published and are now available to individuals who were unable to attend the conference. The two-volume set contains 1472 pages of technical information. A total of 271 papers technical papers has been published; these papers cover all areas of noise control engineering, including machinery noise emission, sound propagation, community noise, surface transportation noise, aircraft noise, instrumentation for noise control engineering and standards for noise control.

The two volume set of INTER-NOISE 86 Proceedings is available for $75.00, and is shipped postpaid both within the United States and overseas (by surface mail). An additional $30.00 per set must be added to overseas orders which are shipped by air. Payment must be made in U.S. funds on a U.S. bank or on a bank that has a correspondent bank in the United States. The INTER-NOISE 86 Proceedings may be ordered from Noise Control Foundation, P.O. Box 2469 Airlington Branch, Poughkeepsie, NY 12603, U.S.A.

INTERNOISE 88

Inter-Noise 88, the seventeenth International Conference on Noise Control Engineering, will be held in Avigon in the South of France from August 30th to September 1rst.

The conference is sponsored by the International Institute of Noise Control Engineering and organized by the industrial and Environmental Noise Group of the French Acoustical Society. It will strongly emphasize the theme: "The Sources of Noise" including the following topics:

— Physical Generation and Radiation Mechanisms
— Measurement and Analysis Techniques

— Location, Identification, Modelling
— Stationnary Sources (machine and equipments, domestic appliances).
— Moving Sources (road, rail, aircraft, ship).
— Techniques for noise reduction at the source
— Active Noise and Vibration Attenuation
— Trends in test codes, labelling, regulations for noise sources.

A large exhibition is scheduled where the latest instrumentation and equipment for noise control will be presented as well as domestic and industrial sound proof equipments.

For further information, please contact:

Inter-Noise 88 secretariat
BP 23
60302 SENLIS CEDEX
Tel. (33) 44 58 34 15
telex: 140 006 F
telecopie: (33) 44 58 34 00